Universität Hamburg
DER FORSCHUNG | DER LEHRE | DER BILDUNG

Characterization of proteostasis factors in the context of cellular safeguarding

Dissertation

zur Erlangung des akademischen Grades

doctor rerum naturalium

(Dr. rer. Nat.)

eingereicht an der

Fakultät für Mathematik, Informatik und Naturwissenschaften der

Universität Hamburg

Von

Qinming Li, Master of Science

2026

Vorsitzender: Prof. Dr. Susanne Dobler

Gutachterinnen/Gutachter: Prof. Dr. Baris Tursun
Prof. Dr. Daniel N. Wilson

Weitere/s Mitglied/er: Prof. Dr. Tobias Lenz

Datum der mündlichen Prüfung: 11.09.2026

Conducted in University of Hamburg
Institute of Cell and Systems Biology of Animals
Biology Department
Research Group: Gene regulation and Cell Fate Decision in *C. elegans*
Supervisor: Prof. Dr. Baris Tursun
Co-supervisor: Prof. Dr. Daniel Nicodemus Wilson

Submitted from Qinming Li
Matrikel-Nr. 7574383
Qinmingli94@gmail.com
Qinming.li@uni-hamburg.de

Eidesstattliche Versicherung

Sofern im Zuge der Erstellung der vorliegenden Dissertationsschrift generative Künstliche Intelligenz (gKI) basierte elektronische Hilfsmittel verwendet wurden, versichere ich, dass meine eigene Leistung im Vordergrund stand und dass eine vollständige Dokumentation aller verwendeten Hilfsmittel gemäß der Guten wissenschaftlichen Praxis vorliegt. Ich trage die Verantwortung für eventuell durch die gKI generierte fehlerhafte oder verzerrte Inhalte, fehlerhafte Referenzen, Verstöße gegen dasDatenschutz- und Urheberrecht oder Plagiate.

Affidavit

I hereby declare and affirm that this doctoral dissertation is my own work and that I have not used any aids and sources other than those indicated.
If electronic resources based on generative artificial intelligence (gAI) were used in the course of writing this dissertation, I confirm that my own work was the main and value-adding contribution and that complete documentation of all resources used is available in accordance with good scientific practice. I am responsible for any erroneous or distorted content, incorrect references, violations of data protection and copyright law or plagiarism that may have been generated by the gAI.

Ort, den | City, date Unterschrift | Signature

Hamburg, 30.03.2026

Abstract

Direct reprogramming (DR) involves the use of cell fate inducing transcription factors (TFs) that directly convert one cell type into another. However, the ability of TFs to reprogram cell identity is highly dependent on the cellular context and is often limited by inhibitory mechanisms. Understanding these reprogramming barriers *in vivo* is essential for unlocking the therapeutic potential of cellular reprogramming and offers valuable insights into the fundamental biology of cell fate determination. In this study, we identified the ubiquitin E3 ligase HECD-1 as a novel safeguard of germ cell identity, preventing ASE neuron conversion in *C. elegans*. Depletion of *hecd-1* via RNAi, or by CRISPR-mediated mutation, consistently induces ASE neuron fate in germ cells. Additionally, smFISH-based assessment of endogenous gene expression confirmed the faithful conversion of germ cells to ASE neuron like cells.

As a critical component of the ubiquitin-proteasome system (UPS), HECD-1 regulates the degradation of target proteins. However, its specific substrates remain poorly characterized. To identify HECD-1 substrates relevant to DR, we conducted mass spectrometry on *hecd-1* mutants to detect proteomic changes, followed by RNAi screening for candidate target genes whose depletion suppresses DR in *hecd-1* mutant animals. We identified several candidate targets (*lmn-1*, *hsp-90*, *cox-4*, *nuo-6* and *hda-1*) that exhibited upregulated protein levels in *hecd-1* mutants and depletion by RNAi suppressed DR. Furthermore, to confirm that DR suppression was not a consequence of germ cell elimination or damage, germline health was assessed in animals with simultaneous depletions for *hecd-1* and the newly identified targets using germ cell reporters such as *sun-1::mRuby*. Additionally, the reprogrammed cells exclusively expressed ASE markers while losing germ cell markers, indicating the faithful conversion of the original cell fate to the new neuronal identity.

This study reveals a multifaceted network orchestrating cellular plasticity following HECD-1 depletion. The strong, paradoxical suppression of HECD-1 depletion mediated DR by *hda-1* RNAi indicated the heterochromatin regulation in repressing the original germ cell fate programs, independent of histone H3 modifications. Additionally, depletion of HECD-1 specifically triggered the mitochondrial unfolded protein response (UPR^{mt}) stress. Upregulation of COX-4 and NUO-6 further indicated the UPR^{mt} stress, and knocking down either gene strongly

suppressed the *hecd-1* depletion mediated DR, highlighting the crucial role of mitochondrial function in DR.

Overall, this study represents the first identification of *hecd-1* as a cellular reprogramming barrier in *C. elegans*, and reveals a network of proteins that promote DR upon loss of HECD-1, thereby contributing to delineating the context of the TF-induced cellular reprogramming.

Zusammenfassung

Die direkte Reprogrammierung (DR) umfasst den Einsatz von zellschicksalbestimmenden Transkriptionsfaktoren (TFs), die einen Zelltyp direkt in einen anderen umwandeln. Allerdings hängt die Fähigkeit von TFs, die Zellidentität umzuprogrammieren, stark vom zellulären Kontext ab und wird häufig durch inhibitorische Mechanismen begrenzt. Das Verständnis dieser Reprogrammierungsbarrieren in vivo ist entscheidend, um das therapeutische Potenzial der zellulären Reprogrammierung zu erschließen, und liefert wertvolle Einblicke in die grundlegende Biologie der Zellschicksalsbestimmung. In dieser Studie identifizierten wir die Ubiquitin E3 Ligase HECD-1 als einen neuartigen Schutzfaktor der Keimbahnidentität, der die Umwandlung in ASE-Neuronen in C. elegans verhindert. Die Reduktion von hecd-1 mittels RNAi oder durch CRISPR-vermittelte Mutation führt konsistent zur Induktion des ASE-Neuronenschicksals in Keimzellen. Zusätzlich bestätigte eine auf smFISH basierende Analyse der endogenen Genexpression die zuverlässige Umwandlung von Keimzellen in ASE-neuronähnliche Zellen.

Als ein wesentlicher Bestandteil des Ubiquitin-Proteasom-Systems (UPS) reguliert HECD-1 den Abbau von Zielproteinen. Seine spezifischen Substrate sind jedoch bislang kaum charakterisiert. Um HECD-1 Substrate mit Relevanz für die DR zu identifizieren, führten wir Massenspektrometrie bei *hecd-1* Mutanten durch, um proteomische Veränderungen zu erfassen, gefolgt von einem RNAi-Screening potenzieller Zielgene, deren Reduktion die DR in *hecd-1* Mutanten unterdrückt. Wir identifizierten mehrere Kandidaten (*lmn-1*, *hsp-90*, *cox-4*, *nuo-6* und *hda-1*), die in *hecd-1* Mutanten erhöhte Proteinspiegel aufwiesen und deren RNAi-vermittelte Reduktion die DR unterdrückte. Um zu bestätigen, dass die Unterdrückung der DR nicht auf die Eliminierung oder Schädigung der Keimbahn zurückzuführen war, wurde die Gesundheit der Keimbahn in Tieren mit gleichzeitiger Reduktion von *hecd-1* und den neu identifizierten Zielgenen mithilfe von Keimzellen-Markern wie *sun-1::mRuby* untersucht. Zudem exprimierten die reprogrammierten Zellen ausschließlich ASE-Marker und verloren Keimzellenmarker, was die zuverlässige Umwandlung des ursprünglichen Zellschicksals in die neue neuronale Identität zeigt.

Diese Studie offenbart ein vielschichtiges Netzwerk, das die zelluläre Plastizität nach HECD-1-Reduktion steuert. Die starke, paradoxe Unterdrückung der durch HECD-1 Reduktion ausgelösten DR durch *hda-1* RNAi weist auf eine heterochromatinvermittelte Regulation der Repression ursprünglicher Keimzellprogramme hin, unabhängig von Histon-H3-Modifikationen. Darüber hinaus löste die Reduktion von HECD-1 spezifisch die mitochondriale UPR^{mt} Stressantwort aus. Die Hochregulation von COX-4 und NUO-6 bestätigte den UPR^{mt} Stress, und die Reduktion eines der beiden Gene unterdrückte die hecd-1-abhängige DR stark, was die entscheidende Rolle der mitochondrialen Funktion in der DR hervorhebt.

Insgesamt stellt diese Studie die erste Identifizierung von *hecd-1* als Reprogrammierungsbarriere in C. elegans dar und enthüllt ein Netzwerk von Proteinen, die nach dem Verlust von HECD-1 die DR fördern und somit zur Definition des Kontexts der durch Transkriptionsfaktoren ausgelösten zellulären Reprogrammierung beitragen.

Table of Contents

1. Introduction

1.1 Cellular reprogramming

1.1.1 Reprogramming to pluripotency

The development of a multicellular organism proceeds from the fertilization of the oocyte and the sperm to form a totipotent zygote, which has the potential to differentiate into distinct fates and form specific tissues. The early stage of mouse embryonic cells are allocated to two primary lineages: the trophoblast lineage, which will form part of the placenta, and the bipotential inner cell mass (from embryonic stem cells are derived) are able to form the three germ layers, each of these layers eventually become specialized and give rise to the tissue of the adult body (Hanna et al., 2010; Yamanaka and Blau, 2010). This differentiation process is tightly regulated by complex transcriptional and epigenetic networks. Once established, the differentiated cellular states are remarkably stable, and such differentiated cells typically do not switch fates under normal circumstances (Ladewig et al., 2013; Smith et al., 2016).

Differentiated cells were long believed to be irreversibly committed to their fate, however, this dogma was challenged by cloning experiments in amphibians (Gurdon et al., 1958) and later in mammals (Wilmut et al., 1997). Using the somatic cell nuclear transfer (SCNT) technique (Figure 1.1. A), John Gurdon and colleagues transferred nuclei from frog somatic cells into an enucleated and unfertilized frog oocyte, which resulted in approximately 35% of cases giving rise to normal tadpoles. Subsequently, the success of Dolly the sheep further created a revolution in science. These profound experiments demonstrated that the nuclei of differentiated cells maintain full genetic potential and can be reprogrammed to a pluripotent state through experimental manipulation (Takahashi and Yamanaka, 2016). However, the success rate of SCNT in mammals remains remarkably low. Decades of study have attributed this low efficiency primarily to epigenetic barriers (Gouveia et al., 2020), and post-implantation, such as immunodeficiency, abnormal offspring syndrome, and premature death (Malin et al., 2022).

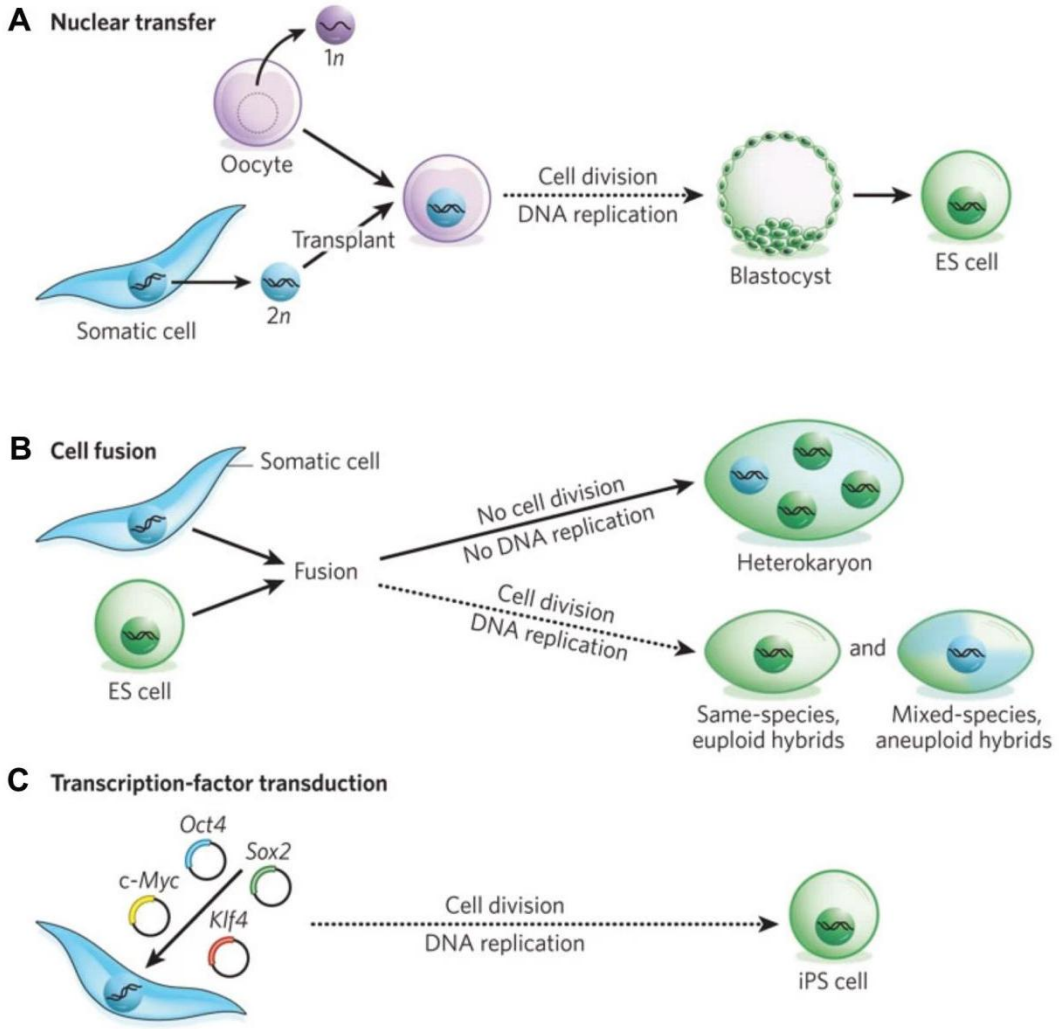

Figure 1.1 Experimental method for the cellular reprogramming. A) Somatic cell nuclear transfer (SCNT): the nucleus of a somatic cell injected into an enucleated oocyte, generating a blastocyst from which embryonic stem cells (ESC) are derived in tissue culture. **B)** cell fusion: two different cell types are fused to a single entity; the tetraploid hybrid cell is able to proliferate. The fused cells can become heterokaryons or hybrids. **C)** Defined factors mediated reprogramming: Introducing four specific genes (Oct4, Sox2, Klf4, c-Myc) into somatic cells using retroviruses can create induced pluripotent stem (iPS) cells. (adopted from Yamanaka and Blau, 2010).

In the late 20th century, SCNT was replicated in many laboratories and successfully applied to clone a wide range of animal species. Concurrently, cell fusion involving the fusion of two or more cell types to form a single entity emerged as a parallel technique, which can generate hybrids or heterokaryons (Figure 1.1. B). Hybrids, characterized by the fusion of nuclei and proliferation capacity, have been observed to adopt a dominant state and the reactivation of inactive X chromosome (Tada et al., 2001). The non-proliferated heterokaryons have multiple distinct nuclei, which showed the activation of silent pluripotency genes such as *Oct4* (Pereira et al.,

2008) and *Nano*g (Silva et al., 2006). Cell fusion method can induce aneuploidy and genomic instability, potentially leading to malignant conversion (Dörnen et al., 2020), but it provided a tool to understand reprogramming. Moreover, it suggested the existence of reprogramming factors that can 'erase' the 'memories' of somatic cells (Takahashi and Yamanaka, 2016).

Encouraged by the SCNT and the analysis of heterokaryons between embryonic stem cell and many types of somatic cell, Takahashi and Yamanaka established a major landmark in the field of reprogramming with the generation of induced pluripotent stem cells (iPSCs) from mouse fibroblasts by ectopic expression of four TFs: OCT4 (octamer-binding TF, also known as POU5F1), SOX2 (SRY-box2), KLF4 (Krüppel-like factor 4), MYC (c-MYC proto-oncogene protein), collectively referred to as OSKM factors (Takahashi and Yamanaka, 2006). Mouse iPSCs are indistinguishable from mouse ES cells in morphology, proliferation, gene expression, and teratoma formation, and even give rise to adult chimeras after being transplanted into blastocysts (Takahashi et al., 2007; Wernig et al., 2007). After successful generation of mouse iPSCs, two groups reported the generation of human iPSCs by using the same combination of factors (Takahashi et al., 2007), and Thomson factors (Yu et al., 2007) which are the combination of *Oct4, Sox2, Nanog,* and *Lin28*. The pluripotent cell state can be induced in a variety of differentiated cell types, for instance, pancreatic β cells, keratinocytes, hepatocytes, and stomach cells (Yamanaka and Blau, 2010) (Figure 1.1.C). While iPSCs appeared remarkably similar to ESCs, subsequent studies revealed notable epigenetic differences, such as global DNA methylation (Liang and Zhang, 2013), suggesting that iPSCs are not identical to embryos in their natural milieu (Takahashi and Yamanaka, 2015). Furthermore, the efficiency of inducing a pluripotent state is low and variable; it depends on factors such as the donor cell type, age, physiological state, the reprogramming factors delivery method, and the barriers of reprogramming (Doss and Sachinidis, 2019).

The studies described above rely on the classical concept of lineage commitment: it was believed that differentiation is unidirectional and irreversible, the undifferentiated and pluripotent state positioned hierarchically ‘above’ the committed and differentiated states. This classical view of lineage specification was depicted by Conrad Hal Waddington as an epigenetic landscape (Figure1.2. A) (Waddington, 1957).

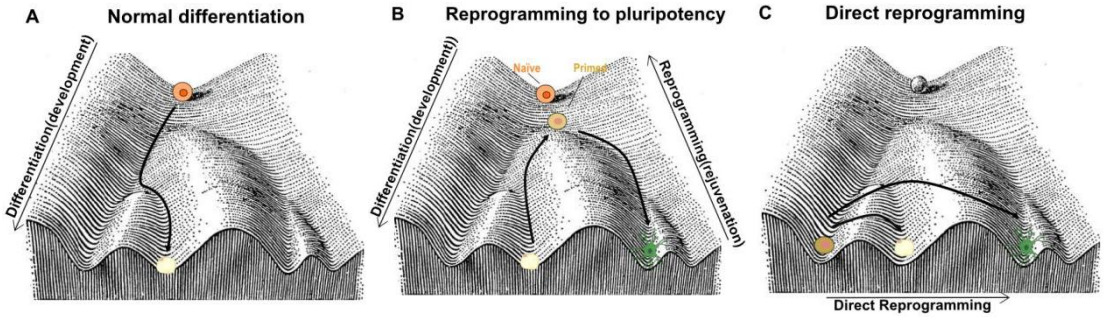

Figure 1.1 Waddington's epigenic landscape of cell fate changes. A) A pluripotent cell (orange) can commit to any somatic lineage (light yellow), which is represented like 'rolls' down a landscape into different groves during normal development. **B)** The discovery of cellular reprogramming to iPSCs demonstrated that a committed cell can reverse course, rolling back up the hill to achieve pluripotency, and subsequently differentiate into a target cell type. **C)** Direct cellular reprogramming has shown that cells can jump directly from one groove to another without passing through a pluripotent state. (Adapted from Waddington, 1957; Ladewig et al., 2013)

This epigenetic landscape described the natural restriction of cell differentiation potential: a pluripotent state of cell moving towards terminal differentiated state is represented as a ball rolling down a hill and segregating into different groves, suggesting that cell fate hierarchy exists (Figure1.2. A) (Ladewig et al., 2013). However, subsequent studies demonstrated that cell fate is reversible and exhibits a high degree of plasticity. The discovery of iPSCs revealed that cell fate transitions can be achieved by employing specific transcription factors that bring a differentiated cell back to a pluripotent state (Figure1.2. B). Furthermore, direct reprogramming, using tissue specific transcription factors allows the conversion of lineage-committed cells into another cell type (Takahashi and Yamanaka, 2015), without passing through the pluripotent state (Figure1.2. C).

1.1.2 Direct Reprogramming

Direct reprogramming, also known as transdifferentiation or direct lineage conversion, is defined as the process by which a cell from one tissue lineage is converted into a cell of a distinct lineage. This phenomenon was first reported by Hadorn and Schläpfer in *Drosophila melanogaster (D. melanogaster)* (Hadorn, 1963; Schläpfer, 1963) through sequentially transplanting male genital imaginal disc cells from larvae into the abdomen of an adult. They observed that few male genital imaginal disc cells lost their development restriction and could form to 'allotypic

structure', for example, cells from leg disk can form a wing and vice versa. This finding suggested that cells could alter their developmental fate, and these results were interpreted as an endogenous phenomenon even though it was triggered by surgical manipulations (Tursun, 2012).

Cellular fate switches, or plasticity, have often been observed as results of pathological or experimental manipulations. For instance, when the eye lens of a newt is removed, pigmented epithelial cells (PECs) from the dorsal iris transdifferentiate to form a new lens (Jopling et al., 2011). Cellular transdifferentiation also occurs naturally during liver regeneration, in the pancreas, and can be induced by injury or activation of NOTCH signalling, as demonstrated by Yanger et al. (Yanger et al., 2013). However, Sprecher and Desplan observed an endogenous transdifferentiation example without manipulation in *D. melanogaster*: during metamorphosis from larvae to adult flies, the photoreceptors of the eyelets switch from expressing blue light-sensitive Rhodopsin (Rh) 5 to green light-sensitive Rh6 receptors, involving a cell fate conversion (Sprecher and Desplan, 2008).

Apart from *D.melanogaster*, natural transdifferentiation also occurs in *Caenorhabditis elegans (C. elegans*), where specialized rectal epithelial cells convert into specific neurons during larval development. Between the L1 and L2 larval stage, the fully de-differentiated rectal epithelial Y cell retracts from the rectum and converts into a PDA motor neuron without any further cell division (Becker and Jarriault, 2016; Jarriault et al., 2008; Richard et al., 2011). The *sox-2* gene and members of the NODE-like (Nanog and Oct4-associated deacetylase) complex are required for this conversion in *C.elegans*, but the role of *sox-2* during Y-to-PDA conversion does not seem to involve neural fate promotion (Kagias et al., 2012). Zuryn and colleagues reported that the conserved H3K27me3/me2 demethylase, JMJD-3.1, works together with the H3K4 methyltransferase SET-1 complex to ensure consistent transdifferentiation of postmitotic hindgut cells into motor neurons in *C. elegans* (Zuryn et al., 2014). The discovery of naturally occurring cell fate conversions revealed the modifiable nature of cell identity. These findings prompted a reassessment of established concepts of cell differentiation and plasticity, thereby paving the way for the notion that transdifferentiation, or direct reprogramming, could also be achieved (Wang et al., 2021).

Direct reprogramming or transdifferentiation can be manipulated by exogenous TF expression, which was first demonstrated by Weintraub and colleagues in 1987. They identified a cDNA that encoded the helix-loop-helix transcription factor MyoD, which was capable of converting phenotypic myoblasts into fibroblasts (Davis et al., 1987) (Figure 1.3). The following experiments showed similar conversion in pigment, nerve, fate, and liver cell lines; however, these processes generated low efficiency, and the resulting muscle-like cells looked aberrant (Weintraub et al., 1989). Nonetheless, MyoD holds a special place in the history of reprogramming, not only as the first evidence that a single TF was capable of reprogramming the cell fate, but also as the foundation for extensive efforts to identify additional TFs involved in lineage conversion (Battistelli et al., 2022).

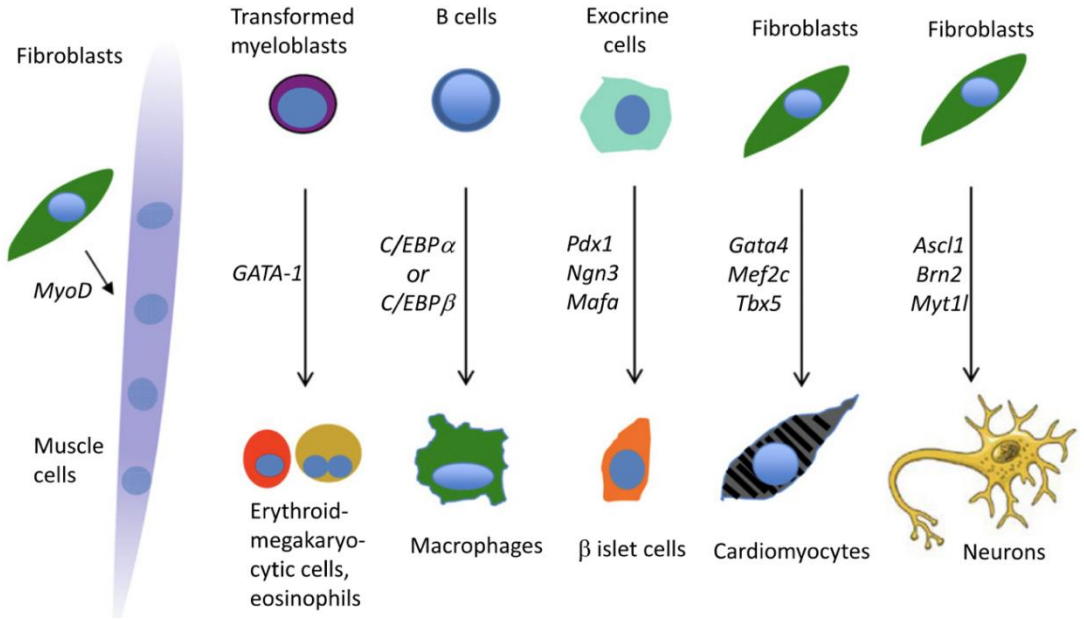

Figure 1.3 Examples of TF-induced transdifferentiation. Davis et al. demonstrated the conversion of fibroblasts into muscle cells using the TF MyoD (Davis et al., 1987). TF GATA-1 was shown to convert myeloblasts into megakaryocytes (Kulessa et al., 1995). Overexpression of C/EBPα or C/EBPβ induced the conversion of B- and T-cell progenitors into macrophages (Xie et al., 2004). Exocrine pancreatic cells were reprogrammed into insulin-producing β-islet cells using the transcription factor combination Ngn3, Pdx1, and Mafa (Zhou et al., 2008). The cocktail of Gata4, Mef2c, and Tbx5 enabled the conversion of mouse fibroblasts into cardiomyocytes (Ieda et al., 2010). Additionally, expression of Brn2, Ascl1, and Myt1l facilitated the conversion of mouse and human fibroblasts into functional neurons (Vierbuchen et al., 2010). (Reprinted from Graf, 2011)

Soon after, the ectopic expression of erythroid GATA-1 was found to be capable of converting avian myeloblasts into either megakaryocyte-erythrocyte precursors or eosinophils (Kulessa et al., 1995) (Figure 1.3). Further insights from the

haematopoietic system also revealed that matured cells can be induced lineage switching, which is differentiated B cells directly reprogrammed into macrophages by ectopic expression of the basic Leu zipper transcription factor C/EBPα or C/EBPβ (CCAAT/enhancer binding protein-α or β) (Xie et al., 2004) (Figure 1.3).

These examples of blood cell lineage conversion, while important for fundamental understanding, remain distant from therapeutic applications. However, in 2008, a significant breakthrough demonstrated therapeutic potential, when Melton and colleagues employed a combination of three transcription factors Pdx1 (pancreatic and duodenal homeobox 1), Ngn3 (neurogenin 3) and MafA (v-maf musculoaponeurotic fibrosarcoma oncogene family, protein A) to convert pancreatic exocrine cells into functional insulin-producing β-islet cells *in vivo* (Zhou et al., 2008). This rapid conversion process appeared stable over months in the absence of transgene expression, and the reprogrammed β-islet cells secreted insulin and rescued hyperglycemia in a mouse model (Vierbuchen and Wernig, 2011; Zhou et al., 2008) (Figure 1.3). Another fascinating example demonstrated that a combination of Gata4, Mef2c, and Tbx5 was sufficient to convert dermal or cardiac fibroblasts into induced cardiomyocyte-like cells (iCMs) (Ieda et al., 2010). Intringuingly, the strategy of iCMs generation *in vivo* exhibited superior quality compared to *in vitro* method, suggesting that additional factors might enhance the reprogramming process *in vivo* (Srivastava and DeWitt, 2016).

In Waddington's model, the different 'valleys' are delineated by 'hills' of differing elevation (Figure 1.2. C), suggesting that interconversion of cells within the same germ layer may require less energy than overcoming the barriers between germ layers. Inspired by the landmark discovery of iPSCs, scientists began to assess direct reprogramming to unrelated cell types (Wang et al., 2021) (Figure 1.3). In 2010, Wernig and colleagues reported the first successful direct conversion of mouse embryonic fibroblasts into induced neurons (iNs) by the expression of Brn2, Ascl1, and Myt1(collectively referred to as BAM) (Vierbuchen et al., 2010). This method was extended to the human cells by supplementing BAM with NeuroD1 TFs (Pang et al., 2011).

In the aforementioned TF-induced direct reprogramming examples, the key TFs, such as MyoD, Ascl1 or GATA4, have been designated as pioneer factors due to the capacity to act as the primary responders by opening the closed chromatin and

recruiting co-binding factors (Keshri et al., 2024). This property elucidates why certain TFs are so powerful and crucial in mediating cell fate reprogramming.

Direct reprogramming is considered as a safer alternative by avoiding the state of pluripotency, which is associated with significant tumorigenic propensity in iPSCs (Ahrens et al., 2019). The potential to apply direct reprogramming *in vivo* offers a promising strategy for regenerative medicine by enabling resident cells to replace those lost due to injury or disease, serving as an alternative to cell transplantation (Fang et al., 2018). Several studies have demonstrated the therapeutic promise of *in vivo* reprogramming in neurological disorders. In a mouse model of Parkinson's disease, Ascl1 combined with Lmx1a and Nurr1 (ALN) was shown to convert endogenous NG2 glia into inhibitory induced neurons (Pereira et al., 2017). Neurod1 was sufficient to convert NG2 glia to glutamatergic and GABAergic iNs in Alzheimer's disease model mice (Guo et al., 2014). Furthermore, the lineage conversion of reactive astrocytes induced by Neurod1 has been utilized to address a focal stroke model in mice (Chen et al., 2020).

Despite these important advances in the field of reprogramming, direct reprogramming has not yet been utilized in clinical applications. Several challenges still need to be overcome, including low efficiency and targeting specificity (Wang et al., 2021). Investigating the molecular mechanism underlying direct reprogramming can help us to understand how cellular fate is maintained, ultimately facilitating the development strategies to overcome these limitations of reprogramming and to precisely manipulate cell identity.

1.1.3 Cell fate safeguarding mechanisms act as barriers to reprogramming

The differentiated state is stable but requires maintenance. Under different environmental conditions like injury, disease, or aging, this state can be lost (Alvarado and Yamanaka, 2014). Under normal conditions, cellular safeguards maintain cell identity. Although it is crucial for the proper function of specialized cells and tissues, many safeguards simultaneously prohibit natural reprogramming and act as barriers to cell fate changes (Brumbaugh et al., 2019).

When cells differentiate to a specialized fate, specific epigenetic states are faithfully maintained, which preserves cell identity (Elsherbiny and Dobreva, 2021). Epigenetic modifications, such as chromatin regulation, DNA methylation, and

histone modifications, reinforce lineage specific programs rather than facilitating pluripotent induction during reprogramming, therefore acting as roadblocks to efficient reprogramming (Armstrong, 2012; Hochedlinger and Jaenisch, 2015; Rasmussen and Helin, 2016). For instance, the histone modification like Histone H3 lysine 9 (H3K9) methylation acts as a barrier during mouse pluripotent reprogramming and SCNT (Chen et al., 2013; Matoba et al., 2014). Another hallmark repressive mark, H3K27 trimethylation (H3K27me3), is tightly associated with transcription repression. Studies imply that the process of establishing pluripotency requires both the silencing of the somatic program through PRC2 (Polycomb repressive complex 2) mediated H3K27me3 deposition (Schuettengruber et al., 2017) and the UTX1 (Ubiquitously transcribed tetratricopeptide repeat) mediated H3K27me3 removal (Fragola et al., 2013; Mansour et al., 2012). Additionally, the elimination of the H3K36me2/3 marks at certain genomic loci was shown to be essential for advancing reprogramming (Vidal et al., 2014), Vitamin C has also been found to decrease the levels of H3K36me2/3 during reprogramming through the activation of downstream vitamin C-dependent H3K36 demethylases, Jhdm1a (Kdm2a) and Jhdm1b (Kdm2b) (Wang et al., 2011). Furthermore, inhibiting DOT1L, a histone methyltransferase targeting H3K79, boosts the efficiency of reprogramming mouse and human somatic cells (Onder et al., 2012).

Reprogramming is likely primarily an epigenetic process, with chromatin modifiers playing essential roles in epigenome remodeling (Buganim et al., 2013). Fidalgoa et al. found that *Zfp281* recruits the NuRD complex to Nanog, suppressing its activation and inhibiting iPSC formation, highlighting NuRD's inhibitory role in pluripotency (Fidalgo et al., 2012). Notably, the chromatin assembly factor complex CAF-1 was identified as a potent roadblock of fibroblasts to iPSCs (Cheloufi et al., 2015). In the context of SCNT, CAF-1 suppression was shown to resist reprogramming through opening of H3K9me3 marked heterochromatin domains (Ishiuchi et al., 2015). In the context of direct reprogramming, suppression of CAF-1 ortholog, the histone chaperone *lin-53*, leads to the direct reprogramming of germ cells to neurons in *C. elegans* (Tursun et al., 2011). Similarly, suppression of other histone chaperones, FACT (Facilitates Chromatin Transcription), has been shown to enhance transdifferentiation processes in various contexts. Specifically, it improves germ cell to neuron and intestine to neuron transdifferentiation in *C. elegans*, as well

as reprogramming human fibroblasts into iPSCs and fibroblast to neuron transdifferentiation (Kolundzic et al., 2018). Recently, the role of the chromodomain-containing chromatin regulator MRG-1 in preventing the conversion of germ cells to neurons was described in *C. elegans*, highlighting the importance of epigenetic regulation in safeguarding cell fate (Hajduskova et al., 2019).

Non-coding RNAs have been considered as new players in the regulation of direct reprogramming (Wang et al., 2021). MicroRNAs regulate gene expression at the post-transcriptional level. Additionally, certain cellular signaling pathways can function as barriers to reprogramming. While p53 plays a key role in apoptosis (Vousden, 2000), several studies have demonstrated that the p53-p21 pathway inhibits reprogramming of somatic cells in both humans and mice (Banito et al., 2009; Brosh et al., 2013, p. 2009; Hong et al., 2009; Marión et al., 2009; Rasmussen et al., 2014; Samavarchi-Tehrani et al., 2010). Similarly, the Wnt/β-catenin signaling pathway plays distinct roles at various stages of both direct and cell fusion mediated mouse reprogramming. Temporal modulation of the Wnt/β-catenin pathway can considerably enhance reprogramming efficiency (Ho et al., 2013; Lluis et al., 2008; Zhang et al., 2014).

Furthermore, the post-translational modification sumoylation has been shown to play a role in regulating somatic cell identity. The depletion of SUMO2 led to an increase and acceleration in the reprogramming process during iPSC generation (Borkent et al., 2016; Cheloufi et al., 2015). Similar to sumoylation, another study used a short hairpin RNA (shRNA) screen to show that silencing of a UPS factor, E3 Ligase *FBXW7* (F-box and WD repeat domain-containing 7), which is involved in ubiquitination, enhances pluripotent reprogramming of mouse embryonic fibroblasts (MEFs) (Buckley et al., 2012). Based on a shRNAs knockdown screen, Qin et al identified other genes that are involved in novel pathways like endocytosis, motility, and adhesion (Qin et al., 2014).

However, considerable gaps remain in our understanding of how distinct biological processes contribute to the safeguarding of cell fate, as well as the mechanisms that enable fate reprogramming when these processes are disrupted. Revealing the molecular strategies by which cells maintain their identity will be essential for advancing the field. In the following section, this study will discuss the advantages of using *C. elegans* as a model organism to uncover unexpected and evolutionarily conserved barriers to reprogramming.

1.2 *C. elegans* as a model organism to study cellular reprogramming

C. elegans is a tiny, non-parasitic nematode ranging from approximately 0.25 millimeters to 1 millimeter long from newly hatched larvae to adulthood. It can be easily found from rotting vegetable matter, where bacterial food sources are abundant (Barrière and Félix, 2006). In 1963, Nobel Laureate Sydney Brenner introduced *C. elegans* as a model to study development and neurobiology (Brenner, 1974). Since then, *C. elegans* has been used as a genetic model organism for biological research across numerous fields, including aging, genomics, cell biology, and neuroscience (Kaletta and Hengartner, 2006; Riddle et al., 1997).

There are several distinct advantages that make *C. elegans* a useful experimental system to study these processes. It is inexpensive to cultivate and can be easily cultured in the laboratory using a diet of the bacterium *Escherichia coli*. *C.elegans* is a self-fertilizing hermaphrodite and has a rapid life cycle of approximately 3 days under optimal conditions. Although males arise at a frequency of <0.2 %, this sexual dimorphism makes them ideal for genetic studies and manipulation: self-fertilizing hermaphrodites can maintain homozygous lines, while males are available for genetic crosses (Corsi, 2006). Their transparent body allows the visualization of individual cells and subcellular components using Nomarski imaging (Differential Interference Contrast, DIC). This transparency also enables the study of developmental processes, screening for mutants affecting cell development and function, isolating cells, and analyzing protein interactions *in vivo* by using fluorescent proteins to tag subcellular compartments or proteins of interest (Boulin et al., 2006; Chalfie et al., 1994; Corsi et al., 2015).

The first genetic studies on *C. elegans* were published in 1974 (Brenner, 1974), revealing several hundred mutants induced by ethyl methanesulfonate (EMS) that impacted behavior and morphology and represented about 100 genes. Six linkage groups were identified, resulting in the creation of a genetic map (Sulston et al., 1983; Sulston and Horvitz, 1977). *C. elegans* has a fixed number of 558 larval and 959 adult somatic cells, which form tissues such as the hypodermis, excretory system, neurons, muscle, intestine, and gonad (J. Kimble, D et al., 1981). Owing to this invariant number of somatic cells, researchers have been able to trace the fate of every cell from fertilization to adulthood in live animals and to generate a complete cell lineage (Kimble and Hirsh, 1979; Sulston et al., 1983; Sulston and Horvitz, 1977).

Furthermore, the morphology of each cell has been reconstructed from electron micrographs, including all the 302 neurons that the adult hermaphrodite possesses (White et al., 1986).

The life cycle of *C. elegans* consists of the embryonic stage, four larval stages (L1-L4), and adulthood. After fertilization, the embryos remain inside the hermaphrodite until they reach approximately the 24-cell stage before being laid. A nearly impermeable eggshell forms, enabling the embryo to develop independently of the mother before hatching into the first larval stage (L1). This marks the first developmental checkpoint for the worm. In case the L1 larva hatches into adverse conditions such as starvation or overcrowding, it does not develop further and molts into the *dauer* stage (Baugh, 2013). In this state, which is characterized by an arrest in feeding and locomotion, the animal can survive for several months (Golden and Riddle, 1984). Otherwise, it progresses sequentially through the L2, L3, and L4 stages before finally reaching adulthood. Each stage ends with a sleep-like period of inactivity called lethargus (Raizen et al., 2008), during which a new cuticle is synthesized underneath the older one, and the old cuticle is shed.

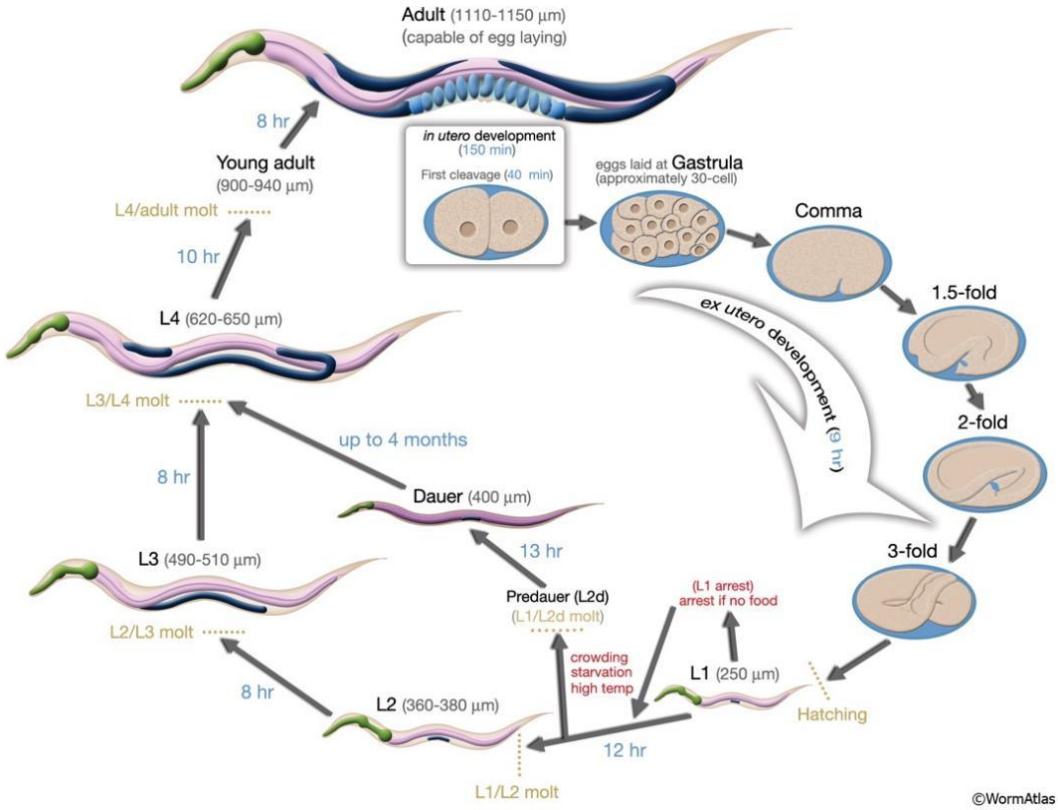

Figure 1.4 The life cycle of *C. elegans*. The life cycle of a hermaphrodite *C. elegans* at 22 °C. Within 3 days, a worm passes through four larval stages and reaches adulthood. The dauer

larvae are skinnier than all the other larval stages. The length of the animal at each stage is marked next to the stage name in micrometers (μm). (Reprinted from WormAtlas).

C. elegans was the first multicellular organism to have its complete genome sequenced (*C. elegans* Sequencing Consortium 1998). The worm genome provided the template for other genome sequencing projects, including the Human Genome Project, completed in 2002. Its tractability as a genetic system has made it a powerful model to study forward and reverse genetics. Forward genetic screens rely on genome-wide mutagenesis in which unknown genes controlling a biological process are sought, whereas reverse genetics relies on target-selected knockdowns by RNAi (Kutscher and Shaham, 2014). Since the complete genome sequence of *C. elegans* has been available for over 20 years, researchers have developed numerous novel experimental strategies that leverage this prior genetic information (Meneely et al., 2019).

Remarkably, approximately 60% of the genes in *C. elegans* have homologs in the human genome (Sonnhammer and Durbin, 1997). Furthermore, key molecular pathways involved in human diseases, such as Notch, Wnt, and Insulin signaling, are highly conserved in *C. elegans* (Baumeister and Ge, 2002). These features make it an excellent model for studying epigenetics, aging, and cellular reprogramming.

Studies in *C. elegans* have demonstrated that ectopic expression of various cell fate-inducing TFs can activate gene expression patterns indicative of a shift toward the target cell type during direct reprogramming (Rothman and Jarriault, 2019). One of the earliest investigations in *C. elegans* revealed that ectopic expression of the homeodomain (HD) TF UNC-30 could induce the expression of genes specific to GABAergic motor neurons. It was shown that upon the ectopic expression of the TF, somatic cells displayed GABAergic neuronal characteristics (Jin et al., 1994). Following the discovery of MyoD, Krause and Weintraub found that overexpression of exogenous HLH-1 in *C. elegans* embryos led most of its cells to adopt muscle characteristics (Fukushige and Krause, 2005). Several similar studies have demonstrated the forced ectopic expression of a single TF is sufficient for *C. elegans* to reprogram blastomeres into all three germ layers: END-1 (endoderm) (Zhu et al., 1998), ELT-2 (intestine) (Fukushige et al., 1998), PHA-4 (pharyngeal) (Kiefer et al., 2007), LIN-26 (epithelial) (Quintin et al., 2001), ELT-1 or ELT-3 (epidermis) (Gilleard and McGhee, 2001) all of which can all induce cell fate changes.

Interestingly, the reprogramming capacity of these TFs is limited to a specific early developmental window. After this period, their efficiency sharply declines in the later developmental stages and becomes nearly ineffective in larvae (Kiefer et al., 2007)(Gilleard and McGhee, 2001). However, ectopic expression of the GATA TF ELT-7 can reprogram fully differentiated pharyngeal cells into intestinal cells, even after mid-embryogenesis (Riddle et al., 2013).

These findings underscore the decline in cellular plasticity as cells become fully differentiated. Yuzyuk et al. demonstrated that the Polycomb group complex 2 (PRC2) protein MES-2/E(z) plays a key role in this loss of plasticity. During embryonic development, PRC2 reorganizes chromatin structure to restrict cellular plasticity over time. Additionally, the ubiquitous expression of TF HLH-1 did not increase reprogramming efficiency in *pha-4* and *end-1* mutants, suggesting that the loss of plasticity is independent of cell fate specification (Yuzyuk et al., 2009).

Studies carried out another TF-induced reprogramming system established in *C. elegans* by Tursun et al.: Using a gustatory glutamatergic ASE neuron-specifying terminal selector TF CHE-1 (Etchberger et al., 2007; Tursun et al., 2011; Uchida et al., 2003), they generated a transgenic worm strain that contained a heat shock inducible TF CHE-1 overexpression (CHE-1^{oe}) in combination with the ASE neuronal fate reporter *gcy-5^{prom}::GFP* (Figure 1.5) (Patel et al., 2012; Tursun et al., 2011; Yu et al., 1997).

Broad overexpression of CHE-1 in early gastrula-stage embryos leads to a broad activation of the ASE neuronal fate, as indicated by *gcy-5^{prom}::GFP* expression, and causes developmental arrest accompanied by morphological deformities. In contrast, during later developmental stages, the initiation of the fate reporter upon CHE-1^{oe} becomes restricted and eventually at the L4 and adult stages, once all tissues have differentiated, the only cells expressing *gcy-5^{prom}::GFP* are a small number of anterior neurons, including RIS, CEP, ASK, and ASI neurons (Patel and Hobert, 2017; Tursun et al., 2011). This suggests that these mature neurons provide specific molecular contexts that enable TF-mediated reprogramming. However, it remains unclear why these particular neurons respond to TF CHE-1^{oe} since they do not bear any obvious relationship to ASE (Patel and Hobert, 2017).

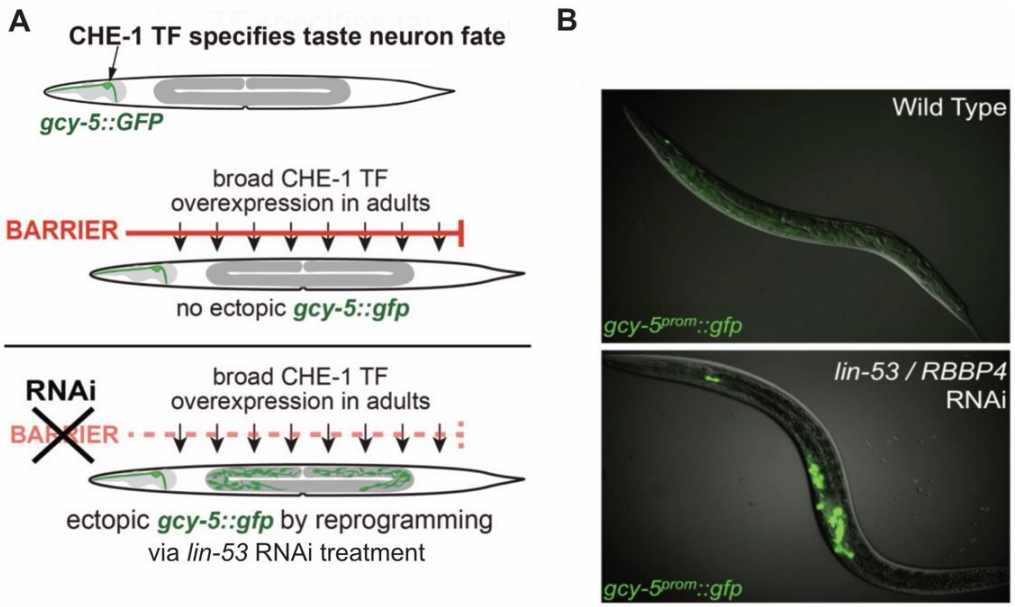

Figure 1.5 *C. elegans* as a transgenic model for studying reprogramming. A) Schematic representation of animals that express *gcy-5^{prom}::GFP* reporter for ASE neuron fate induced by zinc-finger TF CHE-1. Ubiquitous misexpression of CHE-1 in animals does not typically induce ectopic *gcy-5^{prom}::GFP* expression except in a few head neurons. But when a barrier such as *lin-53* is disrupted by RNAi, germ cells exhibit induction of *gcy-5^{prom}::GFP* marker. **B)** Representative microscopy images showing the wild-type state of this transgenic system and the ectopic induction of the reporter *gcy-5^{prom}::GFP* following *lin-53* knockdown by RNAi.

To identify genes whose knockdown enabled the TF CHE-1 induced conversion to ASE-like neuronal cells, a small-scale RNAi screen was carried out by using this CHE-1^{oe} system. This screen identified the conserved histone chaperone LIN-53 (human RBBP7 and RBBP8) as a barrier for germ-cell to neuron conversion (Tursun et al., 2011) (Figure 1.5). It was later shown that the effect of *lin-53* could be phenocopied by removal of the PRC2 complex (*mes2*, *mes-3,* and *mes-6*), indicating that Polycomb-mediated silencing acts as a barrier to reprogramming (Patel et al., 2012). Subsequent research further revealed that such reprogramming is hindered by the GLP1/Notch signaling pathway (Seelk et al., 2016).

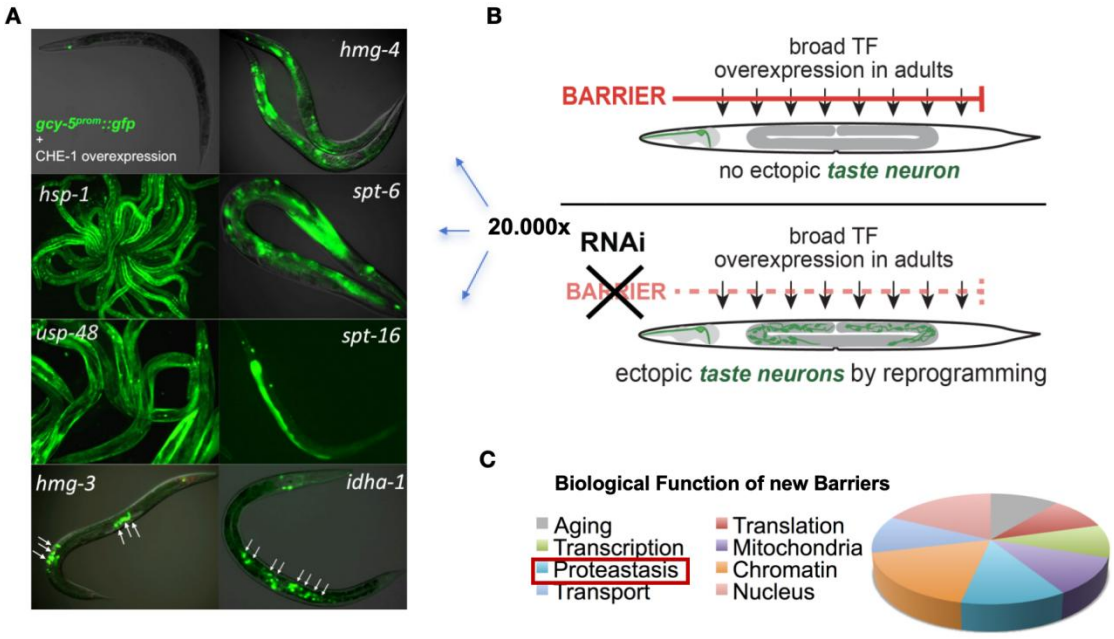

Figure 1.6 Whole genome RNAi screen to identify Reprogramming Barriers. A) Representative images of control animal and ectopic *gcy-5^{prom}::GFP* induction in different tissues from the whole genome RNAi screen. **B)** Schematic representation: The whole genome RNAi screen based on the transgenic system that combines TF CHE-1 with the ASE neuron marker *gcy-5^{prom}::GFP*.**C)** Pie-chart representing 160 genes that act as barriers of direct reprogramming are involved in a wide range of biological functions.

Moreover, 160 new barriers were identified by using this transgenic system in our lab (Figure 1.6 B, C). Among them, our former lab member Ena Kolundžić identified the chromatin regulator FACT as a barrier to reprogramming that inhibits the conversion of intestinal and germ cells into ASE neuron-like cells in *C. elegans* (Figure 1.6 A), and also restricts the reprogramming of human fibroblasts into iPSCs (Kolundzic et al., 2018). Additionally, RNAi-mediated knockdown of *mrg-1* facilitates the conversion of germ cells into neurons that express endogenous pan-neuronal and ASE neuronal markers (Hajduskova et al., 2019).

These findings demonstrate that the histone modifiers and chromatin regulators play crucial roles in preventing cell fate transitions. The fact that reprogramming barriers identified in *C. elegans* are also conserved in mammals highlights the potential of using *C. elegans* as a model organism to identify additional barrier factors and to understand the context of cell fate protection. In this project, we validated newly identified barriers involved in proteostasis from the whole RNAi genome screen (Figure 1.6 C) and investigated their roles by using this transgenic model.

1.3 Proteostasis and Reprogramming

1.3.1 Proteostasis dynamics during development, cell differentiation, and pluripotency

Proteins are involved in almost every biological process. Maintaining a balanced proteome, referred to as protein homeostasis or proteostasis, relies on the proteostasis network (PN). This network regulates the interacting and competing biological pathways for protein balance and proper function. It encompasses protein synthesis, folding, transport, and degradation, all of which ensure that proteins exist in their correct conformations and locations within each cell (Balch et al., 2008; Hipp et al., 2014) (Figure 1.7).

The main players in PN are the chaperones, the UPS, and the lysosome-autophagy systems (Kaushik and Cuervo, 2015). After translation, proteins are synthesized on ribosomes as linear amino acid chains, then folded by molecular chaperones and co-chaperones into unique three-dimensional structures, trafficked in the cytosol to the proper cellular locations, and perform their biological functions (Balchin et al., 2016; Sala et al., 2017) (Figure 1.7). Misfolded, damaged, or aggregated proteins are degraded by the UPS or autophagy pathway (Finley, 2009; Yamano et al., 2016). This complex process is essential for the maintenance of PN components, such as ribosomes, proteasomes, and lysosomes.

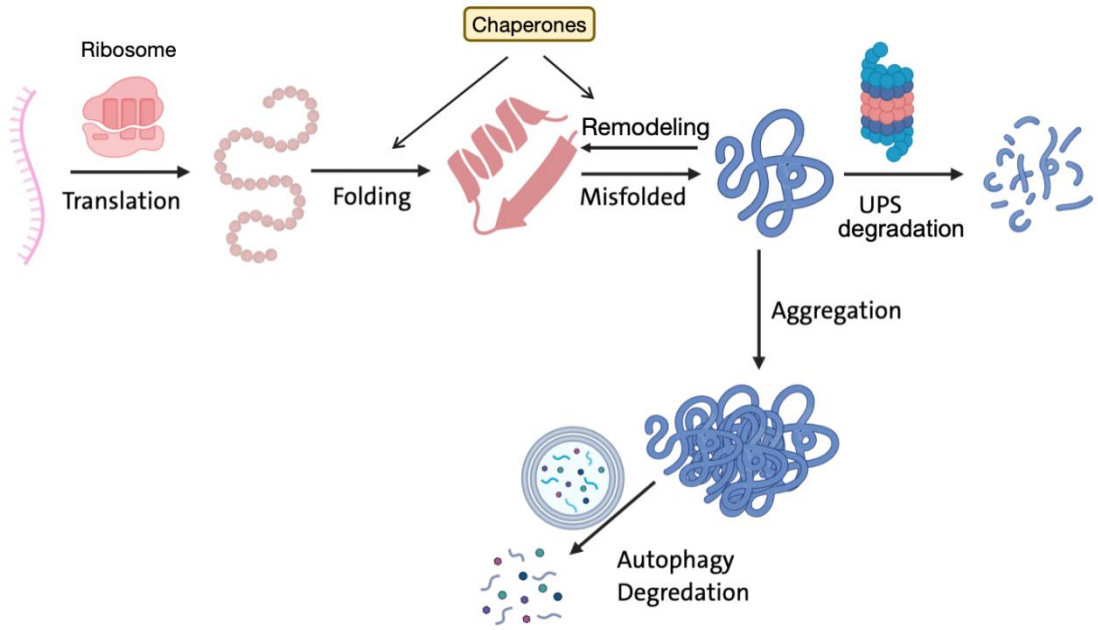

Figure 1.7 Overview of proteostasis network. The scheme illustrates protein synthesis at the ribosome, and molecular chaperones facilitate native protein folding during translation.

Both cytosolic and compartment-specific chaperones are essential for protein quality control, as they support proper folding and prevent unwanted aggregation. If proteins are terminally misfolded or aggregated, proteolysis by the ubiquitin-proteasome system and autophagy for degradation.

During development, cell differentiation triggers a drastic change in the proteome and regulatory systems rapidly detect and rectify disruptions to maintain baseline homeostasis and ensure successful organismal development (Lee et al., 2017; Vilchez et al., 2014). However, metabolic, environmental, and pathological conditions challenge the proteostasis balance, leading to the development of proteotoxicity (Morimoto and Cuervo, 2014). Particularly with age, the ability of various cells and organs to maintain proteostasis under resting and stressful conditions is gradually compromised (Labbadia and Morimoto, 2015; Vabulas et al., 2010). The loss of proteostasis is linked with multiple age-associated disorders, including Alzheimer's, Huntington's, or Parkinson's disease, and cancer (Cohen and Dillin, 2008). Conversely, many studies have shown that maintaining or enhancing the PN into advanced age contributes to extending healthspan and delaying the onset of age-associated diseases (Taylor and Dillin, 2011; Vilchez et al., 2014).

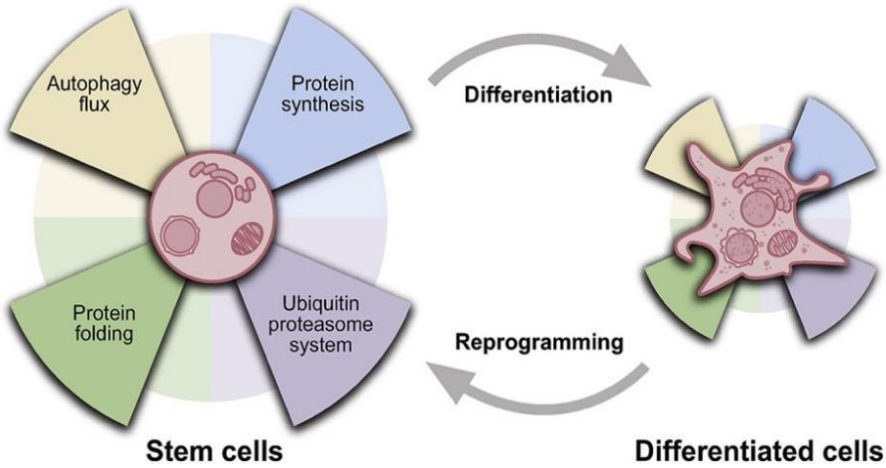

Figure 1.8 Pluripotent stem cells exhibit a powerful proteostasis machinery. Schematic illustration of the proteostasis components that are upregulated in pluripotent stem cells compared with their differentiated counterparts (Reprinted from Llamas et al., 2020).

Growing evidence indicates that proteostasis regulatory mechanisms play a central role in ESC/iPSC self-renewal, pluripotency, and cell fate decisions (Aguilo et al., 2015; Ye and Blelloch, 2014; You et al., 2015). Stem cells are thought to possess a greater capacity of proteostasis compared to differentiated cells (Blanco et al., 2016; Llorens-Bobadilla et al., 2015; Signer et al., 2014) (Figure 1.8). Stem cells must

consistently replenish their population through asymmetric cell division (Knoblich, 2008). Simultaneously, they need to reshape their proteomes as they differentiate into various cell fates, while they can maintain a damage free proteome through proteostasis factors control and PN rewiring during development (Jayaraj et al., 2020; Vilchez et al., 2014).

Thus, a defect of proteostasis could result in impairment of ESC pluripotency and immortality. For instance, ESCs exhibit a higher translational rate that contributes to their increased proliferative activity (García-Prat et al., 2017). Additionally, iPSCs and human ESCs (hESCs) both exhibit higher levels of the chaperonin TRiC/CCT, which decrease as cells differentiate into neuronal progenitors and neurons (Noormohammadi et al., 2016). Similarly, mouse ESCs have an increased level of stress-inducible cytosolic HSP70 (HSPA1), which is another family of chaperones that are required for pluripotency maintenance (Saretzki et al., 2004). Many studies support the finding that levels of chaperones are higher in stem cells than in differentiated cells, suggesting that stem cells have an enhanced ability to ensure the correct folding of proteins (Baharvand et al., 2008; Battersby et al., 2007).

Studies in ESCs and iPSCs have also shown enhanced protein degradation activity, which decreases during differentiation into different lineages. iPSCs and hESCs exhibit high proteasome activity induced by 19S proteasome subunit PSMD11/RPN-6 (Buckley et al., 2012; Vilchez et al., 2012), which promotes weak interaction between the 20S core and the 19S cap to ensure its activity (Pathare et al., 2012; Vilchez et al., 2012). Autophagy, another member of the protein degradation system, also exhibits high levels of activity during early differentiation of hESCs (Tra et al., 2011).

The PN is highly interconnected and interactive. The boosting chaperon activities enhance proteostasis capacity (Jayaraj et al., 2020). Stress responses to protein misfolding often induce translational attenuation (Das et al., 2015). Furthermore, the protein degradation system is considered a determinant of stem cell function (Vilchez et al., 2014). Further details, particularly regarding the UPS, will be discussed in the subsequent chapter.

1.3.2 Ubiquitination by the ubiquitin proteasome system in pluripotency and reprogramming

Ubiquitin was first discovered as a post-translational modification that earmarks proteins for degradation (Ciechanover, 2015). In the early 1980s, Nobel laureates Aaron Ciechanover, Avram Hershko, and Irwin Rose identified the UPS as the cellular machinery responsible for protein degradation and the regulation of cellular homeostasis (Hershko and Ciechanover, 1998). During the process of protein folding, many challenges and disruptions can occur, such as gene mutations, errors in protein translation, oxidative damage, and toxic environmental conditions (Bieschke et al., 2006; Hartl, 2017; Jacobson et al., 2012; Kerem et al., 1990; Lee et al., 2006; Liu et al., 2008). The degradation of misfolded, unassembled, or damaged proteins and control of protein stoichiometries are mainly performed by the UPS (Ciechanover et al., 2000; Shemorry et al., 2013), which consists of several hundred components and is crucial for the balance of proteostasis.

From yeast to humans, ubiquitination processes the enzymatic machinery that covalently attaches ubiquitin to substrate proteins (Pickart and Fushman, 2004; Trempe, 2011). It requires a three enzymatic cascade (Figure1.9. A) (1) E1 ubiquitin-activating enzyme activates ubiquitin in an ATP-dependent manner; (2) activated ubiquitin transfer of cysteine residue from E2 ubiquitin-conjugating enzyme; (3) next, E3 ubiquitin ligase recruits the target protein and mediates the ubiquitin transferred from the ubiquitin-E2 conjugate to a lysine residue on the substrate protein, either directly via a RING E3 ligase or indirectly via a HECT/RBR E3 ligase, which first receives ubiquitin before attaching it to the substrate (Damgaard, 2021; Nandi et al., 2006). Additionally, deubiquitinating enzymes can reverse the reaction by removing or editing ubiquitin modifications (Olguín, 2022). The next step is the recognition of ubiquitin-labeled protein by the 26S proteasome, which also releases the ubiquitin monomers. The protein substrate is then unfolded and translocated into the inner proteolytic cavity of the 20S proteasome for degradation (Zubarev et al., 2022). The E2 enzyme exhibits high selectivity for its E3 binding partner, while the E3 ligase demonstrates considerable substrate specificity. Although the 26S proteasome primarily recognizes polyubiquitin chains as targets, distinct E3 ligases identify substrates based on specific degradation signals, thereby contributing to the overall selectivity and specificity of the UPS (Ciechanover and Iwai, 2004; Pickart, 2001; Saretzki et al., 2004; Weissman, 2001).

The UPS facilitates intracellular protein degradation through ubiquitin-mediated proteolysis; however, ubiquitination involves more than just proteolysis. It also plays a key role in regulating the levels and function of many proteins and signaling pathways that are involved in determining cell fate. Ubiquitination is classified based on the number of ubiquitin molecules attached to a single lysine residue in a protein: monoubiquitination (single ubiquitin) and polyubiquitination (a chain of ubiquitin molecules) (Sewduth et al., 2020). These different types of ubiquitin chains act as 'ubiquitin code' (Fig. 1.9 B); different ubiquitin-protein structures ensure the specificity of protein–protein interactions and target proteins to different pathways and fates. For example, K48-linked polyubiquitination typically targets proteins for degradation by the proteasome (Jin et al., 2008). In contrast, monoubiquitination typically induces a conformational change within the target protein and does not function as a signal for proteasomal degradation. Instead, it is primarily involved in the regulation of protein activity and the mediation of protein-protein interactions (Nakagawa and Nakayama, 2015). For instance, the attachment of a monoubiquitin moiety to histones serves as an epigenetic modification that influences chromatin structure and modulates gene transcription (Fig. 1.9 C) (Fuchs et al., 2012; Groothuis et al., 2006).

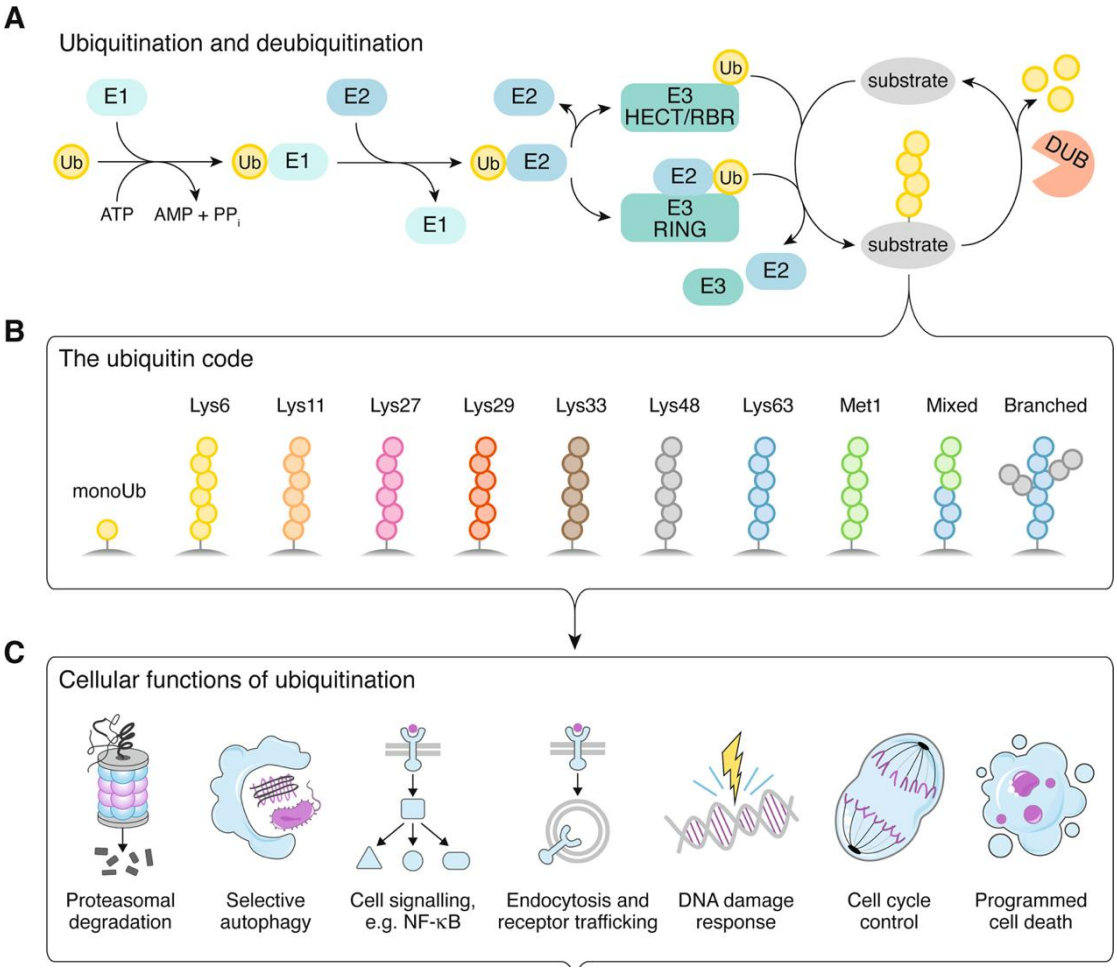

Figure 1.9 Ubiquitination signaling. Schematic illustration shows **A)** Ubiquitination and deubiquitination reactions. **B)** Eight types of homotypic polyubiquitin chains and a broad range of heterotypic, mixed, and branched polyubiquitin chains, collectively called the 'ubiquitin code'. **C)** Examples of cellular functions regulated by ubiquitination. (Reprinted from Damgaard, 2021)

In the last decade, growing evidence has shown that the UPS plays a crucial role in regulating the pluripotency and differentiation of stem cells by promoting the degradation of differentiation-related proteins and maintaining the homeostasis of proteins associated with pluripotency (Buckley et al., 2012; Hernebring et al., 2013; Noormohammadi et al., 2018; Okita and Nakayama, 2012; Selenina et al., 2017; Vilchez et al., 2012). Monoubiquitylation of histones by E3 ligases like RING1, BMI1, RNF20, and Dzip3 plays a crucial role in chromatin architecture and cell fate determination, while deubiquitylases act as key regulators of pluripotency and early development (Endoh et al., 2012; Fuchs et al., 2012; Gu et al., 2016; Inoue et al., 2015; Pengelly et al., 2015; Scheuermann et al., 2010; Yang et al., 2014). In stem cells,

ubiquitin-dependent proteolysis is widely used to regulate the levels of TFs essential for maintaining pluripotency or initiating differentiation (Werner et al., 2017).

During cell differentiation, stem cells must transition from self-renewal to terminal specialization, primarily through the degradation of pluripotency factors (such as OCT4, NANOG, or SOX2) and differentiation inhibitors (such as such as the REST or ID family of transcriptional regulators) (Bahnassawy et al., 2015; Fang et al., 2014; Li et al., 2015; Liao and Jin, 2010), and it is accomplished by the simultaneous production of proteins necessary for the specific functions of the new cell type.

The UPS contributes to ESC function and iPSCs reprogramming by precisely regulating the levels of key TFs, as demonstrated by the shift observed in the balance between pluripotency and differentiation upon interference with the N-Myc-targeting E3 ubiquitin ligase, or following treatment with proteasome inhibitors (Lee et al., 2017; Zhao et al., 2008).

1.3.3 UPS in epigenetics

The UPS, like previously mentioned, controls almost every cellular process, including epigenetics. For instance, under genotoxic stress conditions, the proteasomal deubiquitinase Doa1 directs ubiquitin released from protein degradation toward chromatin to facilitate DNA repair processes (Lis and Romesberg, 2006). In the context of epigenetic modification, the UPS has been demonstrated to perform both proteolytic and non-proteolytic functions (Roy and Ghosh, 2025).

1.3.3.1 In the proteolytic pathway

Several studies have revealed that histone proteins are subject to degradation by the proteasome, although the mechanisms underlying this process remain incompletely understood (Chen and Qiu, 2012). Previously believed to be resistant to degradation, recent evidence indicates that histones exist in a dynamic equilibrium essential for maintaining genomic stability. This concept is reinforced by observations that excess histones can impair transcription and hinder DNA damage repair processes (Singh et al., 2009). Studies conducted both *in vitro* and *in vivo*, particularly in budding yeast, have elucidated mechanisms by which surplus histones disrupt various critical cellular functions (Glowczewski et al., 2000). For example, phosphorylation of histone H3 at Y99 by the DNA damage checkpoint kinase Rad53

is a pivotal step that facilitates ubiquitination and subsequent proteasomal degradation, involving the E2 enzymes Ubc4/5 and the E3 ligase Tom1, though its role in histone degradation remained unclear (Singh et al., 2009). Additionally, RING domain E3 ligases such as Pep5, Snt2, Hel1, and Hel2 have been identified as necessary mediators for histone removal (Singh et al., 2012). In mammalian cells, the E3 ligase complex HUWE1/LASU1 (ortholog of yeast Tom1) has been implicated in histone ubiquitination, though its specific role in degradation requires further clarification (Liu et al., 2007). Histones such as H4, H2B, and H2A.Z are also targeted for degradation to facilitate transcriptional activation and occasionally require 'priming' modifications (Qian et al., 2013; Shmueli et al., 2022).

Besides degradation of excess histone, histone modification enzymes are selectively degraded by ubiquitin-mediated proteolysis to maintain appropriate levels for chromatin regulation. For instance, it highlights that the proteasome degrades key regulators such as histone acetyltransferases (HATs) like CBP (Chen and Li, 2011; Jin et al., 2004; St-Germain et al., 2008) and p300 (Chen et al., 2007), and histone deacetylases (HDACs) (Romani et al., 2016), all of which modulate histone acetylation status and gene activity. The ubiquitin-mediated proteolysis also degrades transcriptional silencing histone mono and dimethyl transferases like G9a and GLPs (Takahashi et al., 2012), and histone demethylases (HDMs) associated with heterochromatin like JARD1C, impacting gene silencing and activation processes (Mersman et al., 2009). Interestingly, the ubiquitin-mediated proteolysis simultaneously degrades both transcription promoting and silencing modifiers, suggesting that cellular context and signaling pathways determine the outcomes in gene regulation (Bach and Hegde, 2016).

1.3.3.2 In the non-proteolytic pathway

The first protein identified as being ubiquitylated was histone H2A (Goldknopf et al., 1975; Goldknopf and Busch, 1977; Hunt and Dayhoff, 1977). Later studies in *D. melanogaster* (Levinger and Varshavsky, 1982), Tetrahymena H2A (Davie et al., 1991; Nickel et al., 1989), and mammalian cells (Huang et al., 1986) revealed that the ubiquitylated forms of histones H2A and H2B are specifically linked to actively transcribed genes.

Pavri et al. demonstrated that elongation efficiency of the transcriptional machinery is affected by factors such as FACT, PAF (elongation regulator complex polymerase associated factor), and H2Bub1(histone H2B is prominently monoubiquitinated at K120). FACT recruits the ubiquitination complex RNF20/RNF40, leading to H2B monoubiquitination (H2Bub1), which promotes displacement of H2A-H2B dimers and facilitates transcription (Pavri et al., 2006). Additionally, H2Bub1 influences epigenetic crosstalk involving histone methylation (e.g., H3K4 and H3K79) (Ezhkova and Tansey, 2004) and histone H2A monoubiquitination at K119 (H2Aub1), resulting in gene repression through H3K27 trimethylation (Cooper et al., 2016). Ubiquitination also mediates non-proteolytic functions, such as activating or repressing TFs and coactivators (e.g., TIF1γ, SRC-3) (Wu et al., 2007). Overall, histone ubiquitination is a versatile mechanism that controls gene expression through various pathways, sometimes independently of protein degradation.

1.4 Aim of the study

Direct reprogramming holds immense therapeutic potential for regenerative medicine; however, its efficiency is restricted by the inhibitory safeguarding mechanisms. Investigating these reprogramming barriers *in vivo* is not only for unlocking the clinical potential of cellular reprogramming but also for providing valuable insights into cell fate determination. A whole genome RNAi screen in *C. elegans* identified proteostasis factors as previously unrecognized barriers to TF-induced direct conversion. In this project, I aim to identify and characterize these factors that act as cellular safeguards.

The decline of proteostasis is widely regarded as a hallmark of cellular senescence and age-related diseases, and it is also involved in almost every biological process, including transcription activity. This project specifically focuses on the E3 ubiquitin ligase HECD-1, whose depletion permits the TF-induced reprogramming of germ cells into ASE neuron-like cells. One part of this work involves assessing the extent to which the germ cells are converted to neurons, as well as exploring the range of alternative cell types into which these germ cells can be reprogrammed. The other component focuses on investigating the mechanisms behind HECD-1 depletion mediated reprogramming. Given that E3 ligases strictly regulate protein degradation pathways, an RNAi suppressor screen targeting the pool of upregulated proteins following HECD-1 dysfunction was performed to identify the core downstream effectors actively driving the reprogramming process. Ultimately, this study seeks to define the role of proteostasis regulating pathways during germ cell fate protection and TF-induced reprogramming of germ cells.

2. Results

2.1 Knockdown of ubiquitin proteasome system factors allows ASE fate marker expression in the germ cells

To identify factors that safeguard cell identity and serve as barriers to reprogramming, a whole-genome RNAi screen was previously conducted in our laboratory. This was achieved by feeding *C. elegans* bacteria from the Ahringer RNAi library (SourceBioscience) with a *C. elegans* strain that carried a transgenic system comprising a heat shock inducible TF CHE-1 in combination with the ASE neuronal fate marker *gcy-5^{prom}::GFP* (Tursun et al., 2011) (see Figure 2.1.1.A). The animals were screened at the L4 stage of F1 progeny for ectopic expression of the ASE fate marker *gcy-5^{prom}::GFP* after broad CHE-1^{oe}. The whole genome screen identified 171 genes that showed ectopic *gcy-5^{prom}::GFP* induction in different tissues. These genes are involved in a variety of biological processes such as proteostasis factors, mitochondrial function, and nuclear factors (Kolundzic et al., 2018). Over the past decade, proteostasis has been demonstrated to play a crucial role in maintaining cellular pluripotency (Noormohammadi et al., 2018). Therefore, this study focused on these candidate genes within the context of germ cell direct reprogramming into ASE neuron-like cells.

First, seven candidate genes identified from the whole-genome analysis were subjected to further validation, which are *hecd-1, eel-1, math-33, usp-39, marc-4, spg-7,* and *plc-3*. Following RNAi-mediated knockdown of these candidates, all of them showed *gcy-5^{prom}::GFP* induction in the germline upon CHE-1^{oe}, which is similar to the previously described germ cell to neuron reprogramming upon depletion of *lin-53*. The penetrance of the phenotype for each candidate was lower than that of *lin-53* RNAi; however, six candidates exhibited a statistically significant increase compared to the negative control, except *plc-3* (Figure 2.1.1 B, C).

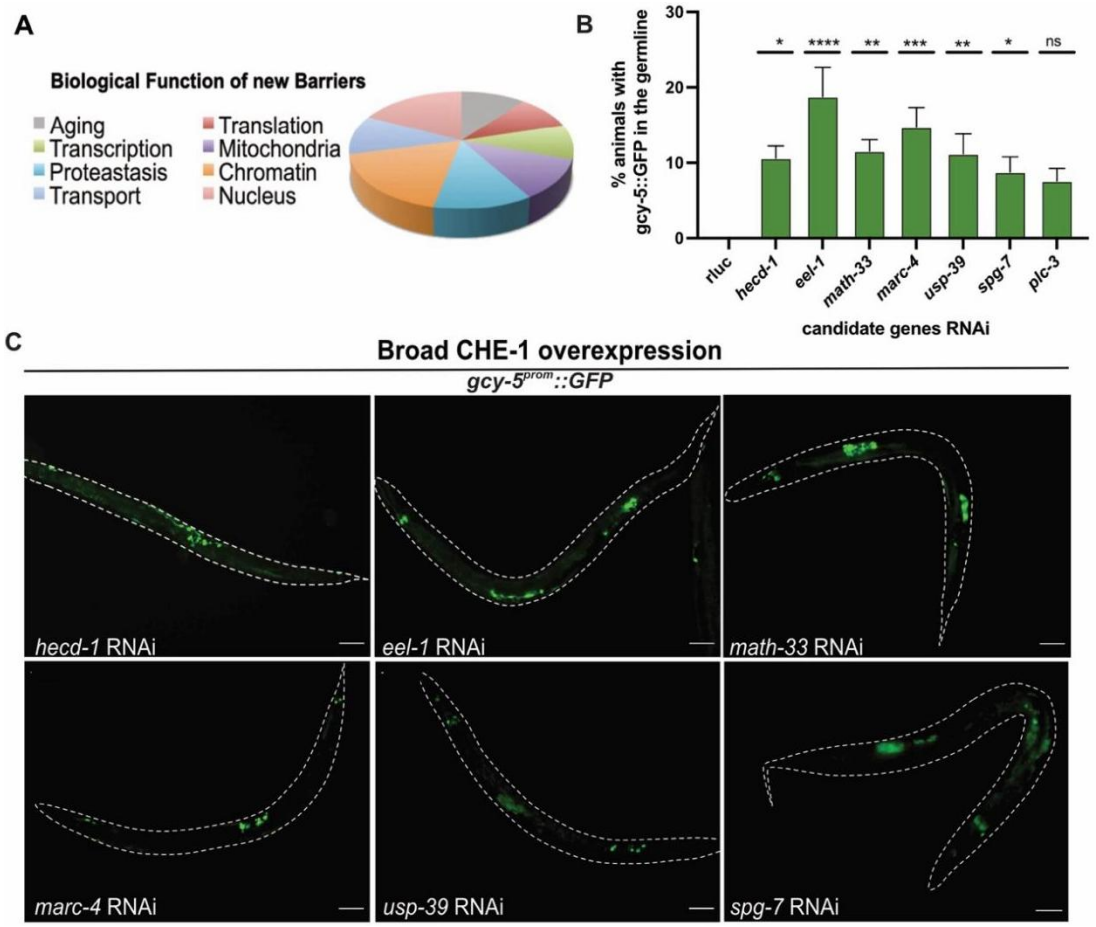

Figure 2.1.1 Depletion of proteostasis factors allow TF induced ASE fate marker expression in the germ line. **A)** Pie-chart representing 160 genes that act as barriers of direct reprogramming are involved in a wide range of biological functions. **B)** Quantification of the CHE-1^{oe} mediated ASE marker *gcy-5^{prom}::GFP* induction in the germ line upon depletion of proteostasis factors in *C. elegans.* One-way ANOVA was used for statistical comparison, *** p<0.001, ** p < 0.01, * p < 0.05, ns not significant. At least 300 animals were counted for each condition. Error bars represent SEM. **C)** Representative images illustrating the germline expression of the ASE marker induced by TF CHE-1 overexpression following RNAi treatment of *hecd-1, eel-1, math-33, marc-4, usp-39,* and *spg-7*.

The RNAi of *plc-3* did not give consistent and reliable phenotypic outcomes; knockdown of *marc-4, spg-7,* and *plc-3* exhibited varying degrees of unhealthiness, developmental delays, and the presence of dead eggs.

Considering the developmental progression of the animals and the qualification of reprogrammed neuron-like cells after RNAi treatments, we decided to select *hecd-1, eel-1,* and *math-33* for further investigation. In this group, knockdown of *math*-33 and *eel-1* resulted in a higher percentage of germ cells being reprogrammed and expressing the *gcy-5^{prom}::GFP* marker. Specifically, *hecd-1* RNAi showed approximately 10% reprogramming efficiency, while *eel-1* RNAi exhibited around

18%, and *math-33* knockdown demonstrated an approximately 12% reprogramming efficiency.

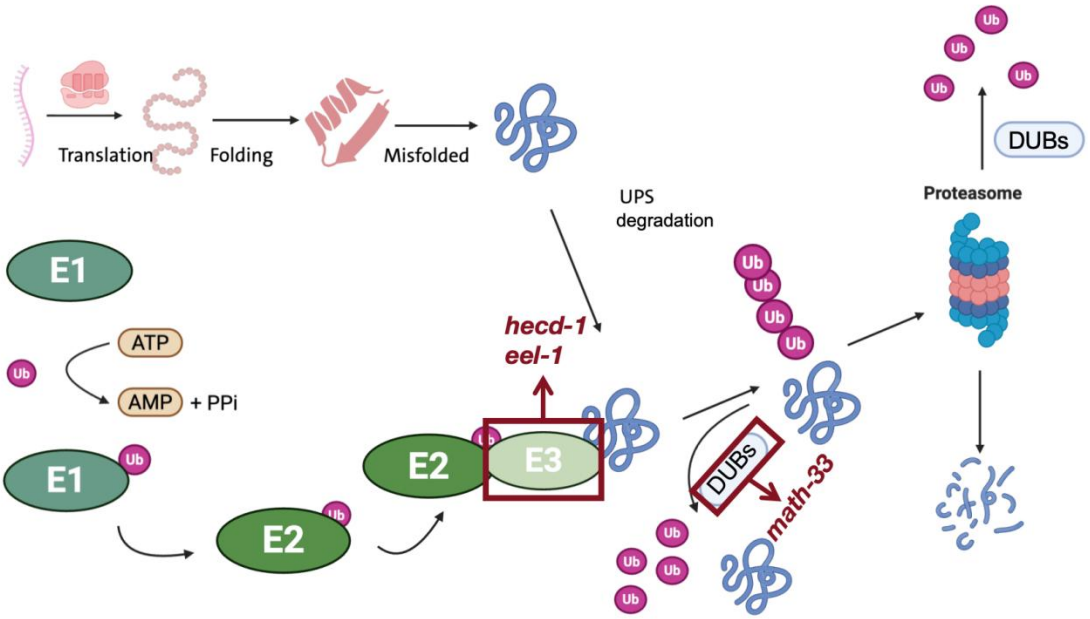

Figure 2.1.2 Candidates in the ubiquitin proteasome system. Schematic representation shows the role of UPS as a degradation pathway within the proteostasis network. It involves a three-step cascade process: ubiquitin activation by E1 enzymes, ubiquitin-conjugation by E2 enzymes, and ubiquitin ligation by E3 ligases. E3 ligases confer substrate specificity and the attachment of ubiquitin molecules to target proteins to the 26S proteasome for degradation. Deubiquitinating enzymes facilitate the removal of ubiquitin chains from substrates, thereby preventing their degradation by the proteasome and recycling free ubiquitin (Giovannini et al., 2025). The red rectangles indicate that *hecd-1* and *eel-1* belong to the E3 ligases, while *math-33* is classified as a deubiquitinating enzyme.

These three candidate genes are all involved in the UPS (Figure 2.1.2), a key protein degradation pathway essential for maintaining cellular protein homeostasis. The role of the UPS in regulating pluripotency was identified through a UPS-targeted RNAi screen (Buckley et al., 2012; Pickart, 2001), and has more recently been reported as a critical regulator of pluripotent stem cell survival and motor neuron differentiation (Zhang et al., 2021).

In this study, we found that these UPS factors inhibit the TF induced conversion of germ cells into specific neuronal cell types, suggesting that the UPS may also contribute to inhibitory mechanisms underlying direct cell reprogramming. Based on this observation, this study further aims to investigate the proteostasis factors regulating pathways involved in germ cell fate protection and TF driven cell reprogramming.

2.2 Overexpression of TF CHE-1 in *hecd-1(ok1437)* mutant allows germ cells to ASE neuron conversion

RNAi often results in a 'partial' loss of function, whereby some level of protein function may be retained. Several studies have demonstrated off-target effects of RNAi at the transcript, protein, and phenotype levels(Alemán et al., 2007; Jackson et al., 2003; Lin et al., 2005). Additionally, several factors can influence the efficiency of RNAi, including bacterial contamination, the freshness and quality of RNAi plates, etc. To validate results obtained from RNAi experiments, analyzing worms carrying mutant alleles of these candidate genes provides an important complementary approach.

First, we attempted to generate available mutant strains in our transgenic system. Two *hecd-1* mutant strains, *hecd-1(ok1437)* and *hecd-1(ok1450),* which carry deletions of approximately 1,150 base pairs and 1,550 base pairs, respectively, were successfully crossed into the transgenic strain expressing heat shock inducible TF CHE-1 and *gcy-5^{prom}::GFP*. After broadly expressing TF CHE-1, both mutants showed ectopic expression of ASE neuronal fate marker *gcy-5^{prom}::GFP* in the germline. In the *hecd-1* RNAi experiments, it was observed that the GFP signal (*gcy-5^{prom}::GFP*) was more proximally located to the vulva, and a similar pattern was detected in the *hecd-1(ok1437)* mutant strain (Figure 2.2.1.B) and the *hecd-1(ok1450)* strain.

Interestingly, *hecd-1(ok1437)* and *hecd-1(ok1450)* both exhibited significantly higher reprogramming efficiency than the *hecd-1* RNAi treatment. In particular, *hecd-1 (ok1437)* showed roughly 10% higher reprogramming efficiency compared to *hecd-1(ok1450)* (Figure 2.2.1.A), and approximately 3-fold increase of reprogramming efficiency compared to the RNAi treatment. These observations suggest that the mutant strains offer a more stable and reliable system, avoiding the limitations and potential failure associated with RNAi based approaches.

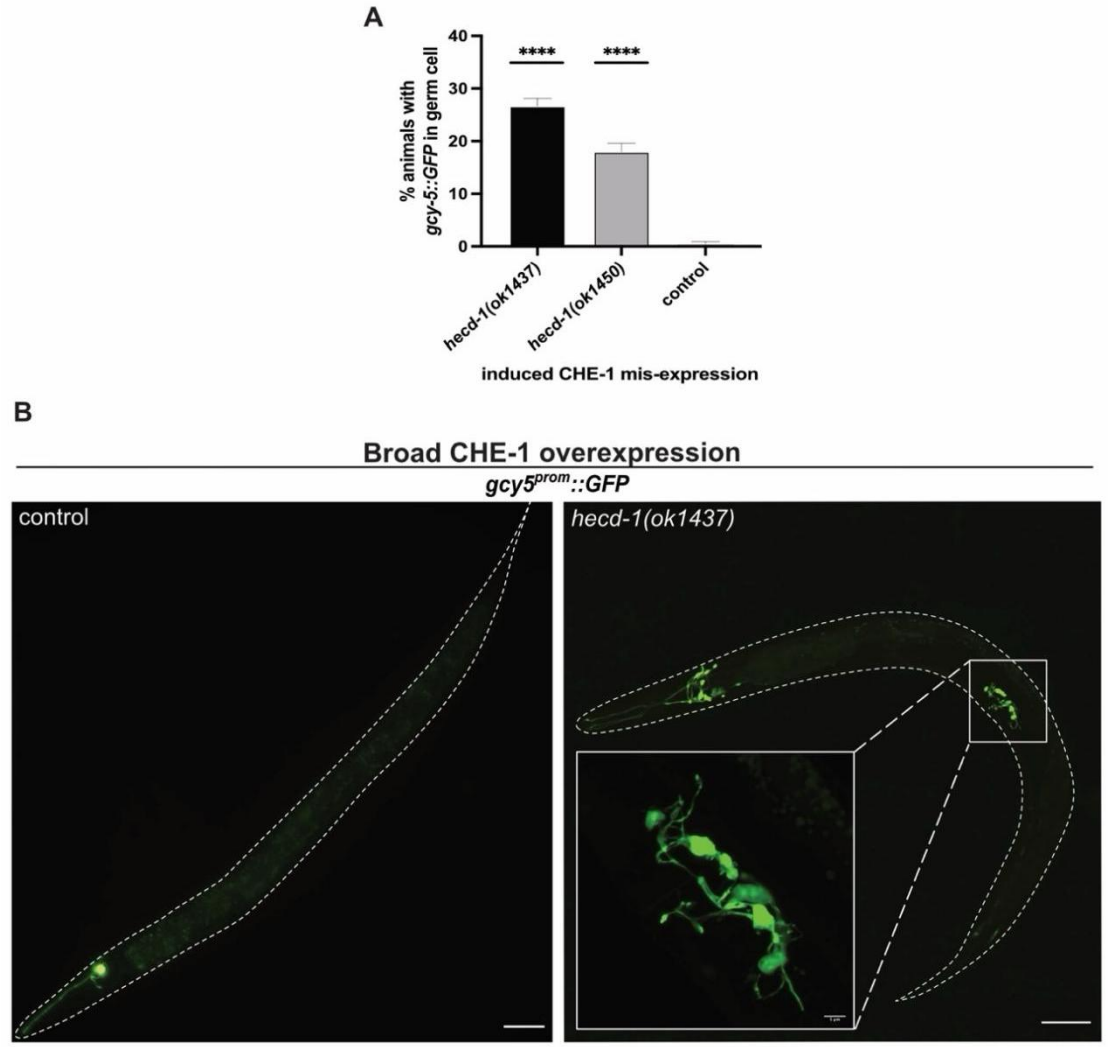

Figure 2.2.1 *hecd-1* mutants allow germ cell conversion to neurons. A) Quantification of the animals showing *gcy-5^{prom}::GFP* induction upon TF CHE-1^{oe} in the germ line of *hecd-1* mutants. Original transgenic strain that before cross *hecd-1* mutant background as a control. Paired Student's t-test was used for statistical comparison, **** indicates $p<0.0001$. At least 300 animals were counted for each condition. Error bars: SEM. **B)** Worms showing ectopic expression of the *gcy-5^{prom}::GFP* reporter in the germline after induction of TF CHE-1. Rectangular boxes indicate the magnified regions, highlighting that converting germ cells have axon/dendritic-like projections. Scale bar: 50µm.

However, the *eel-1* mutant proved to be either lethal or produced no progeny when crossed with the CHE-1^{oe} system. Additionally, the genetic locus of *math-33* is in proximity to the CHE-1^{oe} system cassette, which prevented obtaining a viable strain. Therefore an attempt was made to generate the CRISPR-Cas9 mediated knockout strain. These efforts, however, did not yield any viable animals. Worms carrying knockout alleles of *math-33* or *eel-1* were either lethal or sterile.

Since the knockout approach was unsuccessful, we turned to the tissue specific Auxin inducible degradation system. For this, endogenous MATH-33 was successfully tagged with the auxin-inducible degron (AID) and Human Influenza

Hemagglutinin (3xHA) in the CHE-1^{oe} system strain, but not EEL-1. The AID system facilitates targeted protein degradation via the plant derived protein TIR1 upon auxin treatment (Figure 2.2.2 A). When worms tagged with the degron are combined with transgenic strains expressing TIR1 in specific tissues, this approach enables tissue-specific knockdown of the target protein, allowing the effects to be observed within that particular tissue (Zhang et al., 2015).

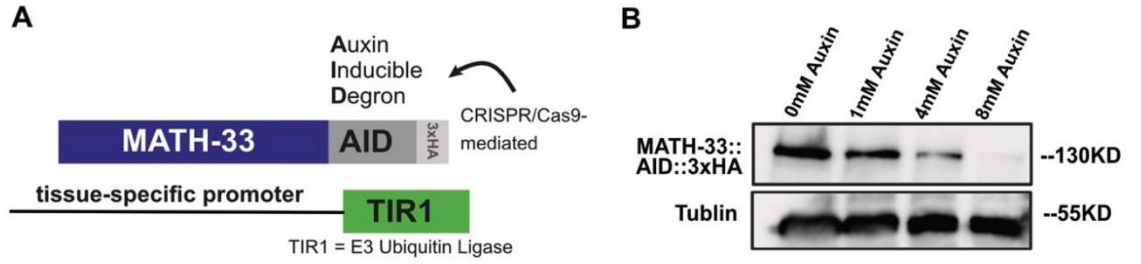

Figure 2.2.2 Tissue specific knockdown by Auxin Inducible Degradation system. A) Schematic diagram illustrating CRISPR-mediated tagging of the endogenous MATH-33 C-Terminal locus with an AID degron and an HA tag. This strain is combined with strains expressing the AID-recognizing TIR1 E3 ubiquitin ligase under tissue-specific promoters to enable targeted protein degradation in specific tissues. **B)** Western blot analysis showing the degradation of MATH-33 protein levels upon treatment with 4 mM auxin, with further depletion observed at 8 mM auxin.

Western blot analysis in the strain expressing TIR1 under a soma-specific promoter revealed nearly complete degradation of MATH-33 upon treatment with 8mM auxin (Figure 2.2.2 B). This new strain can be utilized for further investigations, such as identifying the tissue-specific signaling pathways that contribute to reprogramming following MATH-33 depletion.

Notably, knockdown of *hecd-1* resulted in a comparatively healthier phenotype than knockdown of *eel-1* or *math-33*, and the induced cells displayed a clearer neuronal structure. In contrast, knockdown of *eel-1* or *math-33* typically produced a more diffuse, “cloudy” positive signal; this cloudy pattern was occasionally observed even in the negative control. Overall, *hecd-1* mutants are the available strains that consistently support stable germ cell to neuron conversion upon CHE-1 overexpression, while also exhibiting more convincing neuron like structures. For these reasons, we decided to focus on the *hecd-1(ok1437)* strain in subsequent analyses.

2.3 Converted germ cells in the *hecd-1(ok1437)* mutant background express ASE-specific and pan-neuronal markers

Next, we combined the ASE neuronal fate maker *gcy-5^{prom}::GFP* with subtype neuronal fate makers, including the pan-neuronal reporter *rab-3^{prom}::RFP* (Stefanakis et al., 2015) (Figure 2.3.1 A) and ASE/AWC-specific gene marker *ceh-36^{prom}::RFP* (Hobert, 2016) (Figure 2.3.1 B), to investigate the extent and specificity of germ cell to neuron conversion upon knockdown of *hecd-1*.

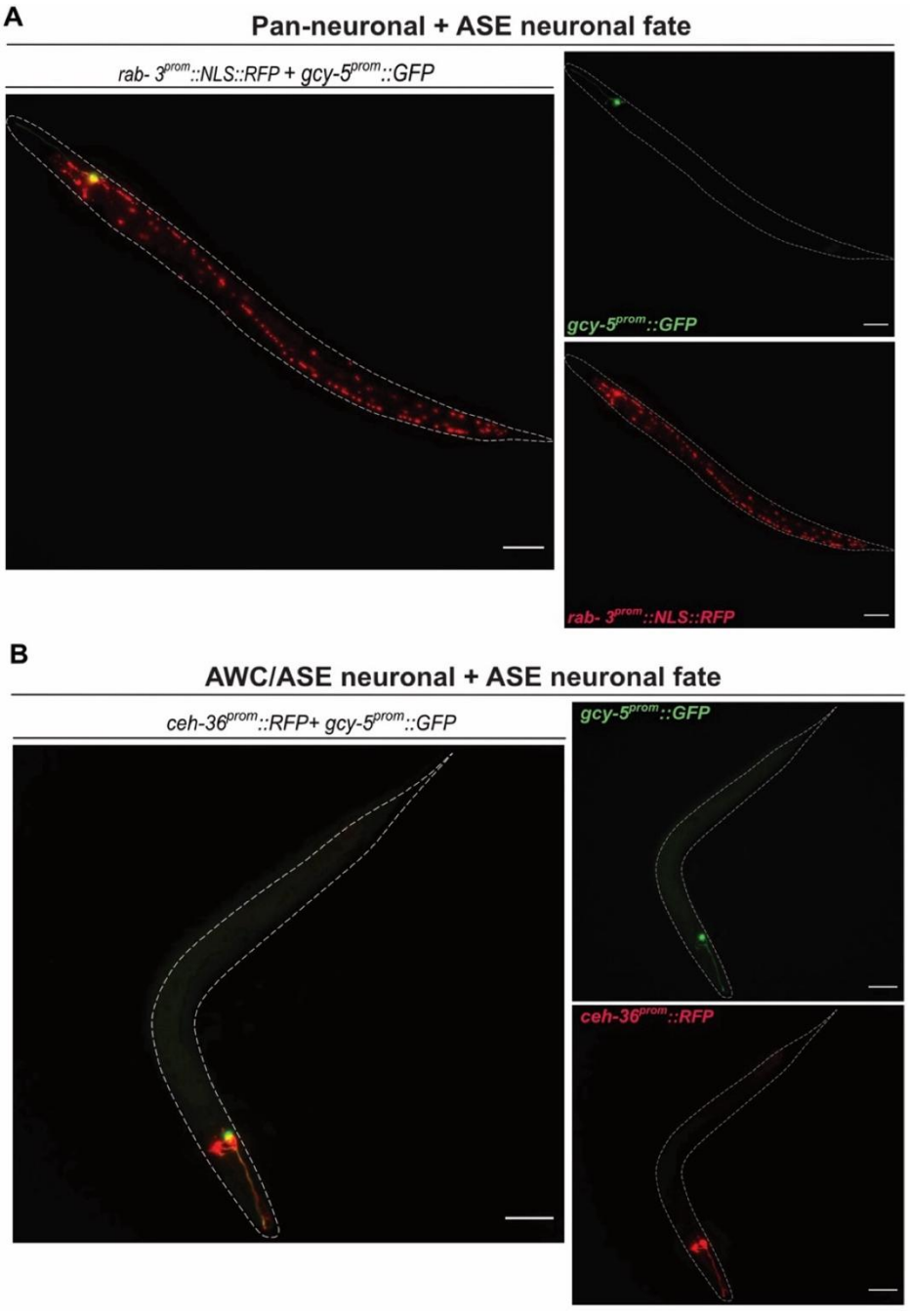

Figure 2.3.1 Transgenic system combined different neuronal markers. The expression of **A)** the pan-neuronal fate marker *rab-3^{prom}::RFP* and **B)** ASE/AWC neuronal fate marker *ceh-*

36^{prom}::RFP can be detected in animals with *gcy-5^{prom}::GFP* in ASE neurons. Scale bars: 50 μm.

In the reprogramming phenotype resulting from CHE-1^{oe}, we observed that, in addition to *gcy-5^{prom}::GFP* expression, reprogrammed cells also expressed the pan-neuronal reporter *rab-3^{prom}::RFP* (Figure 2.3.2 A, C) and the ASE/AWC-specific marker *ceh-36^{prom}::RFP* (Figure 2.3.2 B, D). These findings collectively demonstrate an extensive conversion of germ cells into neuron cells. These data indicate that the reprogrammed cells are not merely activating random genes; rather, they effectively establish a robust, coherent, and highly specific neuronal identity.

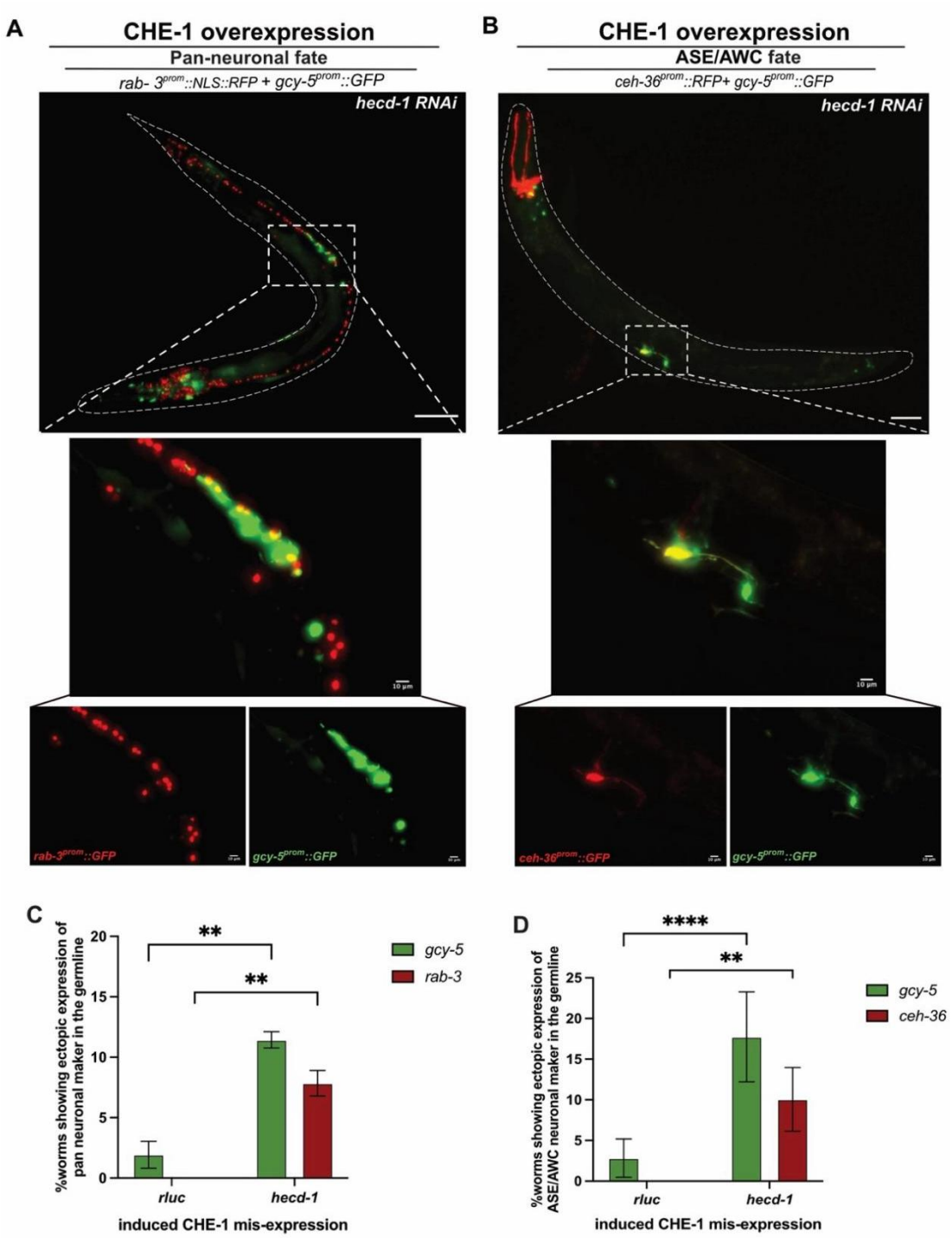

Figure 2.3.2 Knockdown of *hecd-1* allows germ cell conversion to a specific neuronal cell type. After CHE-1^{oe}, the expression of **A)** the pan-neuronal fate marker *rab-3^{prom}::RFP* and **B)** ASE/AWC neuronal fate marker *ceh-36^{prom}::RFP* can be detected in animals with *gcy-5^{prom}::GFP* in the germline. Dashed boxes represent the magnified area. Scale bars: 50µm. Quantification was conducted on animals exhibiting *gcy-5^{prom}::GFP* expression alongside neuronal marker **C)** *ceh-36^{prom}::RFP* expression and **D)** *rab-3^{prom}::NLS::RFP*. Two-way ANOVA was used for statistical analysis. comparison, **** indicates p<0.0001, ** p<0.01. At least 300 animals were counted for each condition. Error bars represent SEM.

To assess whether the expression of the transgenic reporters accurately reflects endogenous gene expression, single-molecule Fluorescent In Situ Hybridization

(smFISH) was performed. Endogenous mRNA transcripts of *gcy-5* and *rab-3* were detected in the reprogrammed germ cells of the *hecd-1(ok1437)* mutant strain (Figure 2.3.3) (S.1), providing evidence that the reporter transgenes faithfully reflect the expression of the endogenous neuronal genes.

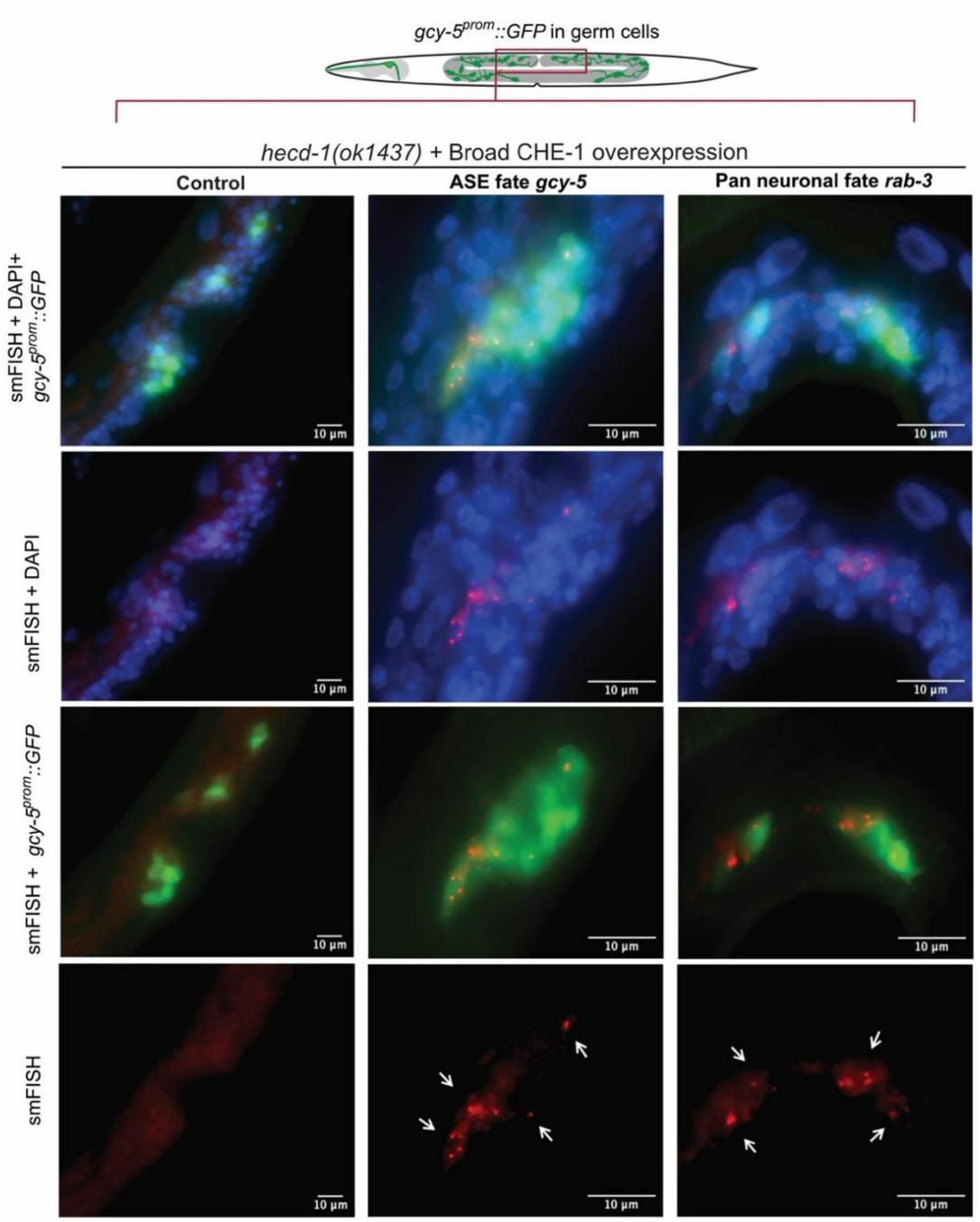

Figure 2.3.3 Endogenous expression of neuronal genes in converted germ cells. smFISH-based visualization of transcripts originating from endogenous neuronal genes *gcy-5* and *rab-3* in the germ cells of *hecd-1(ok1437)* mutant background upon CHE-1^{oe} animals. The mRNAs are displayed as red dots. Control samples were subjected to mock hybridizations. White arrows indicate the positive mRNA transcripts. The smFISH probes utilized in this study are listed in Table 4.9. Scale bar: 10 µm.

Taken together, these results confirmed the faithful conversion of germ cells to ASE neuron-like cells at the molecular level, indicated by the expression of neuronal reporter genes as well as endogenous neuronal genes.

2.4 Knockdown of *hecd-1* allows germ cells conversion to GABAergic neurons

Given that depletion of *hecd-1* enabled the conversion of germ cells into neurons, we next asked whether knockdown of *hecd-1* allows specific conversion of germ cell to neuron since TF CHE-1 specifies the identity of a specific type of glutamatergic neurons, or whether HECD-1 plays a general role in safeguarding the germ cell identity.

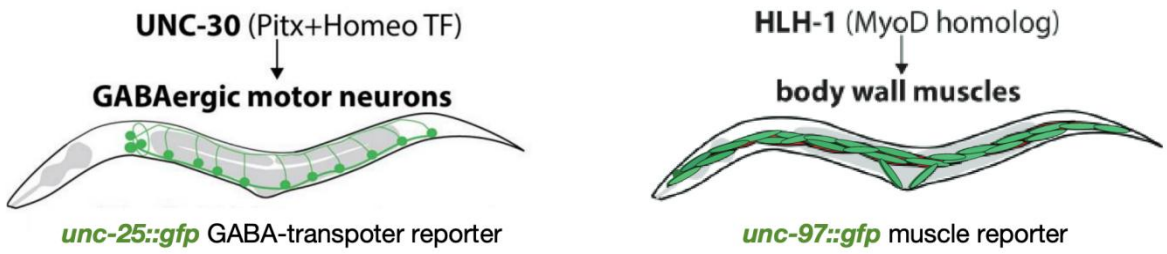

Figure 2.4.1 Transgenic system combined different cell fate makers. Schematic representation of TFs UNC-30 and HLH-1 mediated induction of GABAergic neuron fate and muscle fate in the animals, respectively, visualized by the respective reporters.

To address this question, we examined another neuronal fate: GABAergic motor neurons, which can be induced by TF UNC-30 (Jin et al., 1994). This neuronal fate was identified using *unc-25^{prom}::GFP* as a marker for GABAergic neurons (Figure 2.4.1). It has been demonstrated that *lin-53* functions as a barrier to the reprogramming of germ cells into GABAergic neurons upon induction of TF UNC-30 under the control of a heat-shock inducible promoter (Tursun et al., 2011). Knockdown of *hecd-1* showed *unc-25^{prom}::GFP* expression in germ cells after ectopic expression of UNC-30 (Figure 2.4.2 A, C). Furthermore, the F1 generation RNAi screen of *eel-1* and *math-33* did not result in the induction of the *unc-25^{prom}::GFP* marker.

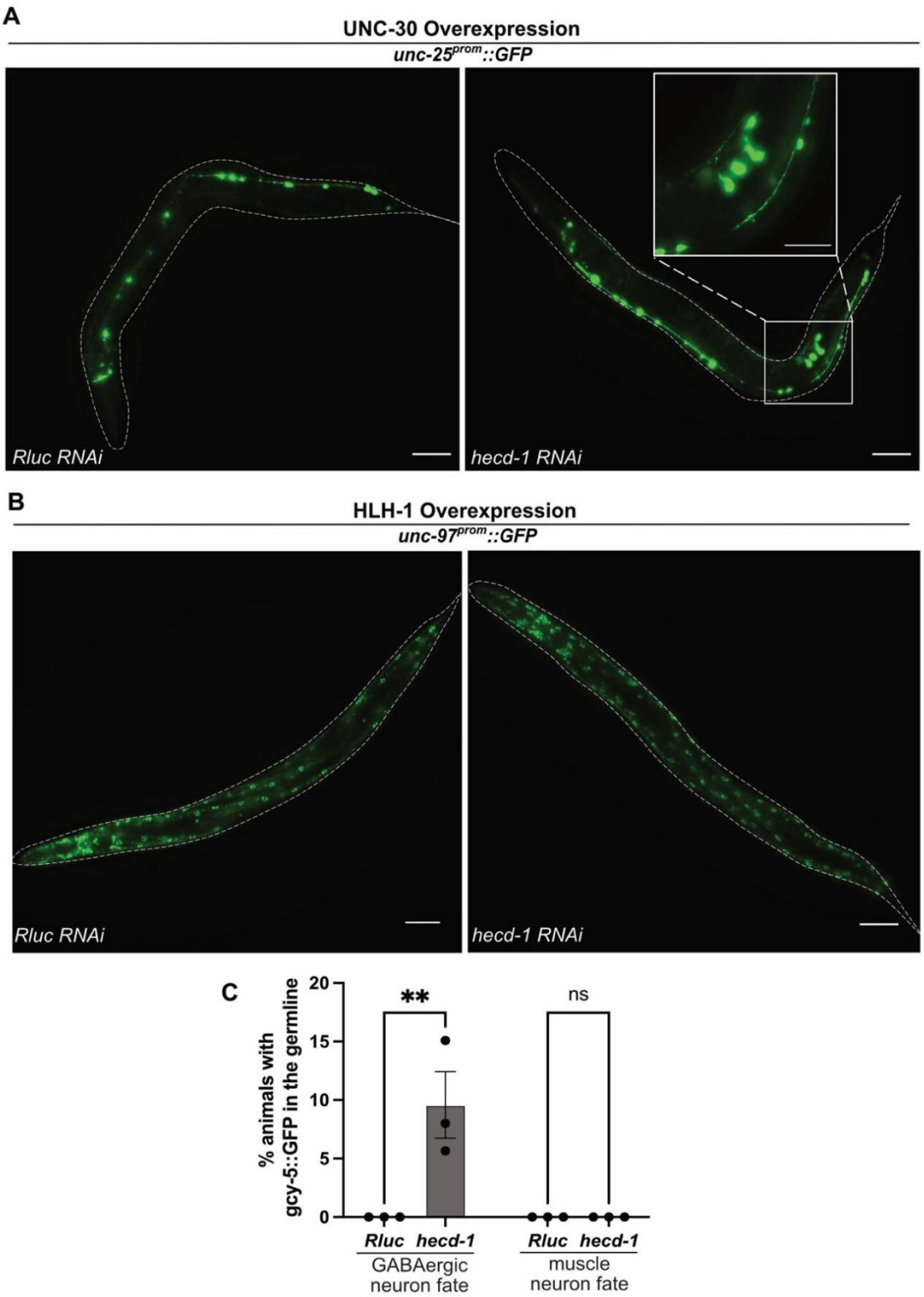

Figure 2.4.2 Depletion of HECD-1 allows germ cells conversion to GABAergic neuronal fate but not to muscle fate. **A)** Representative images of induction of GABAergic neuronal fate reporter *unc-25*^{prom}*::GFP* upon TF UNC-30 overexpression in *control* and *hecd-1* RNAi animals**.** Rectangular boxes indicate the magnified regions. **B)** Overexpression of muscle fate inducing TF HLH-1 does not induce germ cells to muscle conversion in *hecd-1* RNAi animals. **C)** Quantification of germ cell conversion to other fates upon induction of respective TFs. GABAergic neuronal induction can be achieved in 10% of the animals after UNC-30

overexpression, but no muscle induction is observed upon HLH-1 overexpression. Paired Student's t-test was used for statistical comparison, ** $p<0.01$, ns not significant. At least 300 animals were counted for each condition. Error bars represent SEM. Scale bar: 50 µm

Besides examining neuronal fate, another question was whether it is possible to convert germ cells into other tissue types, such as muscle, following knockdown of *hecd-1*. This was examined using a transgenic strain carrying heat shock inducible helix loop helix (bHLH) TF HLH-1 (MyoD homolog) and GFP reporter *unc-97^{prom}::GFP* (Fukushige and Krause, 2005; Harfe et al., 1998) (Figure 2.4.1). However, we did not observe any GFP signal in germ cells, indicating no reprogramming into muscle cells upon any of the *hecd-1* RNAi screens under HLH-1 overexpression conditions (Figure 2.4.2 B, C), nor after knockdown of *math-33* and *eel-1*.

Hence, these results suggest that depletion of HECD-1 is sufficient to enhance permissiveness for reprogramming into neuronal cells, but not into other tissue types like muscle cells. Additionally, the depletion of EEL-1 and MATH-33 hints towards the specificity of germ cell conversion into ASE-like cells.

2.5 Proteomic changes contribute to HECD-1 depletion mediated direct reprogramming

E3 ligases serve as essential mediators within the enzymatic ubiquitination cascade, playing a pivotal role in determining the fate of substrate proteins by imparting a high degree of specificity and selectivity. This regulatory function is critical for modulating protein levels and functional states within cells (Weber et al., 2019).

HECD-1, an E3 ubiquitin ligase, is orthologous to the human HECTD-1 and yeast *Ufd4p*, with its activity closely regulated in terms of chain specificity, determining whether ubiquitination occurs as mono- or poly-ubiquitination, contingent upon the nature of the ubiquitin chains involved (Weber et al., 2019). The ability to produce varied ubiquitin substrate structures is fundamental for directing proteins toward diverse cellular fates. For instance, monoubiquitination is involved in processes such as DNA repair and gene regulation, whereas polyubiquitination with ubiquitin K48 linkages generally targets proteins for proteasomal degradation.

First, we aimed to investigate whether HECD-1 directly influences the transcription factor CHE-1, which is responsible for specifying the ASE neuron fate and is involved in gene regulation (Figure 2.5.1 A). To assess this, Western blot analysis was performed to examine the levels of ectopic CHE-1 expression in different heat shock conditions, due to different heat shock treatment between *hecd-1* RNAi and *hecd-1(ok1437)* mutant (Figure 2.5.1 B). The results showed no significant difference between *hecd-1(ok1437)* and control under 32°C heat shock for 120min, but a higher level of CHE-1 expression in the control compared to *hecd-1(ok1437)* under 37°C 30min for RNAi treatment. These findings suggest that the lack of increased CHE-1 expression in *hecd-1(ok1437)* mutants indicates that CHE-1 activation is unlikely to be the primary mechanism driving reprogramming. Additionally, despite the difference, TF CHE-1 was activated successfully in this transgenic system.

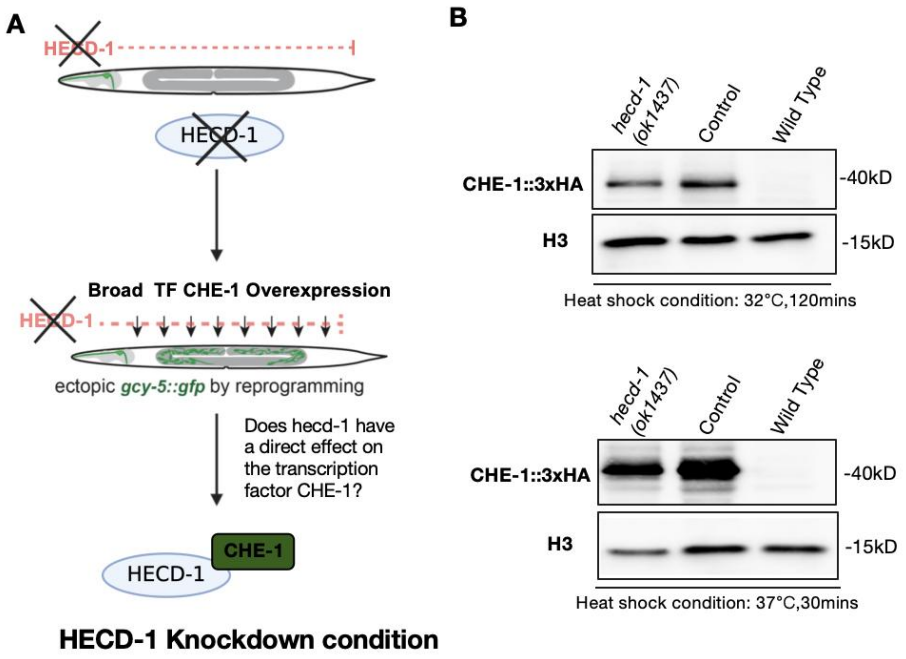

Figure 2.5.1 The effect of HECD-1 on transcription factor CHE-1 is not the primary factor responsible for reprogramming. A) Schematic representation illustrating the potential direct effect of HECD-1 on TF CHE-1 within the transgenic system. **B)** Western blot analysis of CHE-1 expression reveals a significant increase in CHE-1 levels in the control background compared to *hecd-1(ok1437)* mutants under 37°C for 30 minutes, no significant difference between *hecd-1(ok1437)* mutants and controls under 32°C for 120 minutes.

C. elegans hecd-1 was identified in a screen for mutations that lead to reduced ubiquitin-proteasome activity (Segref et al., 2014). When we knock down *hecd-1* using RNAi or a mutant, its target proteins are normally degraded (Figure 2.5.2 A),

but instead accumulate, which leads to reprogramming (Figure 2.5.2 B). So we hypothesized that some of these upregulated proteins might play a role in the reprogramming process. To test this, we planned to perform an RNAi screen of the upregulated proteins in the *hecd-1(ok1437)* mutant strain. It was expected that double knockdown of these upregulated proteins would result in a significant decrease in *hecd-1(ok1437)* mediated reprogramming efficiency (Figure 2.5.1 C), thereby implicating their functional involvement in the process.

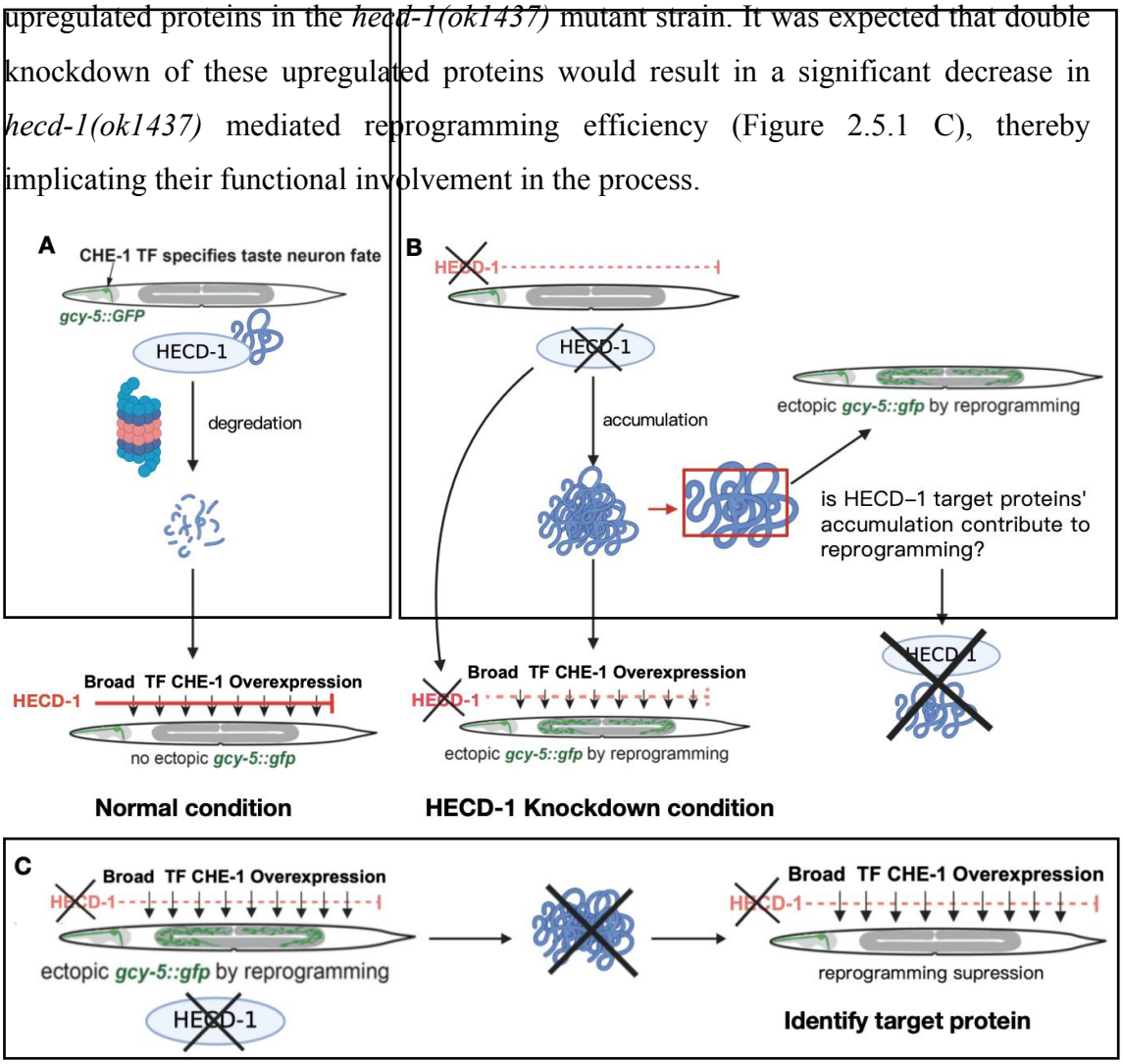

Figure 2.5.2 Hypothesis. A) The schematic illustrates that cells maintain their fate when HECD-1 functions properly, even in the presence of TF CHE-1^{oe}. **B)** The schematic model outlines the hypothesis that the accumulation of proteins resulting from HECD-1 depletion may be a key factor driving direct reprogramming. **C)** Experimental design to identify the key factor driving direct reprogramming: knocking down the accumulated protein responsible for reprogramming should rescue the HECD-1 depletion mediated reprogramming phenotype.

To identify potential mechanisms of HECD-1 depletion mediated reprogramming in *C. elegans*, mass spectrometry was first performed to detect proteomics changes between *hecd-1(ok1437)* and WT strains. A total of 471 proteins were significantly upregulated in the mutant background. This represents a broad range; many of these upregulated proteins may be unrelated to reprogramming and could potentially result from nonspecific aggregation. Therefore, the objective was to

further refine this list to identify candidate proteins that are directly involved in reprogramming. Given that *eel-1*, *math-33*, and *hecd-1* are components of the UPS, we hypothesize that shared proteomic changes among these proteins may function as critical regulators or substrates relevant to the reprogramming process.

Therefore, we also performed mass spectrometry to detect proteomics change in the *hecd-1*, *eel-1,* and *math-33* mutants (Figure 2.5.3 A). The results indicated that HECD-1, EEL-1and MATH-33 were significant downregulated in *hecd-1(ok1437)*, *eel-1(ok1575)* and *math-33(ok2974)* mutants, respectively (Figure 2.5.2 C, D, E). Additionally, the levels of HECD-1 and MATH-33 remained unchanged in the *eel-1* mutant (Figure 2.5.2 D). While the level of MATH-33 was unaffected, EEL-1 expression was increased in the *hecd-1* mutant (Figure 2.5.2 B). Notably, both HECD-1 and EEL-1 were downregulated in the *math-33* mutant (Figure 2.5.2 E).

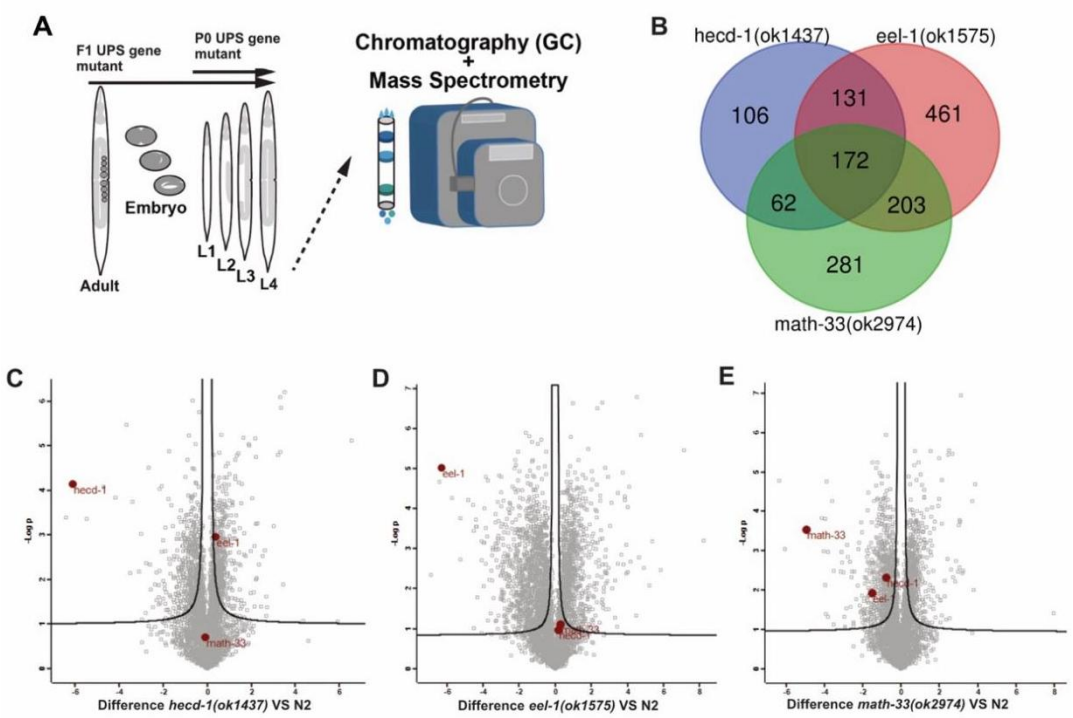

Figure 2.5.3 Proteomic changes in the mutant background of the UPS factors. A) Schematic diagram illustrating the proteomic changes detected by mass spectrometry. Animals were collected at all developmental stages. **B)** Upregulated proteins that are overlapping in the three mutants. These volcano plot graphs showed the significantly downregulated (left side) and upregulated (right side) proteins. **C)** Volcano plot of *hecd-1(ok1437)* mutant compared to WT. **D)** Volcano plot of *eel-1(ok1517)* mutant compared to WT. **E)** Volcano plot of *math-33 (ok2974)* mutant compared to WT. The analysis was performed using Perseus.

Although these individual proteomic profiles provide valuable insights, they do not immediately clarify the functional interplay among these three UPS factors. EEL-1, like HECD-1, is an E3 ubiquitin ligase that promotes target degradation, whereas MATH-33 is a deubiquitinating enzyme that protects target proteins from degradation. While their canonical functions are antagonistic, the mass spectrometry data revealed a striking compensatory regulatory mechanism: the loss of *math-33* significantly downregulates the expression of both HECD-1 and EEL-1 (Figure 2.5.2 E). Consequently, rather than accelerating substrate degradation, as would be expected from the loss of a deubiquitinating enzyme, the *math-33* mutation indirectly leads to the accumulation of HECD-1 and EEL-1 targets due to this compensatory downregulation. Based on this observation, we hypothesized that the core effectors driving the reprogramming process are among the substrates whose degradation is universally impaired across all three mutant backgrounds. Therefore, the subsequent analyses prioritized an overlapping network that was consistently upregulated across the *hecd-1*, *eel-1*, and *math-33* mutants (Figure 2.5.2 B).

Indeed, the analysis revealed many significantly upregulated proteins in all mutants, with 172 proteins identified as overlapping across all three mutants (Figure 2.5.2 B). To test the hypothesis that some of these proteins play a causative role in establishing cellular conversion permissiveness, RNAi experiments in mutant strains can be conducted. These experiments would assess whether targeted knockdown of individual proteins from the overlapping set results in the suppression of reprogramming phenotype, thereby implicating their functional involvement in the process.

Therefore, an RNAi screen was carried out in which *hecd-1* was co-depleted with each of the 172 overlapping upregulated genes. The penetrance of the germ cell conversion phenotype was then scored to identify suppressors that might reduce the reprogramming efficiency associated with *hecd-1* depletion. The RNAi feeding clones were obtained from the Ahringer RNAi library (SourceBioScience) and amplified in the lab using Gibson assembly. To date, 76 of the 172 candidate genes have been tested (Figure 2.5.3).

Protein ID	Gene sequence	gene name	Average % of worms with GFP
control		*rluc*	26.16%
O01805	C44E4.6	*acbp-1*	18.78%
Q95QG8	F36F2.6	*fcp-1*	17.76%
O45444	F35C5.6	*clec-63*	15.85%
Q20476	F46G10.1		18.15%
Q18553	C39H7.1		19.36%
Q21746	R05F9.10	*sgt-1*	16.63%
Q23450	coa-7	*zk20.4*	14.16%
O17347	H42K12.3		18.75%
Q19286;M1Z854;H2KYU8	F10C1.8	*ifb-2*	20.08%
Q09591	M106.1	*mix-1*	16.98%
O44144	C44B12.5	*perm-4*	13.29%
Q5WRN8;G5ECH8;Q27394	C29E6.1a	*let-563*	19.19%
Q9U3C1;Q9U3B9;Q21295	K07F5.13c	*npp-1*	10.28%
G5EFE3	H03A11.2		23.67%
Q18577	C42D4.1		21.98%
G5EG03	T21E8.3	*pgp-8*	20.39%
G5EG78	K09C8.5	*pxn-2*	11.24%
Q22170	T04G9.3	*ile-2*	26.36%
Q22288	T07C4.5	*ttr-15*	22.63%
Q17624	C04C11.2	*arrd-5*	18.13%
Q8WQ99	Y106G6E.6	*csnk-1*	14.33%
Q9U329	W09C5.8	*cox-4*	5.71%
O01634	ZK770.3	*inx-12*	18.77%
Q09508	C03G5.1	*sdha-1*	11.42%
Q9BIB7;H2KZN0	W02D3.11a	*hrpf-1*	22.18%
P43508	F44C4.3	*cpr-4*	13.31%
O02155;Q86NC3	T09B4.5		19.63%
Q95XR1	Y39G10AR.20	*tbca-1*	20.08%
Q9TYS3	D1037.3	*ftn-2*	22.83%
Q21228	K04G2.9		13.20%
P91148	C43E11.7	*ndx-7*	21.83%
O01854	F32B5.1		22.56%
Q95QG8	F36F2.6	*fcp-1*	17.46%
O44511	F42G8.11	*sph-1*	18.56%
Q09372	ZK177.4	*npp-24*	13.30%
Q9GUF2	Y73B6BL.24	*acp-6*	16.51%
G5EBY3	F20G4.3	*nmy-2*	9.09%
O18230	Y57G11C.4	*vti-1*	13.17%
Q09511-2;Q09511	EEED8.7a	*rsp-4*	11.99%
P53993	B0361.8	*algn-11*	13.38%
G5ECM7;G5ECC1	F13G3.10		22.55%
Q4PIU9;Q53U87;Q18100;Q53U86	C18F3.2c	*sax-7*	22.08%
Q20012	F35B12.2	*dhs-20*	24.33%
C1P658;C1P659;B9WRT9;H9G336;H9G334;H9G335;C1P660;O45881	W01F3.3b	*mlt-11*	16.55%
C7FZU4;C7FZU3;Q93791	F54F3.1a	*nid-1*	26.37%
P90901	F38B2.1d	*ifa-1*	15.95%
Q21443	DY3.2	*lmn-1*	1.55%
Q9TZ69	F40G9.3	*ubc-20*	22.49%
Q86S28;Q76NP4;O61907;Q86S27	T27C4.4	*lin-40*	23.89%
Q17510;O76710	B0491.3	*rmd-3*	23.61%
Q9NDC9	T03F6.5	*lis-1*	14.42%
P34422;P34422-3;P34422-2	F44B9.1	*dpf-6*	6.54%
P53014;G8JY79	F09F7.2a	*mlc-3*	9.78%
P30627	ZK637.13	*glb-1*	10.02%
P34669	zk686.3		8.46%
Q19462	F14E5.5	*lips-10*	10.26%
Q9XXA7	H38K22.3	*tag-131*	16.83%
Q9N393	Y54H5A.1		22.14%
Q20655;Q95ZT1	F52D10.3a	*ftt-2*	20.23%
H2KYS1;B0M0L8	C14F11.5b	*hsp-43*	13.80%
Q19203	F08C6.7	*unc-98*	16.37%
A4UVK2;J7SF86	c44c10.9		20.18%
O17347	H42K12.3		18.75%
Q17433;Q9U3L9	B0035.2	*dnj-2*	24.79%
O44441	B0546.1	*mai-2*	14.09%
Q9XX57	Y38H6C.1a	*dct-16*	25.24%
Q8I4G3;Q9XVU9	T03F7.7		24.64%
G5EFJ3	C08E8.4		18.93%
H2L0I2;H2L0I3;Q45EJ8;H2L0I4	ZC8.4a	*lfi-1*	24.56%
Q23543	ZK593.7	*lsm-7*	6.67%
Q03206-2;Q03206;Q94124	K03D3.10	*rac-2*	23.13%
Q17856	CO989.6	*msp-55*	25.12%
I2HAJ8;Q20881	F56D5.6		22.15%
Q18688	C47E8.5	*hsp-90*	2.42%
O17695	C53A5.3	*hda-1*	2.20%
Q23098	W01A8.4	*nuo-6*	0.25%

Table 2.1 Table List of suppressor RNAi screen. 76 of 172 overlapping up-regulated proteins RNAi treatment in *hecd-1(ok1437)* mutant background have been scored, at least 300 animals were counted for each condition.

The results identified several candidates that can rescue the reprogramming phenotype when these upregulated proteins are knocked down in the *hecd-1(ok1437)* mutant compared to the *hecd-1(ok1327)* alone. This suggests that these proteins may play roles in the conversion process. In addition, we observed an improvement in the quality of reprogramming after co-depletion, indicating that some of the upregulated proteins may promote harmful aggregation without directly influencing reprogramming efficiency.

Following screening, 34 genes showed significant suppression of reprogramming efficiency. Notably, *hsp-90 (*previously termed d*af-21*), *lmn-1*, *hda-1,* and *nuo-6* almost completely blocked reprogramming, while *dpf-6*, *lsm-7*, and *cox-4* were also considered important candidates as they showed a strong suppression effect (Figure 2.5.3 A).

Analysis of the protein network revealed that these newly identified suppressors have not been reported to interact with *hecd-1*, and that small protein clusters are formed around *hsp-90, lmn-1,* and *cox-4* (Figure 2.5.3 B)

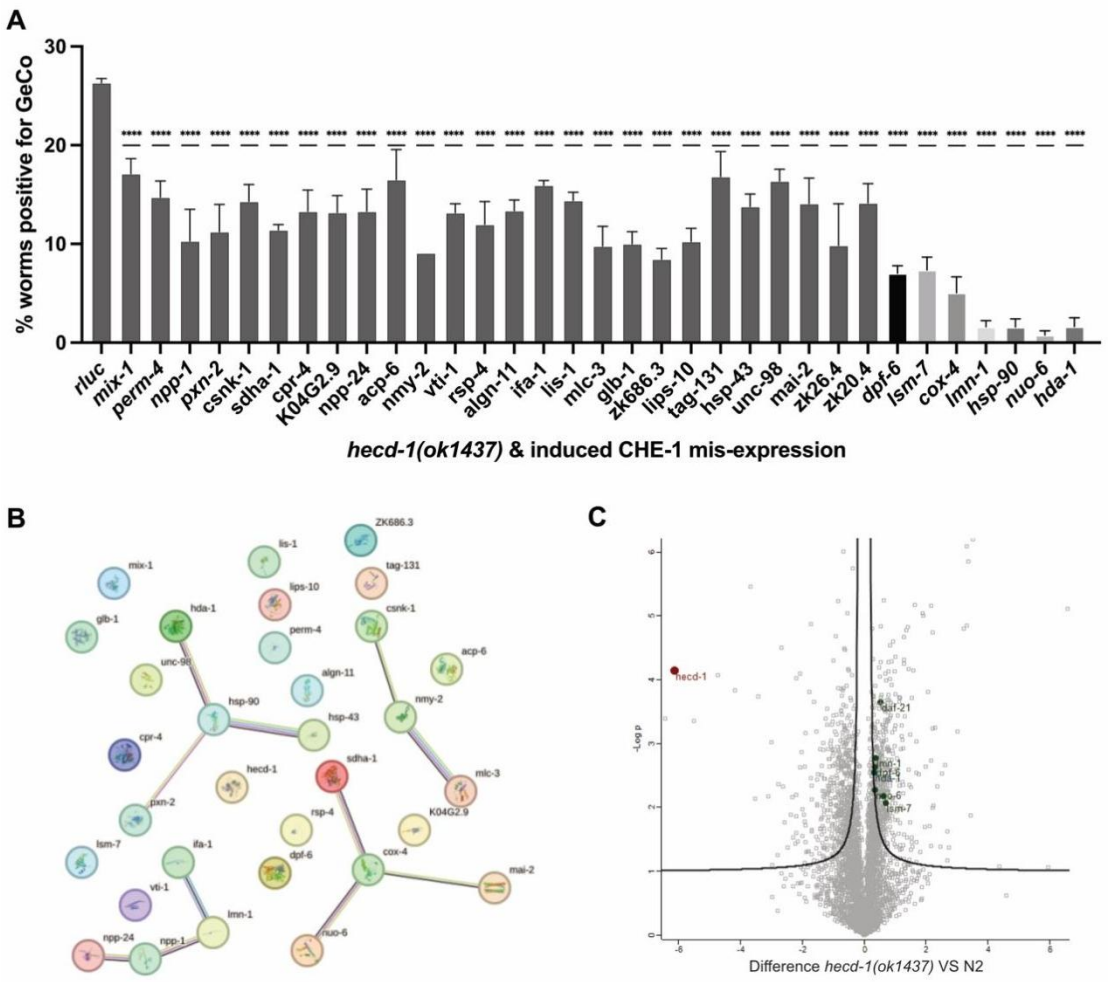

Figure 2.5.4 Knockdown of upregulated proteins that significant suppress *hecd-1* depletion mediated reprogramming phenotype. A) Quantification of the animals showing significant suppression of the TF CHE-1^{oe} mediated ASE marker *gcy-5^{prom}::GFP* induction in the germ line of *hecd-1(ok1437)* mutant background, *Rluc* serves as a negative control, representing the *hecd-1(ok1437)* background alone. **B)** Protein interaction network of the identified significant suppressors analyzed using www.string-db.org. **C)** Candidate gene in the volcano plot of *hecd-1(ok1437)* mutant compared to WT.

LMN-1 represents a notable discovery. Previous studies have demonstrated that RNAi-mediated knockdown of *lmn-1* in *C. elegans* develops into adults that are primarily characterized by female sterility (Hutchison, 2002). Additionally, the F1 generation worms that escaped the lethal effects of the strongest *lmn-1* RNAi exhibited sterility or semi-sterility. In these sterile animals, Liu and colleagues (Liu et al., 2000) observed significant reductions in the number of germ cells.

This raises the next question: whether the suppression effect on reprogramming is because the newly identified target gene truly contributes to reprogramming, or is it simply a consequence of germ cell damage, including potential elimination of affected cells?

2.6 Suppression of direct reprogramming is not a consequence of germ cell elimination via the newly identified target

To confirm that germ cells remain healthy after double knockdown of *hecd-1* and the newly identified targets, we performed DAPI staining to assess the presence and integrity of germ cells (Figure 2.6.1). Fifteen animals were selected from each experimental condition and examined using fluorescence microscopy. We observed that germ cells were absent in 1-2 WT animals following *lmn-1* RNAi treatment. This corroborates previous studies indicating that *lmn-1* RNAi results in a significant reduction in germ cell numbers. However, this effect appears to be less severe in *hecd-1* mutants. Therefore, more precise methods are required to assess germ cell damage and its impact on the reprogramming suppressor screen.

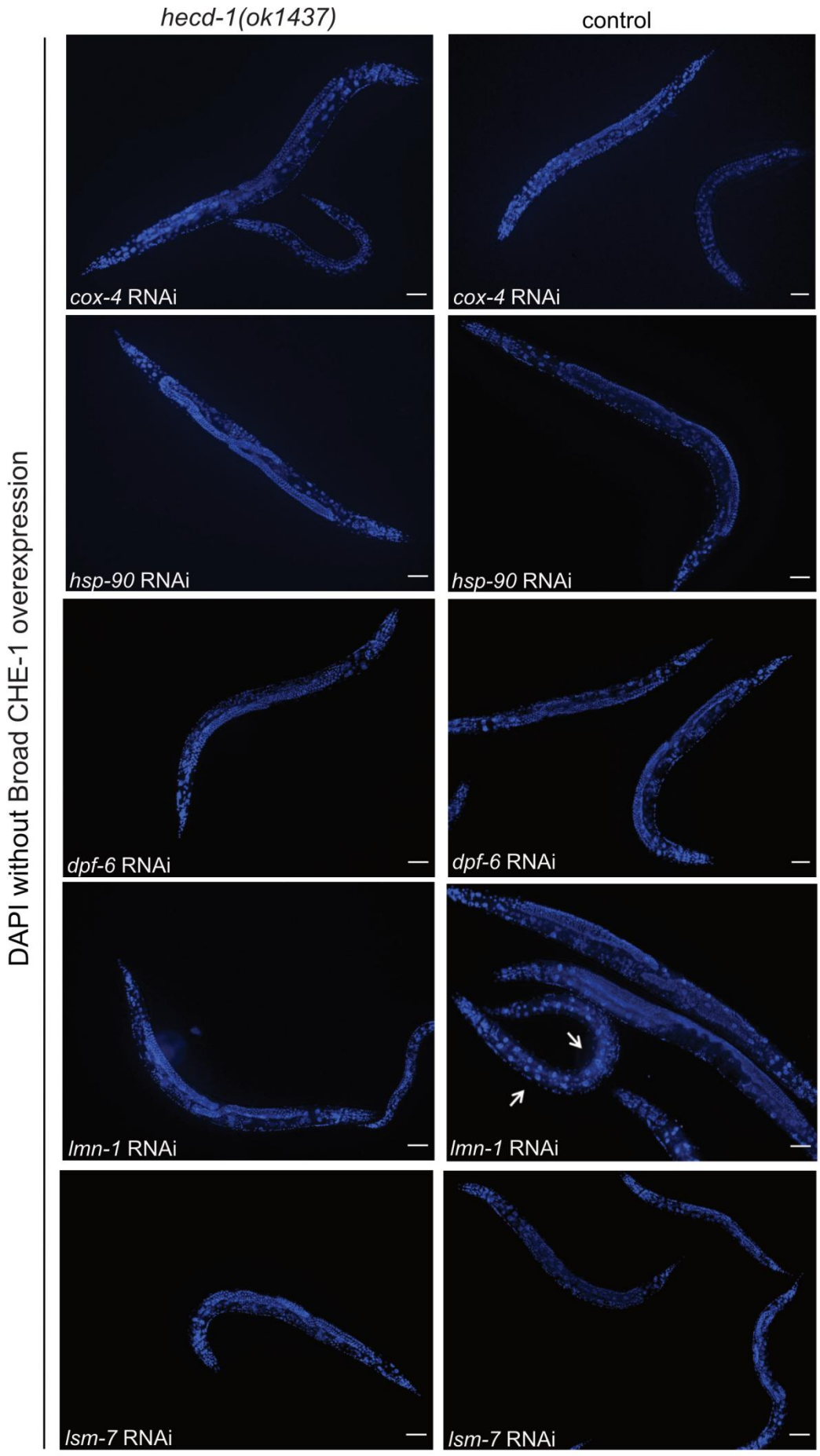
hecd-1(ok1437)
control
DAPI without Broad CHE-1 overexpression
cox-4 RNAi
cox-4 RNAi
hsp-90 RNAi
hsp-90 RNAi
dpf-6 RNAi
dpf-6 RNAi
lmn-1 RNAi
lmn-1 RNAi
lsm-7 RNAi
lsm-7 RNAi

Figure 2.6.1 *lmn-1* RNAi induces germ cell loss. DAPI staining of the whole worm line upon knockdown of candidate targets may potentially contribute to reprogramming in both *hecd-1(ok1437)* mutant background and WT. White arrows indicate control animals in *lmn-1* RNAi and lack a germline. Scale bar: 100 µm.

To further distinguish true reprogramming suppression from germ cell damage, the germ cell specific reporter *sun-1::mRuby* (Figure 2.6.2. A) was used to precisely monitor germ cell integrity. However, as both the *hecd-1* locus and *the sun-1::mRuby* insertion (*ieSi21*) reside on chromosome IV, generating a double homozygous strain is severely hindered by genetic linkage. To avoid this limitation, we generated CRISPR-Cas9 mediated *hecd-1* knockout allele (*hecd-1*$^{-/-}$) within the established *sun-1::mRuby* transgenic background. Following 7036bp deletion, this new *hecd-1*$^{-/-}$ strain retained a healthy and complete germ line (Figure 2.6.2 B).

Upon overexpression of TF CHE-1, the *hecd-1*$^{-/-}$ strain showed approximately the same reprogramming efficiency as the *hecd-1(ok1437)* strain, around 28% (Figure 2.6.2 C). Notably, the majority of ASE neuron like cells did not express the germ cell reporter, suggesting that the initial cell identity was effectively erased during reprogramming (Figure 2.6.2 D).

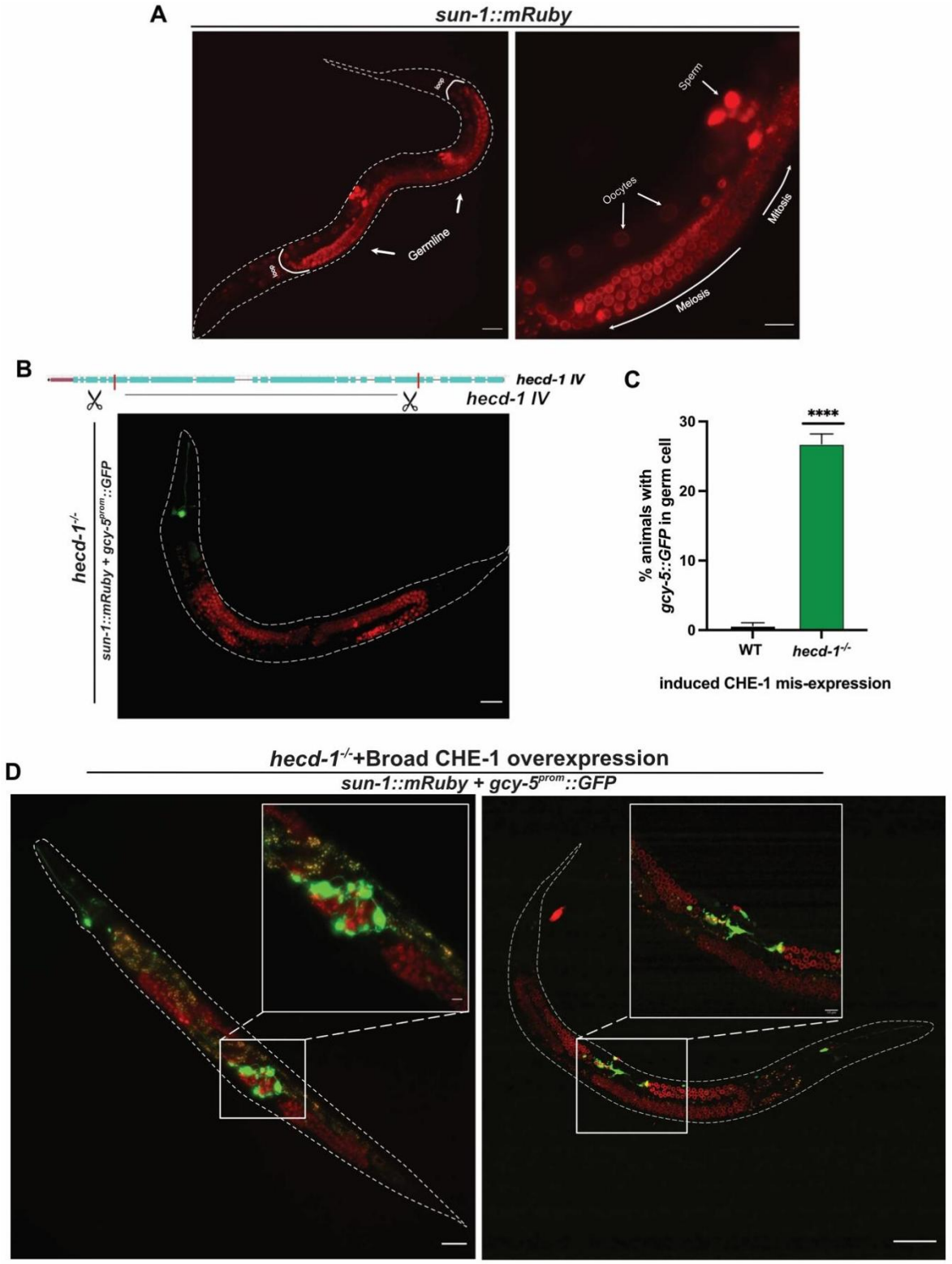

Figure 2.6.2 CRISPR-mediated *hecd-1* depletion allows germ cell conversion upon CHE-1 overexpression. A) The original strain that carries germ cell reporter *sun-1::mRuby*, which is expressed throughout the whole germline and in the early embryo. **B)** Schematic illustration of the deleted genomic regions in *hecd-1*, generated by CRISPR-Cas9 mediated dual sgRNA cleavage, resulting in a 7036 bp deletion. The CRISPR-mediated *hecd-1*$^{-/-}$ strain exhibited a healthy germ line. Scale bar: 50µm. **C)** *hecd-1*$^{-/-}$ showed nearly the same percentage of animals showing *gcy-5*^{prom}*::GFP* induction upon CHE-1^{oe} in the *hecd-1(ok1437)* background. Paired Student's t-test was used for statistical comparison, **** indicates p<0.0001. At least

300 animals were counted for each condition. Error bars: SEM. **D)** Representative microscope images of *hecd-1*$^{-/-}$ upon CHE-1^{oe} condition. Rectangular boxes indicate the magnified regions; most of the converted germ cells predominantly expressed neuronal fate markers. Scale bar: 50 µm.

Furthermore, to validate the results from the *hecd-1(ok1437)* screen, the effects of *lmn-1*, *cox-4*, *lsm-7*, *dpf-6*, and *hsp-90* were independently assessed in the CRISPR-mediated *hecd-1*$^{-/-}$ strain (Figure 2.6.3 A). RNAi targeting *cox-4* and *hsp-90* in *the hecd-1*$^{-/-}$ background resulted in a slightly reduced suppression of reprogramming compared to the *hecd-1(ok1437)* background. In contrast, the other three candidate genes showed no significant difference in their effects. This difference may be attributed to the fact that HSP-90 is an important component of the molecular chaperone system, while COX-4 is involved in mitochondrial function. Both proteins are highly interconnected and interact extensively with the protein degradation system within the broader PN. Consequently, alterations in *hecd-1* are likely to subsequently influence the activity of mitochondrial and molecular chaperone components.

In general, the *hecd-1*$^{-/-}$ strain showed a similar phenotype to *hecd-1(ok1437)*, confirming the suppression observed in the germ cell to neuron reprogramming efficiency as seen previously (Figure 2.6.3 A, B). Additionally, the *hecd-1*$^{-/-}$ strain provided further evidence that the original germ cell identity was entirely converted to neuronal cells. While there are minor differences observed in the effects of *cox-4* and *hsp-90* (Figure 2.6.3 B), these distinctions do not compromise the reliability of the *hecd-1*$^{-/-}$ model for further investigating the mechanisms of germ cell elimination through the co-depletion of *hecd-1* and target genes.

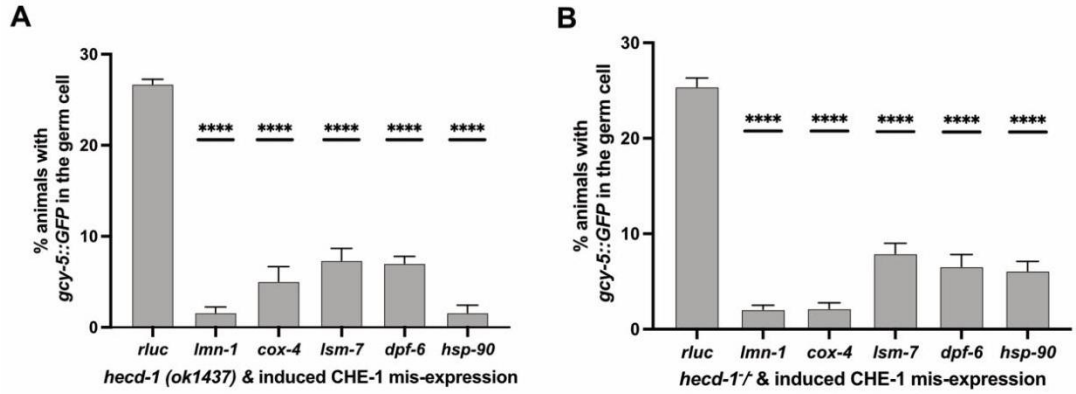

Figure 2.6.3 Reprogramming efficiency in the *hecd-1*$^{-/-}$ strain is comparable to that observed in the *hecd-1(ok1437)* strain. A) B) Quantification of animals showing *gcy-5*^{prom}*::GFP* induction following CHE-1^{oe} in the germ line upon knock down of candidate targets may potentially contribute to reprogramming in *hecd-1(ok1437)* background **A)** and

CRISPR-mediated *hecd-1*$^{-/-}$ background **B)**. Ordinary one-way ANOVA was used for statistical comparison, **** p<0.0001. At least 300 animals were counted for each condition. Error bars: SEM.

By scoring the germ cell maker to assess the health of germ cells in the condition with (Figure 2.6.4 A) and without CHE-1^{oe} (Figure 2.6.4 B), It was observed that *lmn-1* RNAi resulted in a statistically significant difference compared to the negative control and other candidate genes. These findings suggest that knockdown of *lmn-1* compromises germline integrity; however, the extent of this impairment is insufficient to completely inhibit the reprogramming process, indicating that *lmn-1* is a key candidate involved in this mechanism.

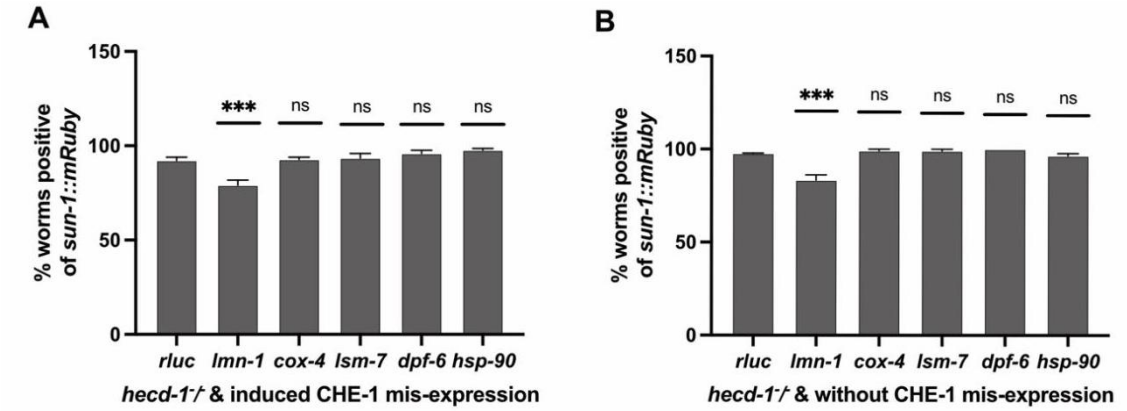

Figure 2.6.4 The integrity of the germline after co-depletion of *hecd-1* with candidate genes. **A) B)** Quantification of animals showing *sun-1::mRuby* induction in *hecd-1*$^{-/-}$ background upon knock down of candidate targets potential contribute to reprogramming with heat shock **A)** and without heat shock **B)**. Ordinary one-way ANOVA was used for statistical comparison, *** p<0.001, ns not significant. At least 300 animals were counted for each condition. Error bars: SEM.

By using this newly developed CRISPR/Cas9-mediated *hecd-1* knockout strain in conjunction with a germ cell marker, we confirmed the high fidelity of germ cell fate transdifferentiation. This process was characterized by the disappearance of the original cell identity and the subsequent adoption of a neuronal fate. This strain is a viable model that exhibited a similar suppression of reprogramming upon knockdown of the newly identified targets. Importantly, it demonstrates that *lmn-1* RNAi indeed affects germ cell viability, as suggested by previous studies; however, this effect is insufficient to counteract the reprogramming suppression induced by the intervention.

To investigate the effect of embryonic development, P0 generation RNAi was performed. The animals were selected at the newly hatched stage and transferred to RNAi plates when the germline was already established. They were then screened at

the L4 stage following broad CHE-1^{oe} in both *hecd-1(ok1437)* (Figure 2.6.3 A) and *hecd-1*$^{-/-}$ strains (Figure 2.6.3 B). The results showed that only *lmn-1* RNAi significantly decreased the reprogramming phenotype induced by HECD-1 depletion, it strongly suggested that *lmn-1* plays a role independent of the cell cycle in postmitotic cells in the context of reprogramming.

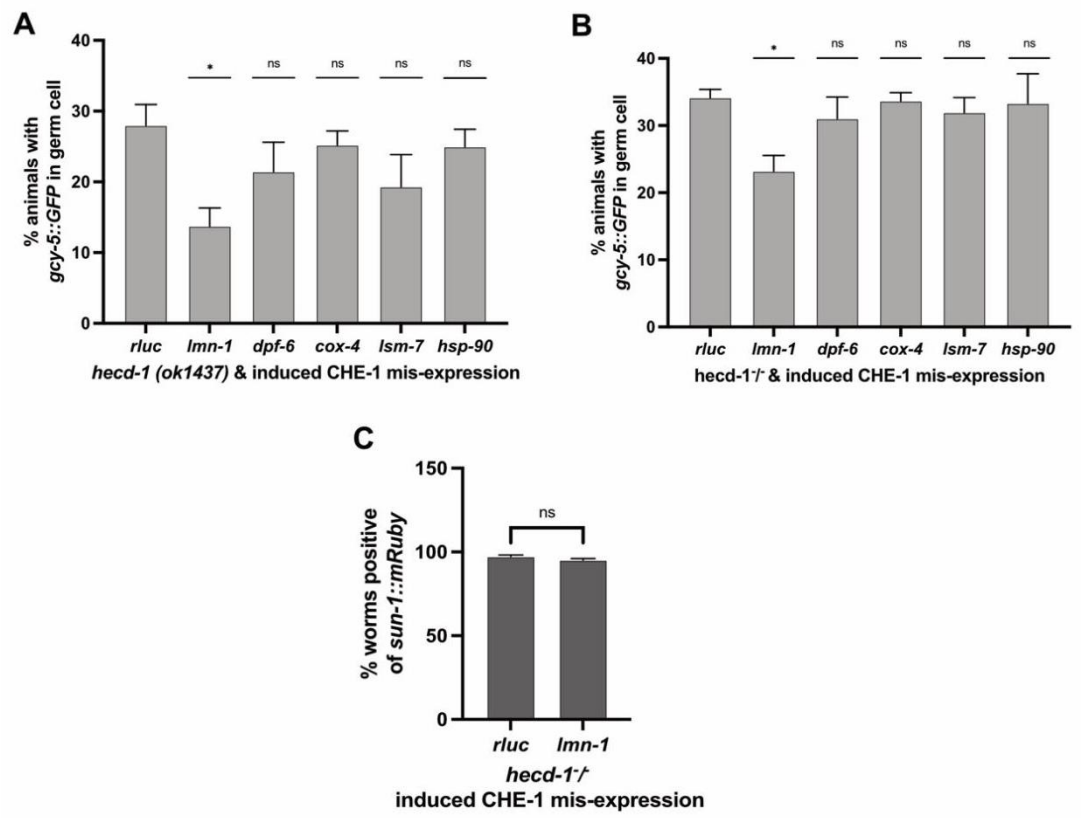

Figure 2.6.5 P0 generation RNAi screen of candidate genes depletion in *hecd-1(ok1437)* and *hecd-1*$^{-/-}$ background. **A) B)** Quantification of P0 generation animals showing *gcy-5*^{prom}*::GFP* induction following CHE-1^{oe} in the germ line upon knock down of candidate targets may potentially contribute to reprogramming in *hecd-1(ok1437)* mutant background **A)** and *hecd-1*$^{-/-}$ background **B)**. Ordinary one-way ANOVA was used for statistical comparison, * $p < 0.05$, ns not significant. At least 300 animals were counted for each condition. Error bars: SEM. **C)** Quantification of P0 generation animals showing *sun-1::mRuby* induction in *hecd-1*$^{-/-}$ background upon knockdown of *lmn-1* upon CHE-1^{oe}. One-tail student t-test was used for statistical comparison, ns not significant. At least 300 animals were counted for each condition. Error bars: SEM.

In the *hecd-1*$^{-/-}$ background P0 generation RNAi experiments, germline integrity was also assessed by scoring the germ cell marker *sun-1::mRuby*. *lmn-1* RNAi showed no significant difference compared to the negative control in this assay. Furthermore, we observed that even germ lines exhibiting signs of deterioration, such

as a reduction size or a decreased number of germ cells, without complete germ cell loss, were still capable of inducing reprogramming (Figure 2.6.6).

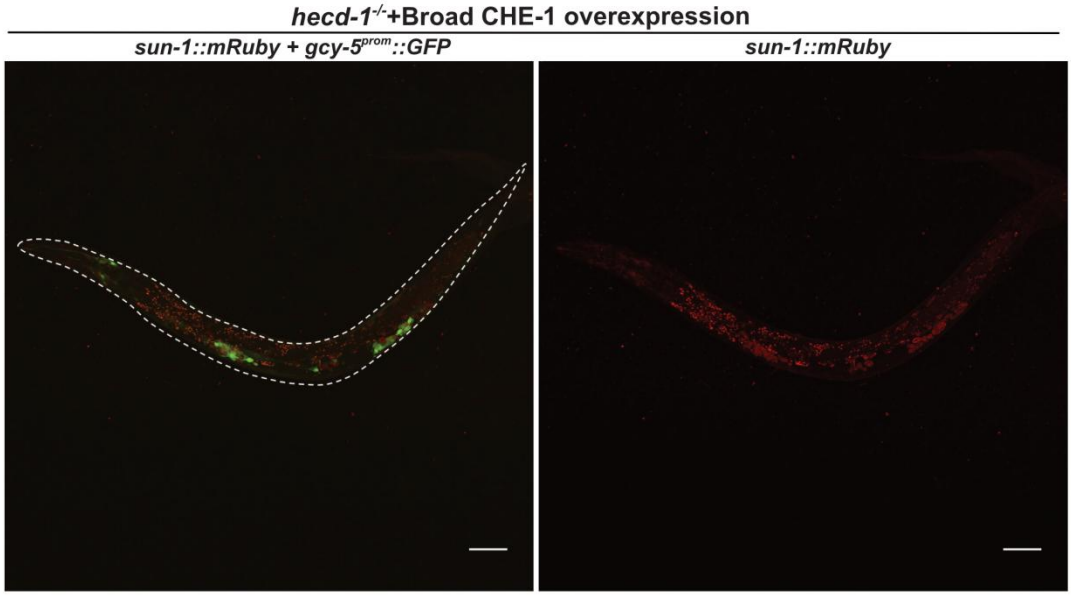

Figure2.6.6 Reduction size or a decreased number of germ cells were still capable of inducing reprogramming. Representative microscope images of *lmn-1* RNAi in *hecd-1*$^{-/-}$ strain upon CHE-1^{oe} condition. The animals exhibit incomplete germ cell development, but the surviving germ cells can still be reprogrammed into ASE neurons. Scale bar: 50 μm.

Taken together, these findings suggest that the suppression of the reprogramming phenotype by the candidate gene is not solely due to germ cell elimination.

2.7 Knockdown of *lmn-1* and *hps-90* both significantly suppress the reprogramming phenotype induced by lin-53 depletion

To investigate whether the suppressive effect is specific to the *hecd-1* depletion background or represents a general mechanism in germ cell to neuron conversion, we performed double RNAi by combining *lin-53* with these candidate target genes as a control, because germ cell conversion after *lin-53* knockdown is well established and is the reprogramming example we routinely use as a positive control in our lab.

We first placed P0 generation L4 stage worms onto double RNAi plates and screened at the L4 stage of F1 progeny (Figure 2.7.1 A). The results indicated that, while the percentage of germ cell to ASE neuron conversion showed no significant difference following knockdown of *lsm-7* and *dpf-6*, the knockdown of *cox-4*, *hsp-90*, particularly *lmn-1*, significantly decreased the reprogramming efficiency induced by *lin-53* RNAi treatment. Notably, depletion of *lmn-1* appeared to reduce approximately

half of the reprogramming phenotype observed with *lin-53* RNAi. Additionally, *lin-53* RNAi in *hecd-1*$^{-/-}$ background was performed, which resulted in low numbers, and germ cell marker expression was rarely observed after double depletion of *lin-53* and *hecd-1*.

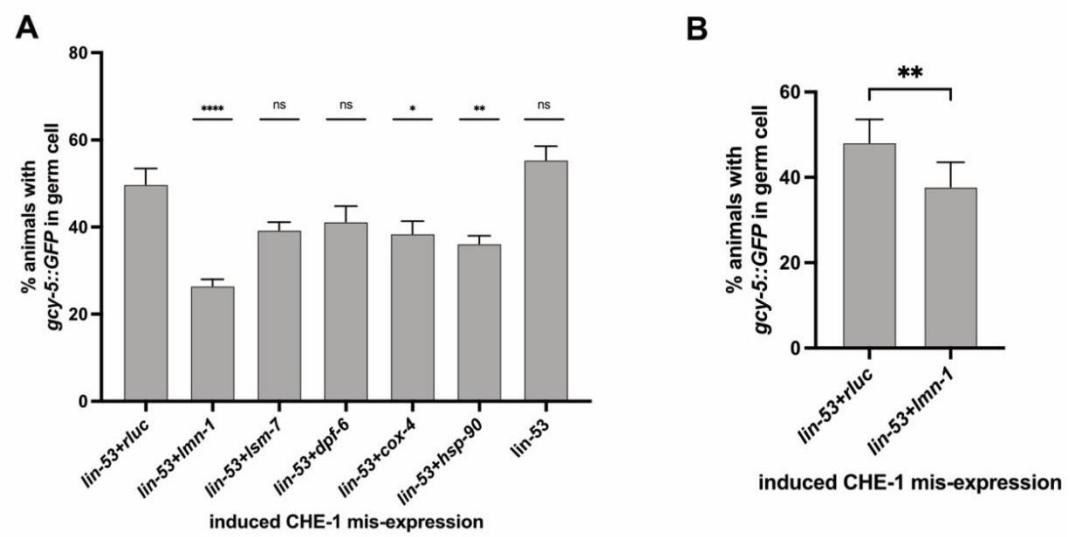

Figure 2.7 Knockdown of *lmn-1* significantly suppresses the reprogramming phenotype induced by *lin-53* RNAi. A) Quantification of double RNAi knockdown was performed using *lin-53* with *rluc* as the control, *lin-53* in combination with *lmn-1*, *lsm-7, dpf-6*, *cox-4*, and *hsp-90* as the experimental groups. The animals remained on double plates throughout the experiment. Ordinary one-way ANOVA was used for statistical comparison, **** $p<0.0001$, ** $p<0.01$, * $p < 0.05$, ns not significant. At least 300 animals were counted for each condition. Error bars: SEM. **B)** Quantification P0 generation animals showing *gcy-5*^{prom}*::GFP* induction in the germ line in double RNAi of *lin-53* with *lmn-1*, and *lin-53* with *rluc*. One-tailed paired t-test was used for statistical comparison, * $p < 0,05$. At least 300 animals were counted for each condition. Error bars: SEM.

However, the impact of *lmn-1* depletion on germ cell damage still persists, and this impact can be mistakenly interpreted as a suppression effect, as previously described. Therefore, P0 scoring was also performed to accurately assess the effectiveness of the suppression (Figure 2.7.1 B). Combining these results, knockdown of *lmn-1* and *hsp-90* strongly suppresses the reprogramming phenotype mediated by the *lin-53* knockdown, suggesting that knockdown of *lmn-1* and *hsp-90* plays a general suppressive role in the conversion of germ cells to ASE neurons.

2.8 Loss of HECD-1 does not lead to significant alterations in histone H3 modification

Next, our goal was to investigate the underlying mechanisms that enable reprogramming to occur following HECD-1 dysfunction. Due to the limited research available on the E3 ligase HECD-1, its substrates remain largely unidentified.

However, LMN-1 and H3K9me3 are interconnected in chromatin organization, suggesting that modifications in heterochromatin and nuclear lamina interactions may play a critical role in chromatin remodelling and cellular reprogramming processes.

In the context of TF-mediated reprogramming, the chromatin state of the initial cell type and the accessibility of target genes for the fate inducing TF are critical determinants of reprogramming potential. One key mechanism regulating chromatin accessibility is histone methylation. Since LMN-1 is associated with H3K9me3, the next investigation was how the chromatin methylation state is affected following the mutant or knock out of HECD-1. To test this, we started by performing the whole worm WB to analyze two classical histone methylation marks: repressive histone mark histone H3 lysine 9 trimethylation (H3K9me3), and active chromatin mark histone 3 lysine 4 trimethylation (H3K4me3). The results showed H3K9me3 and H3K4me3 levels remained unaltered compared to the control (Figure 2.8.1 A).

This suggests that global chromatin status does not change in a way that can be detected at the whole worm level, but it might change in specific tissues. To visualize the chromatin status in different tissues, immunostaining was performed, and the levels of H3K9me3 and H3K4me3 were analyzed, especially in the germ line (Figure 2.8.1 C). The fluorescence intensity of immunostained germ lines showed no significant difference between the *hecd-1(ok1437)* mutant and the control.

Subsequently, a broader panel of histone H3 modifications using Western blotting was examined, including additional histone methylation and acetylation markers. However, no significant differences were observed between HECD-1depletion background and controls (Figure 2.8.1 B).

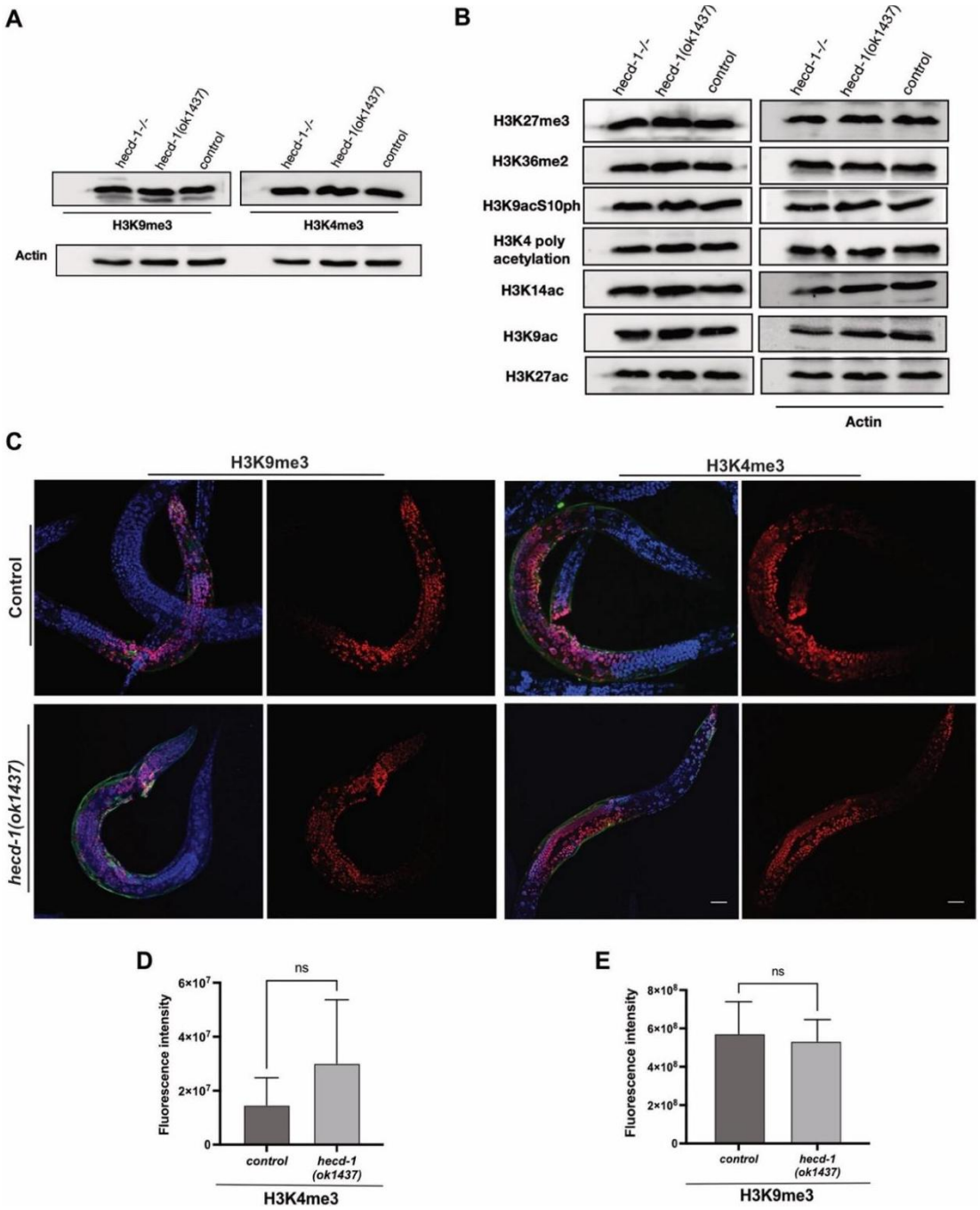

Figure 2.8 HECD-1 depletion does not drive global histone3 modification status changes. **A)** Western-blot analysis of H3K4me3 and H3K9me3 levels of whole worms treated with *hecd-1*$^{-/-}$, *hecd-1(ok1437),* and control. **B)** Western-blot analysis of H3K27me3, H3K36me2, H3K9acS10ph, H3K4 poly acetylation, H3K14ac, H3K9ac and H3K27ac levels of whole worms treated with *hecd-1*$^{-/-}$, *hecd-1(ok1437)* and control. **C)** Immunostaining of whole worms against H3K9me3 and H3K4me3 upon *hecd-1*$^{-/-}$, *hecd-1(ok1437),* and control. Red signal represented the histone methylation antibodies, green signal represented the MYO-3, which serves as an internal positive control to verify successful tissue permeabilization and overall immunostaining efficiency, and blue signal represented the DAPI. Scale bar: 50µm. **D)** Quantification of fluorescence intensities of immunostaining against H3K9me3 and H3K4me3. Paired t-test was used for statistical comparison, ns not significant; n:4. Error bar represents SEM. Scale bar: 50µm

Taken together, these observations suggest that HECD-1 mediated reprogramming is not primarily driven by global histone H3 modification changes. Specifically, the levels of H3K9me3 do not exhibit significant differences between the loss of HECD-1 and controls, indicating that the upregulation of LMN-1 may play an intermediary role in the reprogramming process.

2.9 HDA-1 acts as a suppressor of germ cell identity

In the process of validating HSP90 and LMN-1, RNAi screens were further conducted to identify additional suppressors of HECD-1 depletion mediated reprogramming, focusing primarily on proteins within the network that interact with LMN-1 and HSP-90. RNAi-mediated knockdown of *nuo-6* and *hda-1* each nearly completely rescued the reprogramming phenotype (Figure 2.9.1 A), despite being identified after the histone modification analysis.

We also confirmed the presence and integrity of germ cells by using the CRISPR strain carrying germ cell marker *sun-1::mRuby* and *hecd-1*$^{-/-}$ background. Despite the fact that *hda-1* and *nuo-6* RNAi caused severe embryonic lethality, especially *hda-1*, the surviving worms still retained germ cells (Figure 2.9.1 B).

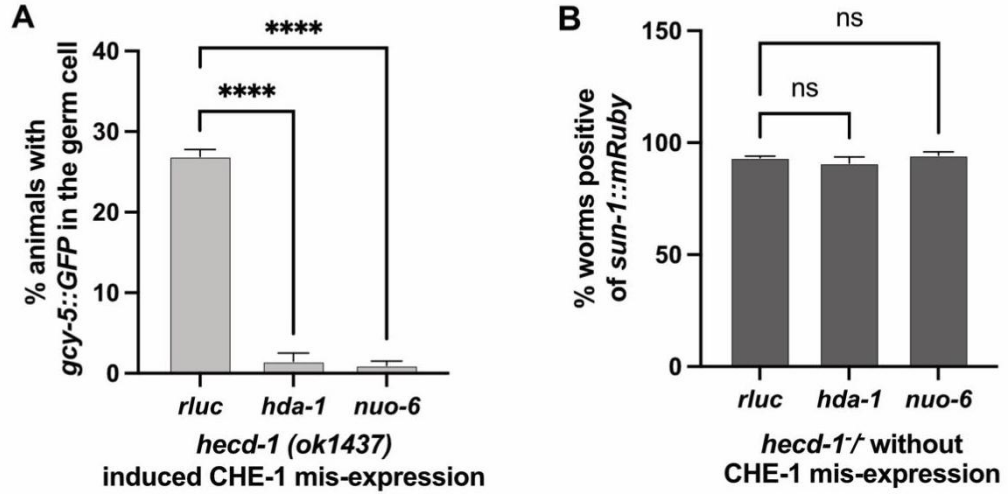

Figure 2.9.1 knockdown of *hda-1* and *nuo-6* rescues the reprogramming phenotype. A) Quantification of animals showing germ cell maker *gcy-5*^{prom}*::GFP* induction in *hecd-1(ok1437)* background upon knock down of *hda-1*, *nuo-6,* and control with CHE-1^{oe}. Ordinary one-way ANOVA was used for statistical comparison, **** $p<0.0001$. At least 300 animals were counted for each condition. Error bars: SEM. **B)** Quantification of animals showing germ cell marker *sun-1::mRuby* induction in *hecd-1*$^{-/-}$ background upon knock down of *hda-1*, *nuo-6,* and control without CHE-1^{oe}. Ordinary one-way ANOVA was used for statistical comparison, ns, not significant. At least 300 animals were counted for each condition. Error bars: SEM.

To further investigate the effect after embryonic development, RNAi of *hda-1*, *nuo-6,* and the control was performed in P0 generation. The results indicated that the

animals maintained a healthy and complete germline (Figure 2.9.2 B). Furthermore, knockdown of *hda-1* still suppressed the reprogramming efficiency of the *hecd-1* knockout (Figure 2.9.2 A), whereas the knockdown of *nuo-6* showed no significant difference.

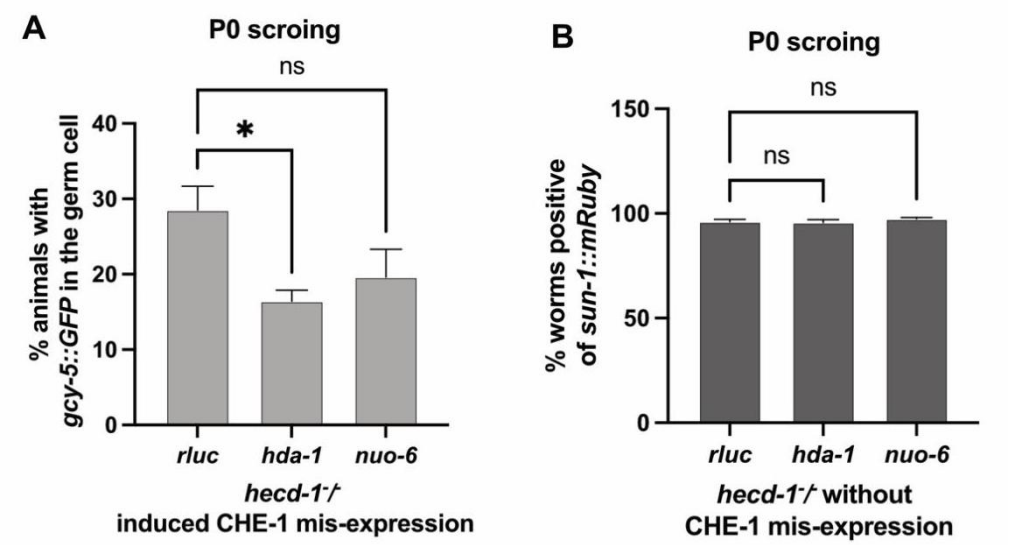

Figure 2.9.2 knockdown of *hda-1* rescues the reprogramming phenotype in P0 generation. A) Quantification of P0 generation animals showing germ cell maker *gcy-5^{prom}::GFP* induction in *hecd-1$^{-/-}$* background upon knockdown of *hda-1*, *nuo-6,* and control with CHE-1^{oe}. Ordinary one-way ANOVA was used for statistical comparison, * $p < 0,05$, ns not significant. At least 300 animals were counted for each condition. Error bars: SEM. **B)** Quantification of P0 generation animals showing germ cell marker *sun-1::mRuby* induction in *hecd-1$^{-/-}$* background upon knockdown of *hda-1*, *nuo-6,* and control without CHE-1^{oe}. Ordinary one-way ANOVA was used for statistical comparison, ns not significant. At least 300 animals were counted for each condition. Error bars: SEM.

Taken together, the results from both the F1 and P0 generations suggest that *hda-1* and *nuo-6* may function as core suppressors of the reprogramming phenotype induced by *hecd-1* depletion. Knockdown of either gene reduced the reprogramming efficiency from approximately 30% to nearly 0%.

The result for *hda-1* was unexpected. *hda-1* is an ortholog of the human genes HDAC1 and HDAC2, which encode histone deacetylases. HDACs have been implicated in heterochromatin silencing (Hayakawa and Nakayama, 2011). Under normal assumptions, depletion of these HDACs would be expected to increase reprogramming efficiency upon HECD-1 depletion by promoting heterochromatin desilencing. However, we observed the opposite effect: *hda-1* depletion significantly reduced reprogramming efficiency in the HECD-1 depletion background. This finding suggests that the silencing function of HDACs may be required to suppress the germ

cell fate. When HDA-1 accumulates due to HECD-1 depletion, this may lead to even stronger silencing of the germ cell fate. In this scenario, the original germ cell identity becomes further repressed. Conversely, knockdown of *hda-1* reduces this silencing capacity, allowing the germ cell fate to become dominant again and thereby impairing reprogramming.

Several studies have demonstrated the interactions between lamin proteins and HDACs: In many laminopathies, histone methylation and acetylation are severely affected (Columbaro et al., 2005; Evangelisti et al., 2016; Pellegrini et al., 2015). Also, Lamin A/C has been shown to interact with HDAC2 to promote its deacetylase activity (Mattioli et al., 2018). To explore this relationship in *C. elegans*, the *lmn-1::GFP* strain with the *hecd-1(ok1437)* strain was crossed first. Cells located in the middle region of the animal showed noticeable *lmn-1::GFP* accumulation, which corresponds to the area where we typically observe reprogramming (Figure 2.9.3). Therefore, further work is required to determine whether the upregulation of *lmn-1* is connected to changes in *hda-1* activity.

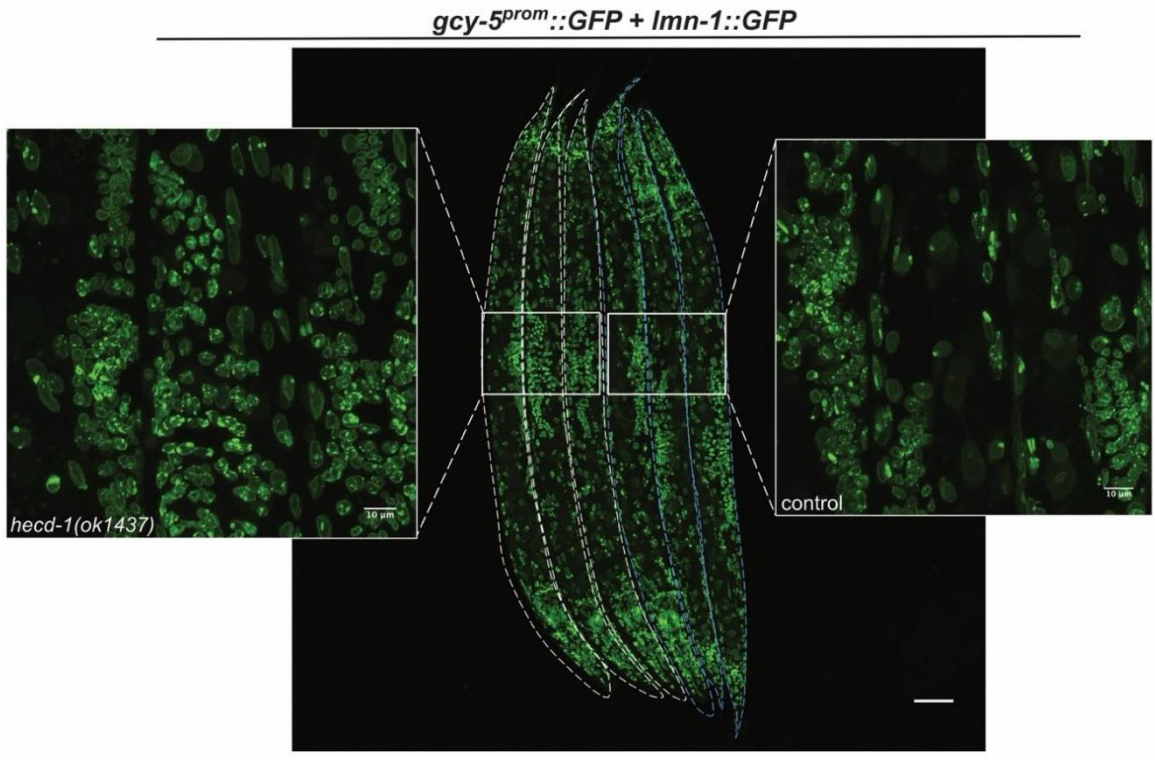

Figure 2.9.3 *lmn-1::GFP* in *hecd-1(ok1437)* and control. Representative image illustrating *lmn-1::GFP* induction in *hecd-1(ok1437)* (white dotted line) and the control (blue dotted line) in the transgenic system that combines heat shock inducible CHE-1 and *gcy-5^{prom}::GFP*. Rectangular boxes indicate the magnified regions, unlabeled scale bar: 50 µm.

Another new candidate gene, *nuo-6*, is an ortholog of human NDUFB4 (NADH: ubiquinone oxidoreductase subunit B4). NDUFB4 is a subunit of NADH-ubiquinone oxidoreductase complex I, which is essential for cellular respiration and energy production in mitochondria. An upregulated level of NUO-6 points out the presence of mitochondrial stress, which may be activated as a consequence of the accumulation of misfolded proteins resulting from *hecd-1* dysfunction. However, knockdown of *nuo-6* almost blocks the reprogramming, suggesting that the stress pathway is not merely a harmful consequence but also plays a crucial role in the reprogramming process.

2.10 Loss of HECD-1 specifically triggers the UPR^{mt}

HECD-1 has been linked to reduced ubiquitin proteasome activity and mitochondrial maintenance, implying a potential impact on energy production or metabolism (Segref et al., 2014). Based on this evidence, we hypothesize that dysfunction of HECD-1 compromises proteostasis, leading to the aggregation of misfolded proteins and the induction of stress responses. When the quantity of unfolded or misfolded proteins exceeds a compartment's protein folding capacity, eukaryotic cells activate organelle specific signaling pathways, known as unfolded protein responses (UPRs), to manage this stress (Pellegrino et al., 2013). Two cellular compartments with essential protein folding functions, the ER and mitochondria, are equipped with distinct protein stress responses, known as the ER UPR (UPR^{ER}) and the mitochondrial UPR (UPR^{mt}), respectively (Figure 2.10.1). Research in iPSCs has shown that the UPR is activated during reprogramming (Simic et al., 2019), so we hypothesized that these stress signaling pathways might serve as triggers that initiate the reprogramming program.

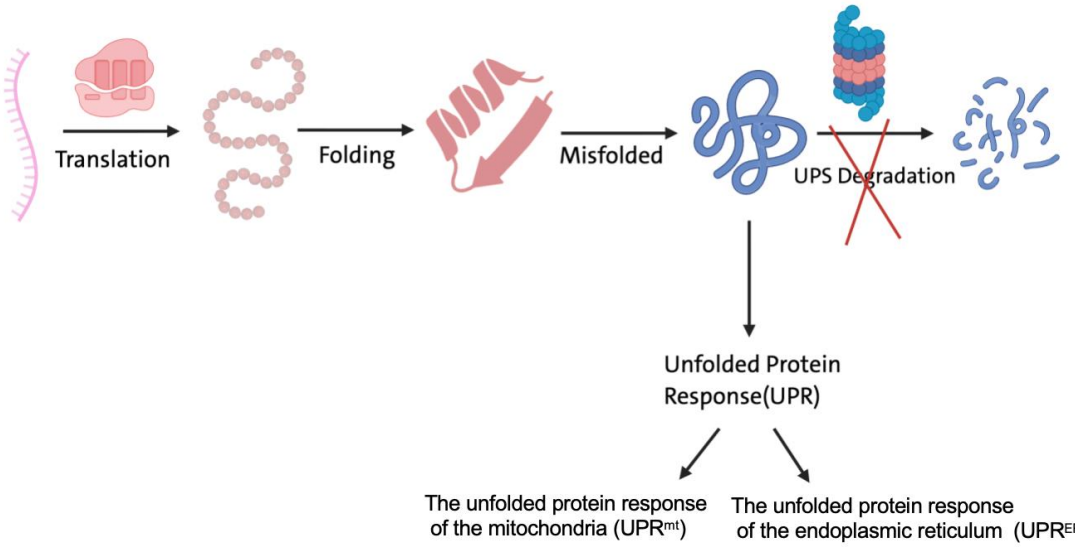

Figure 2.10.1 The unfolded protein accumulation triggers the unfolded protein response. Schematic representation when UPS degradation system defect, misfolded protein accumulation triggers the unfolded protein response: the endoplasmic reticulum unfolded protein response (UPR^{ER}), which monitors the integrity of the endoplasmic reticulum (ER), the mitochondrial unfolded protein response (UPR^{mt}), which monitors mitochondrial quality.

To investigate these stress pathways, we crossed specific fluorescent reporters: *hsp-6::GFP* (Yoneda et al., 2004) and *hsp-4::GFP* (Hertel et al., 2013) into the *hecd-1* knockout background. In the context of HECD-1 deficiency, there was a significant induction of the mitochondrial stress reporter, as shown by increased fluorescence intensity of *hsp-6::GFP* (Figure 2.10.2 A, C); however, there was no detectable activation of the ER stress reporter (*hsp-4::GFP)* was observed (Figure 2.10.2 B, D).

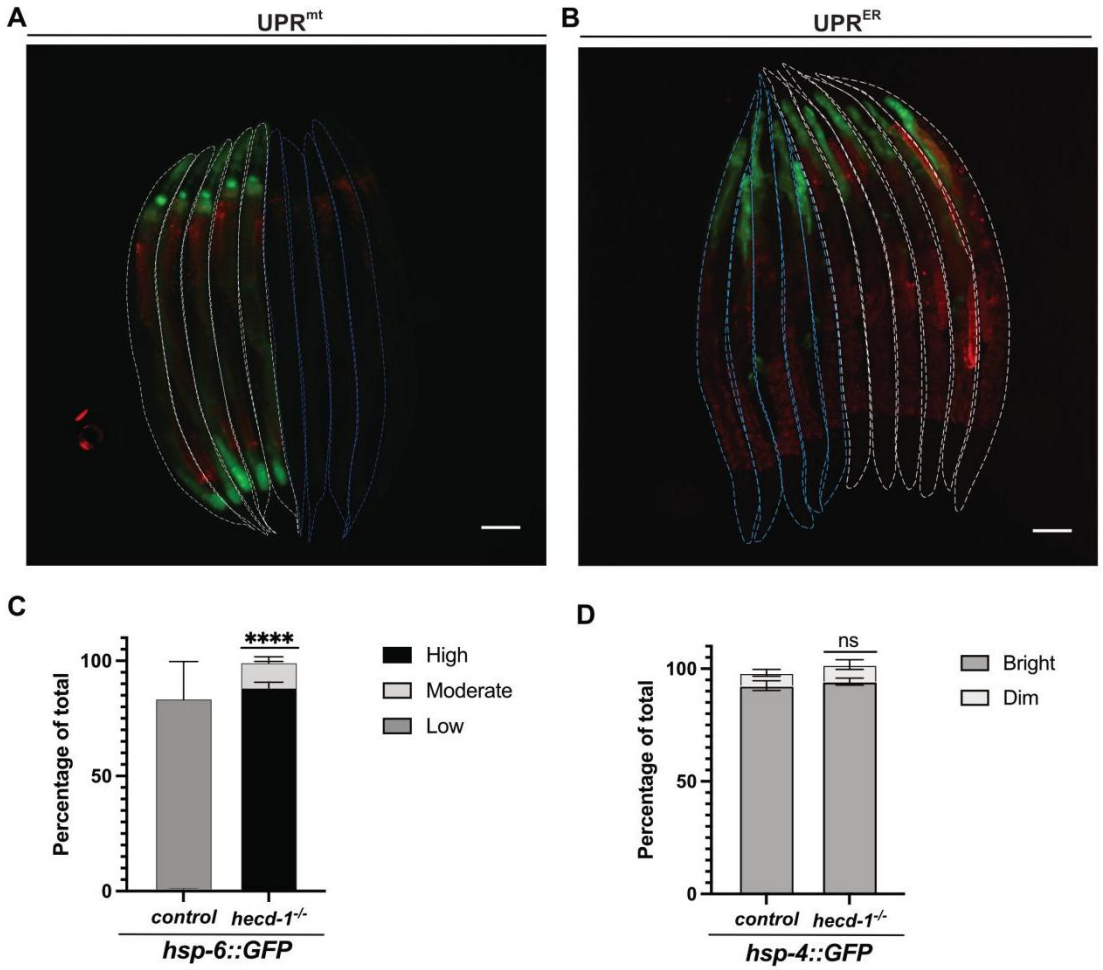

Figure 2.10.2 HECD-1 depletion induces mitochondrial unfolded protein response. A) Representative image illustrating *hsp-6::GFP* induction upon *hecd-1*$^{-/-}$ (white dotted line) and control (blue dotted line), scale bar: 100 µm.. **B)** Representative image illustrating *hsp-4::GFP* induction upon *hecd-1*$^{-/-}$ (white dotted line) and control (blue dotted line). **C, D)** Quantification of *hsp-6::GFP* **C)** and *hsp-4::GFP* **D)** induction upon *hecd-1*$^{-/-}$ compared to control. Ordinary two-way ANOVA was used for statistical comparison, **** $p<0.0001$, ns not significant.

These results indicate that loss of HECD-1 specifically triggers UPR^{mt} stress. The previously observed protein level changes in HSP-90, COX-4, and NUO-6 previously indicated the presence of mitochondrial stress. In addition, knockdown of all three candidate genes strongly suppressed the reprogramming phenotype caused by *hecd-1* depletion, suggesting that they may play important roles in the reprogramming process mediated by loss of HECD-1.

3. Discussion

3.1 UPS factors act as reprogramming barriers of germ cell to ASE neuron conversion

The field of cellular reprogramming offers a promising approach for generating human tissues for therapeutic applications. It holds significant potential for advancing regenerative medicine and disease modelling. However, its clinical translation is currently constrained by critically low efficiencies, primarily due to robust biological barriers that impede the reprogramming process (Brumbaugh et al., 2019; Haridhasapavalan et al., 2020). The first barrier to reprogramming was identified by Tursun and colleagues, who characterized safeguarding mechanisms that maintain cellular identity during germ cell to neuron conversion and described the role of the histone chaperone LIN-53 within this protective framework (Tursun et al., 2011). Since then, a number of reprogramming barriers have been identified in *C. elegans* as well as in other species, which serve to preserve cellular identity across a diverse range of tissues and cell types (Ebrahimi, 2015; Kolundzic et al., 2018). While epigenetic regulation plays a crucial role in cellular safeguarding mechanisms, emerging evidence indicates that cell fate determination is governed by a complex network in which alterations in one component can trigger a cascade of events, ultimately leading to changes in cell fate. Despite these advances, our understanding of the underlying mechanisms remains limited.

The UPS factors, specifically *hecd-1*, *eel-1,* and *math-33,* were identified as barriers of germ cell to ASE neuron conversion. Knockdown of any of these genes consistently resulted in detectable conversion of germ cells to ASE neurons upon ectopic expression of the TF CHE-1. Ubiquitination by the UPS is a key posttranslational modification, and its role in the regulation of pluripotency was recently uncovered in a UPS-targeted RNAi screen (Buckley et al., 2012). Among these three validated genes, two HECT E3 ubiquitin ligases: *eel-1* and *hecd-1*, which are homologs of HUWE1 (Zahreddine et al., 2010) and HECTD1 (Chen and Greenwald, 2015), respectively, as well as *math-33*, a deubiquitinating enzyme homolog of UPS7 (McCloskey and Kemphues, 2012). In *C.elegans*, EEL-1 promotes DNA damage-induced germ cell apoptosis (Ross et al., 2011) and can regulate neuronal function and development (Opperman et al., 2017). MATH-33 has been

implicated in processes related to metabolism and longevity (Heimbucher et al., 2015), its human ortholog, USP7, is known to associate with chromatin and participates in epigenetic control of gene expression (Pozhidaeva and Bezsonova, 2019). The other type of HECT E3 ubiquitin ligase, HECD-1, is involved in quality control regulation during development and can act as both a positive and a negative modulator of Notch activity in *C. elegans* (Chen and Greenwald, 2015). Further details on this will be discussed in the subsequent chapter.

Taking those together, we identified three UPS factors as barriers in the context of TF-mediated reprogramming. These findings pose a novel regulatory role of posttranslational mechanisms in cell fate determination.

3.2 E3 ligase HECD-1 safeguards germ cell identity

This study identified HECD-1 as a novel barrier to TF-induced reprogramming. Unlike MATH-33 and EEL-1, or other previously identified barriers in our group, deletion and knock out of HECD-1 are compatible with survival. Critically, this non-lethal property is conserved in humans; missense variations of the human ortholog HECTD1 have been reported as non-lethal in clinical samples (Zerafati-Jahromi et al., 2025).

Depletion of *hecd-1* via RNAi or CRISPR-mediated mutation successfully induced an ASE neuron fate, validated by reporter expression and the disappearance of germ cell maker expression and switch to neuronal marker expression (Figure 2.6.1 C). Furthermore, smFISH results supported endogenous expression of neuronal genes during this process. This extensive and specific conversion into neuron-like cells suggested HECD-1 plays a crucial role in cell fate safeguarding. However, the current understanding of the function of *hecd-1* remains incomplete.

HECD-1 is a member of the HECT (Homologous to E6AP C Terminus) domain E3 ligase family. Numerous studies have demonstrated that E3 ligases are important players in cancer progression, explainable by their regulatory participation in most cellular processes, including cancer relevant processes, highlighting their potential as specific therapeutic targets (Sampson et al., 2023). In particular, several HECT E3 ligases contribute to tumorigenesis by modulating the ubiquitination levels of substrates that exhibit either tumor suppressive or oncogenic functions (Bernassola et al., 2019). The ortholog of HECD-1, HECTD1, has been reported to regulate diverse

biological processes, including signal transduction, gene transcription, development, and lipid homeostasis (Aleidi et al., 2018; Sarkar and Zohn, 2012; Sugrue et al., 2019; Tran et al., 2013). The yeast ortholog of HECD-1, *Ufd4p*, functions as a quality control ubiquitin ligase involved in clearing misfolded and aggregated proteins, with evidence for feedback regulation in this process (Hwang et al., 2010; Ju and Xie, 2006; Theodoraki et al., 2012). In *C. elegans*, studies have demonstrated that HECD-1 is involved in chromatin remodelling during developmental processes (Lampersberger et al., 2023) and directly influences the Notch signalling pathway, which is essential for cell fate decision (Chen and Greenwald, 2015).

Although the specific substrate of HECD-1 remains unknown, mutations in *hecd-1* that lead to reduced ubiquitin-proteasome activity have been reported previously (Segref et al., 2014). This suggests that dysfunction of HECD-1 may cause the accumulation of misfolded proteins, thereby disrupting proteostasis. Stem cells are thought to exhibit elevated proteostasis capacity, and defects in this system can impair the maintenance of pluripotency in ESCs as described before. In this study, knockdown of HECD-1, a component of the PN, induced reprogramming events. The possible explanations may account for this finding: First, both iPSCs and hESCs have thus far been generated only *in vitro* and not *in vivo*, indicating that the *in vivo* environment is more complex and may permit reprogramming. Second, some HECT-type E3 ligases have been shown to play dual roles in tumorigenesis by functioning as both tumor promoters and suppressors (Kao et al., 2018; Koganti et al., 2018). Third, subsequent mass spectrometry analyses revealed increased levels of another E3 ligase, EEL-1, as well as an additional barrier we identified, indicating that proteostasis represents a dynamic and compensatory system: a defect in one component may trigger elevated activity in others to maintain overall proteostasis.

3.3 Cellular safeguard mechanism of HECD-1 may be cell type specific and protect against specific fates

RNAi-mediated depletion of *hecd-1*, *hecd-1* loss-of-function mutants, and *hecd-1* knockout all allowed reprogramming only in germ cells. This is consistent with previous findings on the histone chaperone LIN-53 (Tursun et al., 2011) and FACT complex members (Kolundzic et al., 2018). These observations suggest the existence of tissue-specific cell fate maintenance mechanisms. One possible explanation is the

intrinsic plasticity of germ cells, which may enable them to be reprogrammed more easily upon perturbation compared to other cell types. This idea is supported by the results from a whole genome RNAi screen performed by Ena Kolundzic (Kolundzic et al., 2018), which also forms the basis of our current project. This screen revealed that germ cells exhibited the highest percentage of reprogramming phenotype, accounting for approximately 58% of the total number of observed conversion events.

These results suggest that HECD-1 plays a role in safeguarding cell fate against reprogramming towards at least neuronal lineages, such as ASE and GABAergic neurons. However, no HLH-1-mediated reprogramming towards muscle fate was observed. These findings are also similar to the previous reports involving depletion of FACT complex and LIN-53, both of which allow reprogramming to neuronal fate, not to the muscle fate. These negative results may provide a hint towards a target selectivity of HECD-1, considering that human orthologs of *hecd-1* variants are associated with a variable (Zerafati-Jahromi et al., 2025), highlighting its important role in neurodevelopment. Together, these results raise the possibility that HECD-1 may specifically restrict the developmental potential towards a neuronal differentiation pathway, while different factors might function to inhibit the activation of other, non-neuronal differentiation programs.

3.4 Proteomic changes by HECD-1 depletion contribute to reprogramming

It is well established that cells use ubiquitylation controls nearly every step of transcription, including the direct regulation of TFs (Mark and Rape, 2021). Because overexpression of the TF CHE-1 is induced by heat shock, and heat shock itself can be perceived as a form of cellular stress, the slightly reduced CHE-1 expression levels observed in the *hecd-1* mutant compared to the control. This likely reflects an endogenous attempt to mitigate proteotoxic stress and maintain proteostasis. Nevertheless, CHE-1 expression remained markedly higher than in the WT, demonstrating that the heat-shock inducible transgenic overexpression system had been successfully established.

Drastic proteomic changes have been observed during reprogramming of somatic cells to pluripotency, including alterations in mitochondrial proteins and chromatin modification proteins (Hansson et al., 2012). In the context of the direct reprogramming, we did not solely compare the protein level changes between the

hecd-1 mutant and WT. To distinguish the actual drivers of cellular reprogramming from non-specific protein aggregation resulting from impaired degradation due to loss of function of HECD-1, we performed an RNAi suppressor screen, which provided compelling functional validation of our hypothesis.

Crucially, rigorous experiments utilizing the germ cell marker strain further confirmed that the suppression was not a secondary artifact caused by germ cell elimination. Although the knockdown of *lmn-1* partially compromised germline integrity, the suppressive effect on reprogramming remained statistically significant even after accounting for this partial loss of cells. Notably, *hecd-1* depletion mediated reprogramming is predominantly localized to the proximal germline near the vulva. We observed that as long as the germ cells within this specific anatomical region remained viable, reprogramming events could still be detected, even if the overall structural integrity of the germline was perturbed. Therefore, the profound reduction in reprogramming efficiency reflects a genuine mechanistic requirement for LMN-1 in the cell fate transition, rather than mere tissue destruction.

Taken together, one function of *hecd-1* is to regulate ubiquitin-proteasome activity, and loss of *hecd-1* leads to the accumulation of misfolded proteins. Mass spectrometry data support this conclusion by revealing an upregulated pool of proteins. Knockdown of these upregulated proteins produced two distinct outcomes. First, knockdown of accumulated proteins that are harmful to the proteostasis environment did not affect the reprogramming phenotype; in some cases, it even contributed to a healthier phenotype with improved reprogramming qualification. Second, and more importantly, knockdown of candidate genes that truly contribute to the reprogramming led to a suppressive effect on the *hecd-1* depletion phenotype, and this effect was independent of germ cell elimination, indicating a genuine role for these genes in the reprogramming process.

3.5 Knockdown of HSP-90 and LMN-1 general suppress TF CHE-1 mediated germ cell to ASE neuron conversion

Results from the RNAi suppressor screen indicated that HSP-90 and LMN-1 almost block the HECD-1 depletion mediated reprogramming phenotype (Figure 2.6.2). Furthermore, these two genes were also required for LIN-53 depletion

mediated reprogramming, but they did not exert as strong a suppressive effect as observed with HECD-1 depletion. The observed differences may reflect distinct pathways in which LIN-53 and HECD-1 function. Previous studies have linked LIN-53 to reprogramming through its association with the Polycomb repressive complex 2 (PRC2) (Patel et al., 2012), which is the sole identified methyltransferase with activity toward H3K27 and is responsible for all H3K27 methylation in mouse ESCs (Højfeldt et al., 2018; Laugesen et al., 2019). The following experiments showed no significant change in the level of H3K27me3, suggesting that LIN-53 and HECD-1 operate through different pathways during TF-mediated reprogramming.

Hectd1, the human ortholog of HECD-1, has been shown to regulate the intracellular localization and secretion of HSP90 in the context of neural tube defects (Sarkar and Zohn, 2012). Unlike conventional chaperone systems, HSP90 appears to be a specialized chaperone primarily involved in signal transduction pathways, including those mediated by TFs and protein kinases (Buchner, 1999; Taipale et al., 2014). It has been described as a crossroads of genetics and epigenetics, highlighting its dual role in safeguarding genome integrity and enabling rapid adaptation to environmental stresses through modulation of genomic mutations and epigenetic states (Wong and Houry, 2006). Over the past decade, several small-molecule inhibitors targeting HSP90 have been developed and recognized as promising anticancer agents (Whitesell and Lindquist, 2005). Interestingly, HSP90 also functions as a chromatin remodeling regulator responsive to environmental cues, capable of switching chromatin between permissive and non-permissive transcriptional states (Condelli et al., 2019).

While no direct evidence currently establishes a connection between LMN-1 and HECD-1, our research suggests the potential of LMN-1 to serve as a substrate for HECD-1. *C. elegans* possesses a single lamin gene, *lmn-1* (also known as Ce-lamin) (Lui et al., 2000). In mammals, the lamin protein family is encoded by three lamin genes and is classified as A-type and B-type lamins (Butin-Israeli et al., 2012). Lamins are among the most prominent and extensively studied proteins in animals, and lamin-associated diseases in humans are referred to as laminopathies (Worman et al., 2010). Changes in nuclear morphology, including alterations in shape, size, lobulation, and the appearance of heterochromatin and nucleoli, are used to assess tumor development (Zink et al., 2004). Heterogeneous expression of nuclear lamins,

particularly Lamins A/C, has been observed in tumor cells obtained from cancers of the ovary (Capo-chichi et al., 2011), colon (Willis et al., 2008), gut (Machiels et al., 1995), blood (Agrelo et al., 2005), prostate (Helfand et al., 2012), lung (Wu et al., 2009), and breast (Capo-chichi et al., 2011). These findings suggest that lamin A/C expression could serve as a potential biomarker for cancer risk (Willis et al., 2008). A decrease in lamin B1 expression has been noted in gastrointestinal (Moss et al., 1999) and lung cancers (Broers et al., 1993), whereas increased levels have been reported in malignant prostate cancer and hepatocellular carcinoma, indicating its potential as a diagnostic and prognostic marker (Coradeghini et al., 2006). Recent research also identified lamin B deficient and lamin A/C enriched microdomains within prostate cancer cell nuclei, which are associated with specific chromosomal regions and decreased gene expression.

LMN-1 represents a notable finding. During direct reprogramming of germ cells into neurons, the nuclear morphology also changes, similar to that observed in tumor development, indicating that alterations in nuclear architecture are essential for the transition from one cell type to another. Notably, heterogeneous expression of lamin genes plays an important role in this process.

3.6 HDAC represses germ cell identity

Histone ubiquitylation is known to influence other chromatin modifications, such as acetylation (Ricci et al., 2002; Turner et al., 2002) and methylation (Briggs et al., 2002; Sun and Allis, 2002). Furthermore, LMN-1 acts as an essential component in maintaining the spatial organization of H3K9me3 dependent heterochromatin (Harr et al., 2020; Van Steensel and Belmont, 2017), as well as the observation that hypermethylated H3K4 decreases following the overexpression of wild type lamin A in C2C12 myoblasts (Håkelien et al., 2008). Additionally, inhibition of HSP90 leads to a switch from active to repressed chromatin by degrading Trithorax Group (TrxG) which induces H3K4me3 (Jarosz, 2016; Kingston and Tamkun, 2014; Schuettengruber et al., 2007). Therefore, we hypothesized that changes in cellular processes and proteomic profiles may be required to render a cell permissive for TF mediated reprogramming by increasing chromatin accessibility for TF binding. However, no differences were observed in histone H3 modifications of HECD-1-dysfunctional worms, suggesting that the effect may not be mediated through histone H3 modifications.

Although *hda-1* showed an apparent upregulation in the mass spectrometry data analysis, its expression level was very close to the threshold, and knockdown of *hda-1* resulted in a significant suppression effect on HECD-1 depletion mediated reprogramming. HDA-1 is an ortholog of the human genes HDAC1 (histone deacetylase 1) and HDAC2 (histone deacetylase 2), which are frequently found overexpressed in various types of cancer (J. Song et al., 2005). Histone acetylation is removed by HDACs, and chromatin regions bound by HDACs are typically transcriptionally inactive (Shahbazian and Grunstein, 2007). While drugs targeting HDACs are commonly employed to enhance reprogramming efficiency, in our case, inhibiting HDAC activity did not improve reprogramming but nearly completely rescued the reprogramming phenotype induced by HECD-1 depletion. This counterintuitive finding parallels the clinical reality of HDAC inhibitors in oncology, where their anticancer mechanisms are highly context-dependent and notably non-uniform. Indeed, elevated levels of HDACs are frequently implicated in maintaining aberrant cell states in various cancers and tumors (Eckschlager et al., 2017).

During reprogramming, repression of the original cell fate is a crucial initial step. As a key transcriptional repressor, this study suggests that *hda-1* may primarily suppress the germ cell identity rather than the reprogrammed cell identity. Knockdown of *hda-1* contributes to maintaining germ cell identity; thus, the increased level of *hda-1* resulting from HECD-1 depletion could further inhibit germ cell identity, thereby creating a permissive environment for reprogramming (Figure 3.1).

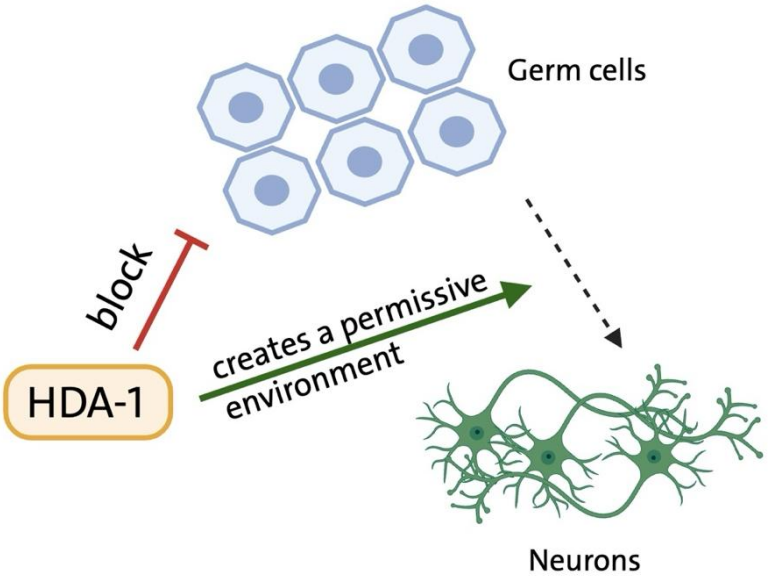

Figure 3.1 HDA-1 functions as a suppressor of germ cell identity. HDA-1 inhibits germ cell fate and creates a permissive environment that facilitates the reprogramming process.

Lamin A/C has been reported to function as a scaffold that facilitates the recruitment of histone-modifying enzymes, such as PCAF and HDAC2, to chromatin (Murray-Nerger and Cristea, 2021; Santi et al., 2020). Studies also show the co-expression of lamin A/C and HDAC2 favors histone deacetylation, strongly suggesting that lamin A/C contributes to HDAC2 activation and promotes its recruitment to specific gene promoters (Mattioli et al., 2018).

In this context, it remains unclear whether LMN-1 and HDA-1 are directly substrates of HECD-1 or whether the increased levels of LMN-1 directly lead to elevated HDA-1 activity. Alternatively, other relationships may exist between LMN-1 and HDA-1. For example, increased lamin could serve as a nuclear scaffold that physically anchors and stabilizes the repressive chromatin state mediated by HDACs, further reinforcing gene silencing during reprogramming. These possibilities highlight the complex interplay between nuclear architecture and chromatin modification in regulating cell fate transition.

3.7 The potential role of UPR^{mt} for HECD-1 depletion mediated reprogramming

Upon loss of HECD-1, the imbalance of proteostasis triggers the UPR, specifically activating the UPR^{mt} as indicated by the strong induction of the marker *hsp-6::GFP*. Previous studies have shown that the HDAC HDA-1 and the histone demethylases JMJD-3.1 and JMJD-1.2 are essential for UPR^{mt} related gene expression (Merkwirth et al., 2016; Shao et al., 2020). Since both JMJD-3.1 and

JMJD-1.2 function as H3K27me3 demethylases and no changes were observed in global H3K27me3 levels, the activation of the UPR^{mt} in this context is likely mediated through the HDA-1 dependent pathway.

In the suppressor screen, the candidates *nuo-6* and *cox-4* are both upstream triggers of UPR^{mt} activation. NUO-6 is an ortholog of human NDUFB4 (NADH: ubiquinone oxidoreductase subunit B4), and COX-4 is an ortholog of human COX4I1 (cytochrome c oxidase subunit 4I1) and COX4I2 (cytochrome c oxidase subunit 4I2). The mitochondrial protein-folding environment can be compromised by excessive reactive oxygen species (ROS) produced mainly by the NADH-ubiquinone oxidoreductase (complex I) and the ubiquinol cytochrome c oxidoreductase (complex III) of the electron transport chain (Hamanaka and Chandel, 2010; Tormos et al., 2011). Reprogramming somatic cells with the TFs Oct4, Sox2, Klf4, and c-Myc induces oxidative stress and markedly elevates ROS levels in both *in vitro* (Banito et al., 2009) and in *vivo* (Chiche et al., 2017; Mosteiro et al., 2016) settings. Our results indicate that ROS signaling is activated during reprogramming; importantly, depletion of ROS significantly impairs reprogramming efficiency. These observations align with previous reports suggesting that ROS signaling must be maintained at optimal levels to facilitate the transition to pluripotency (Zhou et al., 2016).

Several studies have shown that cells undergo substantial metabolic and mitochondrial remodeling during reprogramming in order to achieve the newly acquired cellular state (Bukowiecki et al., 2014; Rastogi et al., 2019; Xu et al., 2013). In addition, mitochondria can influence nuclear function by modulating the levels of key metabolites that affect gene expression, including ATP, acetyl-CoA, NAD+, and ROS (Andreux et al., 2013). Based on this, we hypothesized that activation of the UPR^{mt} may regulate transcriptional activity. During mitochondrial stress, ATFS-1 (a key regulator of UPR^{mt}) is not imported into mitochondria and instead accumulates in the nucleus, where it directly promotes the transcription of nuclear genes such as *hsp-6*. Within the specific reprogramming context of this study, we propose that UPR^{mt} facilitates the transcriptional activation of the cell fate inducing TF CHE-1. By potentially enhancing the endogenous regulation of TF CHE-1 or synergizing with it at target chromatin loci, UPR^{mt} provides the critical transcriptional boost required to overwrite the original germ cell identity and establish the new neuronal network.

To systematically summarize the role of the UPR^{mt} in facilitating direct reprogramming, we propose a comprehensive mechanistic model (Figure 3.2). This model aims to guide further investigation into how HECD-1 functions as a cellular safeguard and exerts its effects through its mitochondrial functions, influencing transcription activity and the promotion of molecular chaperones.

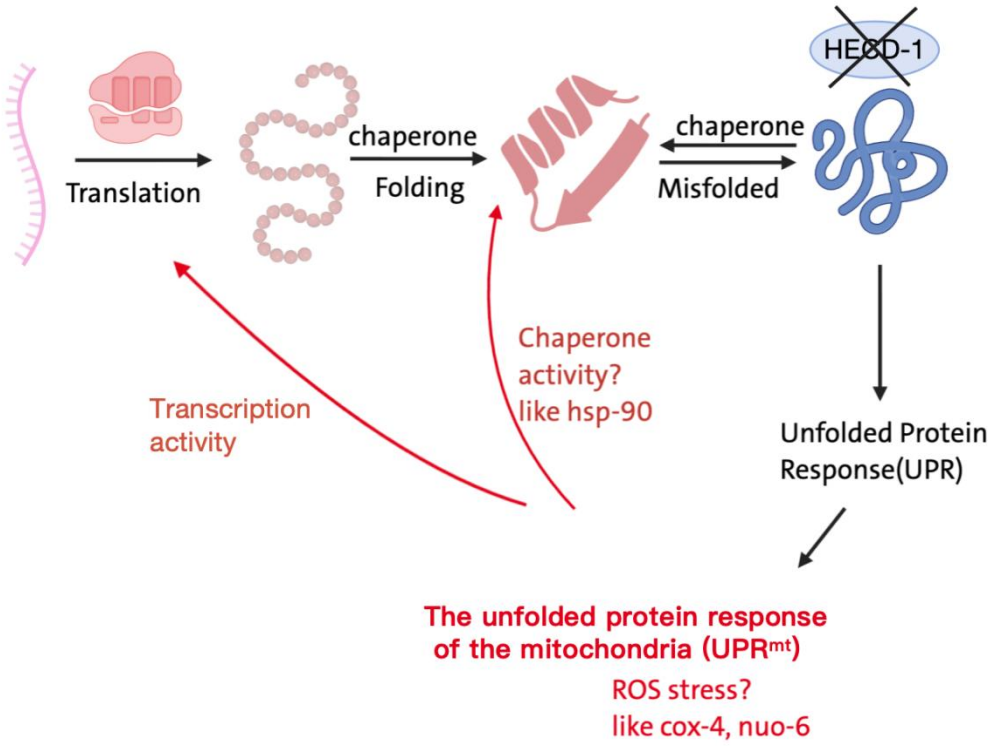

Figure 3.2 Proposed model of the potential role of UPR^{mt} in HECD-1 depletion mediated reprogramming. Impaired HECD-1 mediated protein degradation leads to an accumulation of misfolded proteins, which activates UPR^{mt}. This targeted activation may drive processes essential for cellular plasticity: (1) generating a transient ROS signal through mitochondrial components such as COX-4 and NUO-6, that promotes metabolic remodeling to enhancing transcriptional activity needed to establish the new cell fate; (2) increasing molecular chaperone activity (e.g., HSP90) to maintain proteostasis and may assist in the folding of newly synthesized proteins required for neuronal differentiation.

3.8 Conclusions and future perspective

Proteostasis is a highly interconnected system, and dysfunction of any single component can trigger a cascade of changes that appear unrelated but are, in fact, tightly linked. In this study, loss of HECD-1 led to the significant upregulation of 471 proteins and enabled the reprogramming of germ cells into ASE neurons upon TF CHE-1^{oe}. This study confirms the expected role of HECD-1 in protein degradation but also reveals its previously unappreciated function in safeguarding cell fate in *C.*

elegans. Most reprogramming barriers identified are chromatin regulators that directly influence gene accessibility, thereby determining whether TFs can successfully induce cell fate changes (Cheloufi et al., 2015; Kolundzic et al., 2018; Tursun et al., 2011). The conventional dogma of molecular biology is a hierarchy from DNA to RNA to protein; the proteome is typically viewed as a downstream consequence of genomic and epigenomic regulation. In this context, the identification of an E3 ubiquitin ligase as a barrier of reprogramming broadens our understanding of how cell fate protection mechanisms operate.

This study's mechanistic investigations revealed a counterintuitive role for the histone deacetylase HDA-1 in this process. Typically, HDACs contribute to chromatin condensation and gene silencing; thus, it would be expected that the knockdown of *hda-1* would induce a more open chromatin state and facilitate reprogramming. Paradoxically, in the context of HECD-1 depletion, the knockdown of *hda-1* achieved the exact opposite effect: it promoted the maintenance of the original germ cell identity, thereby rendering the cells highly refractory to reprogramming. Additionally, the Western blot results demonstrate that the regulation of HDA-1 is independent of global histone H3 marks, including H3K27me3, H3K9me3, and H3K36me2/3. Further investigation is to ensure the effect of *hda-1* by performing ChIP-Seq to determine how HDA-1 selectively erases the germline program to license neuronal reprogramming.

Furthermore, the specific activation of UPR^{mt} following HECD-1 depletion suggests that the stress pathway actively contributes to the reprogramming process. To determine conclusively whether the UPR^{mt} functions as a causal driver or merely as a secondary consequence of HECD-1 dysfunction, future studies should focus on ATFS-1, the master transcriptional regulator of the UPR^{mt}. Knocking down *atfs-1* would effectively disable the UPR^{mt} transcriptional program. If knockdown of *atfs-1* suppresses the *hecd-1* depletion induced reprogramming phenotype, it would demonstrate that ATFS-1 dependent UPR^{mt} activation is mechanistically required for cell fate conversion. Conversely, if the reprogramming phenotype persists despite the loss of ATFS-1, this would indicate that UPR^{mt} activation is simply a byproduct of proteotoxic stress. In that case, elevated levels of ROS – potentially generated through the accumulation of mitochondrial substrates such as NUO-6 and COX-4 – may instead serve as the direct trigger for reprogramming. This alternative model could be

readily evaluated by treating animals with specific ROS inhibitors. Therefore, to understand the exact relevance of the UPR^{mt} in the reprogramming process, it is crucial to experimentally uncouple the transcriptional stress response from the metabolic byproducts of mitochondrial dysfunction.

Overall, this study underscores the potential of *in vivo* cellular reprogramming as a powerful tool for uncovering the mechanisms that safeguard cell fate. Strikingly, it was observed that the perturbation of a single gene (*hecd-1*) can trigger a profound systemic cascade, which ultimately drives the direct transdifferentiation of germ cells into neurons. The success of reprogramming relies not only on epigenetic modifications but also on additional factors. It is proposed that changes in nuclear morphology induced by *lmn-1*, together with the ability of HSP90 to promote the proper folding of newly synthesized proteins, collaboratively execute the cell fate transition. Conversely, stable nuclear morphology and protein folding are equally essential for maintaining cell fate. In a broader context, unraveling these deeply conserved safeguarding mechanisms in *C. elegans* holds translational potential for human biology, offering crucial insights for the advancement of regenerative medicine and the development of future cellular therapies.

4. Materials

The reagents, chemicals and kits are given in the relevant section.

The Equipment was purchased from Eppendorf, Bio-rad Laboratories, Thermo Fisher Scientific.

Ultra pure water was produced by using Millipore Super-Q System.

Sanger sequencing was performed by Eurofins Genomics, Ebersberg.

Oligonucleotide synthesis was performed by Sigma-Aldrich, Taufkirchen and Eurofins Genomics, Ebersberg.

Repair templates for CRISPR were synthesized from integrated DNA Technologies (IDT).

Genome-wide *C.elegans* RNAi collection (Ahringer) was purchased from Source BioScience.

4.1 *C.elegans* strains

Table 4.1 *C.elegans* strains used and generated in the study

Name	Genotype
N2	*C.elegans* wildtype variant Bristol
BAT028	*otIs305 (hsp::che-1::3xHA) V; ntIs1 (gcy-5::GFP) V*
BAT326	*otIs263 [ceh-36p::tagRFP]; otIs305 [hsp::che-1::3xHA]; ntIs1 [gcy-5::GFP]V*
BAT527	*otIs355 [rab-3::NLS::TagRFP]; otIs305 [hsp-16.2p::che-1::3xHA, rol-6(su1006)] ntIs1 [gcy-5p::GFP, lin-15(+)] V*
BAT522	*otIs305 [hsp::che-1::3xHA] ntIs1 [gcy-5::GFP] V.; otis393 [ift-20::NLS::tagRFP]*
BAT684	*juIs8 [unc-25::GFP]; barEx147 [hsp-16.2/4::unc-30]*
BAT713	*barIs90 [hsp-16.2/4::unc-30; rol-6(su1006)]; juls8[unc-25::gfp]*
BAT730	*otIs355 [rab-3::NLS::TagRFP] IV; barEx147 [hsp-16.2/4::unc-30]*
BAT857	*hecd-1(ok1437)* IV; *otIs305 [hsp-16.2p::che-1::3xHA, rol-6(su1006)], ntIs1 [gcy-5p::GFP,lin-15(+)]* V
BAT852	*otIs305 (hsp::che-1::3xHA) V, ntIs1 (gcy-5::GFP) V; hecd-1 (ok1450) I*
RB1334	*C34D4.14(ok1450) IV.*
RB1319	*C34D4.14(ok1437) IV.*
CA1199	*unc-119(ed3) III; ieSi38 IV.*
CA1200	*ieSi57 II; unc-119(ed3) III.*
CA1219	*unc-119(ed3) III; ieSi21[sun-1p::sun-1::mRuby::sun-1 3'UTR + Cbr-unc-119(+)] IV*

CA1319	*plk-2(ok1936) I; ieSi21[sun-1p::sun-1::mRuby::sun-1 3'UTR + Cbr-unc-119(+)] IV; sun-1(ok1282) V.*
LW0698	*lmn-1::gfp[lmn-1p::lmn-1::gfp::lmn-1 3'UTR) + pMH86(dpy-20(+)]*
VC1100	*Y67D8C.5(ok1575) IV.*
RB2194	*math-33(ok2974) V.*
BAT2263	*barSi83(math-33::AID degron::3xHA) ; V.*
BAT2295	*ieSi38 [sun-1p::TIR1::mRuby::sun-1 3'UTR + Cbr-unc-119(+)] IV.; barSi83(math-33::AID degron::3xHA) ; V.*
BAT2369	*otIs305 (hsp::che-1::3xHA) V, ntIs1 (gcy-5::GFP) V; hecd-1 (ok1437) IV; pJKL380.4 [lmn-1p::lmn-1::gfp::lmn-1 3'UTR) + pMH86(dpy-20(+)]*
BAT2370	*barSi87[hecd-1mutant(CRISPR KO)] IV;unc-119(ed3) III; ieSi21 [sun-1p::sun-1::mRuby::sun-1 3'UTR + Cbr-unc-119(+)] IV*
BAT2371	*barSi87[hecd-1mutant(CRISPR KO)] IV;unc-119(ed3) III; ieSi21 [sun-1p::sun-1::mRuby::sun-1 3'UTR + Cbr-unc-119(+)] IV; otIs305 (hsp::che-1::3xHA) V; ntIs1 (gcy-5::GFP) V*
BAT2372	*barSi83(math-33::AID degron::3xHA) V; otIs305 (hsp::che-1::3xHA) V; ntIs1 (gcy-5::GFP) V*
SJ4100	*zcIs13[hsp-6::GFP] V*
SJ6	*zcIs4 [hsp-4::GFP] V; upr-1(zc6) X.*
BAT2525	*barSi87[hecd-1mutant(CRISPR KO)] IV;unc-119(ed3) III; ieSi21 [sun-1p::sun-1::mRuby::sun-1 3'UTR + Cbr-unc-119(+)] IV;zcIs13 [hsp-6::GFP] V*
BAT2526	*barSi87[hecd-1mutant(CRISPR KO)] IV;unc-119(ed3) III; ieSi21 [sun-1p::sun-1::mRuby::sun-1 3'UTR + Cbr-unc-119(+)] IV;zcIs4 [hsp-4::GFP] V*

4.2 Bacterial strains

Table 4.2 Bacterial strains used in the study

Name	Genotype	Purpose
Escherichia coli: OP50	uracil auxotroph *E. coli* bacteria	Food source for *C.elegans*
Escherichia coli: OP50 (carb-resistant)	uracil auxotroph *E. coli* bacteria antibiotic-resistant	Food source for *C.elegans*
Escherichia coli: MACH1	F–Φ80lacZΔM15ΔlacX74 hsdR(rK–,mK+)ΔrecA1398 endA1 tonA	Transformation
Escherichia coli: HB101(DE3)	F-, mcrA, mcrB, IN(rrnD-rrnE)1, rnc14::Tn10(DE3 lysogen: lavUV5promoter -T7 polymerase	Transformation into RNAi bacteria (express dsRNA)

4.3 Oligonucleotides

Table 4.3.1 List of oligos used for CRISPR repair template

Name	Sequence	Application
math-33 _AID_homo1_F	GATCACAAATCACCCATCCAACAT TCAAGTGAAGCTGCGATCCGAATC TTGAACGGATCCGGAGGTGGCGGG CCTAAAGATCCAGCCAAAC	Amplify *math-33* AID system knock in
math-33 _AID_homo1_R	gagagaaagagattgcacagggagaggaaagaaactt ggcgatcataacaaccgtttgaaTCAAGCGTAA TCTGGGACGTC	Amplify *math-33* AID system knock in
math-33 _AID_homo2_F	aatactcgccgtaaaaagacataaaaataatgataaaata aatcccctattttccagTTCCACAAGTGTAC ATTGGTCTAGATCACAAATCACCC ATCC	amplify *math-33* AID system knock in
math-33 _AID_homo2_F	gatcgtattggttcaaacagagagagagaggggagaga gagagagagaaatagagagaaagagattgcacagg	amplify *math-33* AID system knock in
math-33 _AID_clean F	aatactcgccgtaaaaagac	amplify *math-33* AID system knock in
math-33 _AID_clean R	gatcgtattggttcaaacagag	amplify *math-33* AID system knock in
math-33 _AID template _clean F	CGAATCTTGAACGGATCC	amplify *math-33* AID system knock in
math-33 _AID template _clean R	AGCGTAATCTGGGACGTC	amplify *math-33* AID system knock in

Table 4.3.2 List of oligos used for genotyping

Name	Sequence	Application
hecd-1 (ok1437) fwd	ggatggagttcacacggagt	genotyping *hecd-1* (*ok1437)* strain
hecd-1 (ok1437) rev	attggtggtagcgtctttgg	genotyping *hecd-1* (*ok1437)* strain
hecd-1 (ok1450) fwd	ggatggagttcacacggagt	genotyping *hecd-1* (*ok1450)* strain
hecd-1 (ok1450) rev	attggtggtagcgtctttgg	genotyping *hecd-1* (*ok1450)* strain
eel-1 (ok1575) fwd	tgtgctgggagtatgagctg	genotyping *eel-1* (*ok1450)* strain
eel-1 (ok1575) rev	aacgacagtgtgcgaacttg	genotyping *eel-1* (*ok1450)* strain
math-33 (ok2974) fwd	gaaagttcgcggactgaatc	genotyping *math-33* (*ok2974)* strain

math-33 (ok2974) rev	cttgtcggtcattgtgtcgt	genotyping *math-33* (*ok2974)* strain
math-33 _AID_frw	ACAACGGCGAGAAAGTCAAC	genotyping *math-33* _AID CRISPR mutant
math-33 _AID_rev	AATGAGAACACGACACGGTC	genotyping *math-33*_AID CRISPR mutant
L4440 plasmid_rev	cgagtcagtgagcgaggaag	to sequence insert in L4440 RNAi plasmid
L4440 plasmid_frw	CGACGTTGTAAAACGACGG	to sequence insert in L4440 RNAi plasmid

Table 4.3.3 List of oligos used for Gibson assembly

Name	Sequence	Application
GB_*Lys-7*_fwd	aagtgctcatcattggaaaaGCAGGACAAGGATCCTTTG	Amplify *lys-7* for RNAi clone
GB_*Lys-7*_rev	agttttcgccccgaagaacgGCAAACTGCTTGACAGATG	Amplify *lys-7* for RNAi clone
GB_*pud-1.2*_fwd	acgtgacgcgtggatccccGATAATCAGACTGGAAGTC	Amplify *pud-1.2* for RNAi clone
GB_*pud-1.2*_rev	atatcgaattcctgcagcccGTGAAAGTGGTAGTCGATTC	Amplify *pud-1.2* for RNAi clone
GB_*hsp-90*_fwd	acgtgacgcgtggatccccCCAATGACTGGGAAGATC	Amplify *hsp-90* for RNAi clone
GB_*hsp-90*_rev	atatcgaattcctgcagcccGATTTGAGTTTGGTTCTCC	Amplify *hsp-90* for RNAi clone
GB_*ifb-2*_fwd	acgtgacgcgtggatccccGAAATCAAGGCTGAATACG	Amplify *ifb-2* for RNAi clone
GB_*ifb-2*_rev	atatcgaattcctgcagcccCTCGACAAGCTTTCTGTAG	Amplify *ifb-2* for RNAi clone
GB_*mlt-11*_fwd	acgtgacgcgtggatccccGAAAGGGATACAACGTCAAG	Amplify *mlt-11* for RNAi clone
GB_*mlt-11*_rev	atatcgaattcctgcagcccGAAGTGACTGAACTGATTG	Amplify *mlt-11* for RNAi clone
GB_*atfs-1*_frw	aagtgctcatcattggaaaagcatggaatcactacttg	Amplify *atfs-1* for RNAi clone
GB_*atfs-1*_rev	agttttcgccccgaagaacgatttttcttcccttcttctc	Amplify *atfs-1* for RNAi clone

4.4 sgRNAs

Table 4.4 List of sgRNAs used in this study

Targeted gene	sgRNA name	Sequence
*math-33*_C-terminal	gBT160	GAATCAGTTCAAGATTCGGA
*eel-1*_c-terminal	gBT163	TCCAGAATTGGTGTATACAG
*eel-1*_N-terminal	gBT164	GACCCGGAAGAGCTTGAACT
sgRNA1_*hecd-1*	gBT166	GTTGAGGGATCCTTACCTGG
sgRNA2_*hecd-1*	gBT167	ACCAGAAGAAGATGGAACAG

4.5 Antibodies

Table 4.5.1 Primary antibodies used in this study

Name	Type	Species	Company
PA23	Anti-HA-HRP	Rat	Santa Cruz
PA20	Anti-alpha-Tubulin	Mono;mouse	Sigma
PA24	Anti-H3K9me3	Poly;rabbit	Abcam
PA10	Anti-H3K39me2	Mono;mouse	Dr. Hiroshi Kimura; Graduate School of Frontier Biosciences Osaka University
PA45	Anti-Histone H3	Poly;rabbit	Abcam
PA47	Anti-H3K4me3	Poly;rabbit	Abcam
PA48	Anti- H3K9 ac	Poly;rabbit	Abcam
PA49	Anti- H3K14 ac	mono; rabbit	Abcam
PA63	Anti-H3K9AcS10ph	Poly;rabbit	GeneTex
PA72	Anti-myosin heavy chain A	Mono;mouse	Hybridoma Bank
PA105	Anti-H3K27me3	Mono;mouse	Abcam
PA181	Anti-H3K27ac	Poly;rabbit	Abcam
PA197	Anti-H3K9AcS10ph	Poly;rabbit	Abcam
PA200	Anti-actin	Mono;mouse	Santa Cruz Biotechnology

Table 4.5.2 Secondary antibodies used in this study

Name	Type	Species	Company
SA2	IgG-HRP	anti-mouse	Santa Cruz
SA4	IgG-HRP	anti-rabbit	Santa Cruz
SA7	AlexaFluor488	anti-mouse	Mol. Probes
SA9	AlexaFluor568	anti-rabbit	Mol. Probes

4.6 smFISH probes

Table 4.6 smFISH probes used in this study

Probes set	Sequence	Fluorophore
gcy-5_set1	cattcggatgctccaagaac caattccaactcgaagcgtc caattggaagagttccacca tatcgcattcggtatattcc tcccactacaacatctacat tattggtatcagccaactgg tgccactcgatcaaattgga tttacagtagtcttggtcgt cttaaggttgcctcaacatc atccgcactggatatagatc cgatcttgttaatgcctcat tacgagctcgactctttaca ggaccactaattgcgcataa ccaatactcctcattgtcaa tctttcccaaacttgtttgt tggagttagtccatttgcaa ctactgtgaatgactcccaa atttctaacagcatccgcaa tgccatcccgtataagtaaa tagtaaccatttgcggcata gcggtagagattttgaccaa tcatgttaactagtgccact ccgtgacaattgcgaagacg cgtttttctttttgtggcat gtgatcttcgactatttggc actttctccggttatagttg gctatgatgtttggtggtta atttctccttctcttcttta ggtccatcgatagataatcc gatatcctgaagtgatcctc aaagttcataccctctgcaa ggcaagtagctgaacgtaga ctcccaatccaaaatctgtt tacgatttcctccttttttc aagtattaactccggtcgga acttgcaaatttgctcagct gttctgcaacttgttttgga tctccaattgattccacttt tgtcggtaacccagaaacac ggaaccttgaagctcttaca gcccactattaattccaatt atggatagaccaacgacacc gtatccccaaataggcaata tttccattactttccattct tgtgcagcttctgacatatg	Fluor Red 610

	tctcctcttgaacttgtttc tgtttccattacacctttc gattttgtgtcactgtcagt	
rab-3_set1	caaagttctgatcgggttgt atcaggagcttgaacatgta tccaactgatgaatttccga catcacagtaacggaagagg gtagagacgaaggcagaagt cactttgaaatcgattccga tttgtctccacggaacacag ggtatcccagatttgaagtt gatagtaggcggtggtgatg cagaatgaatcccattgctc actcttcattagtgatgtca gcaccaatcctgaacactat tttcccatgagtatgtcttg ccaaccaaaacaacttgagc ttcagagtccatatcacatt ccctatccatagatacaact aagttgatcagcaagttggc ggctgatgtttcgaagaatt cctttacattaatgttctcc tctccaccaacttctcaaaa tctgccatcttatcacaaat ctgtgggtccttatccaaac ttcgagcttctgtccttttg aattgcattgctgttgagca attgcgtttggaatttggga agagctacgcgcttttagaa cctagatgttgagagaggga tttacgatccatatatctgg taattaaaccaactacgccc ggggaatatgattgaacgtt gctctgggaattgtttggaa ggcgactatgattagttaga tgggaactgggaagtcacta aatcaatctttcagcgggtg cctcgaaaataatttcctcc	Fluor Red 610

4.7 Kits

Table 4.7 Kits used in this study

Name	Company
QIAquick PCR Purification Kit	Qiagen
NucleoSpin® Gel and PCR Clean-up	Macherey-Nagel
NucleoSpin® Plasmid Isolation Kit	Macherey-Nagel
Trans-Blot® Turbo™ RTA Midi	Biorad

Nitrocellulose Transfer Kit	

4.8 Plasmid

Table 4.8 Plasmid used in the study

Name	Company
dBT46	Empty L4440 plasmid
dBT187	*myo-2::mCherry*

4.9 Chemicals, solutions and antibiotics

Table 4.9.1 Chemicals and reagents used in this study

Name	Company
4′,6-diamidino-2-phenylindole	Carl Roth GmbH + Co. KG
Acetic Acid	Carl Roth GmbH + Co. KG
Agar-Agar, Kobe I Kobe I, pulv.	Carl Roth GmbH + Co. KG
Agarose NEEO Ultra-Qualität Roti®garose	Carl Roth GmbH + Co. KG
Alpha ketogluterate	*Sigma*
Ammonium peroxydisulphate ≥98 %, p.a., ACS	Carl Roth GmbH + Co. KG
Amphotericin B Fungizone	USBiological
Bacto Tryptone, BD Difco	A. Hartenstein GmbH
Bacto Peptone, BD Difco	A. Hartenstein GmbH
Bacto Yeast Extract	
Bovine Serum Albumin	Sigma Aldrich
Calcium Chloride, Dihydrate	*Calbiochem*
Cholesterin (Cholesterol)min. 95 %, Ph. Eur.	Carl Roth GmbH + Co. KG
Dextran Sulfate	*Sigma Aldrich*
Dipotassium phosphate	Carl Roth GmbH + Co. KG
EDTA (Ethylenediaminetetraacetic acid)	Carl Roth GmbH + Co. KG
Ethanol unvergaelt ca. 99%	Universität Hamburg
Ethanol vergällt ca. 99%	Universität Hamburg
Ethylene Carbonate	Sigma Aldrich
Gelatin	Carl Roth GmbH + Co. KG
Glucose	Carl Roth GmbH + Co. KG
Glycerol 98%	Carl Roth GmbH + Co. KG
Glycin PUFFERAN®	Carl Roth GmbH + Co. KG
Hefeextrakt / Yeast Extrakt	AppliChem
Hydrochloric acid 37 %	Carl Roth GmbH + Co. KG
Hydrogen Peroxide 30 % p.A.	Carl Roth GmbH + Co. KG
Indole-3-acetic acid, 98+% (Auxin)	Alfa Aesar
IPTG min. 99 %, dioxanfrei, animal free	Carl Roth GmbH + Co. KG

LB-Agar (Luria/Miller)	Carl Roth GmbH + Co. KG
LB-Medium (Luria/Miller)	Carl Roth GmbH + Co. KG
Magnesiumchlorid-hexahydrat	Carl Roth GmbH + Co. KG
Magnesium sulphate	Carl Roth GmbH + Co. KG
Methanol	Carl Roth GmbH + Co. KG
Potassium chloride	Carl Roth GmbH + Co. KG
ROTIPHORESE®Gel 30 (37,5:1)	Carl Roth GmbH + Co. KG
ProLong™ Diamond Antifade Mountant	ThermoFischer
ProLong™ Diamond Antifade Mountant with DAPI	ThermoFischer
RNase away	M&P Molecular Bio Products
Roti-Stock 20x SSC	Carl Roth GmbH + Co. KG
Sodium Acetate	Carl Roth GmbH + Co. KG
Sodium azide	Fluka-Sigma
Sodium chloride	Carl Roth GmbH + Co. KG
Sodium dodecyl sulfate	Carl Roth GmbH + Co. KG
Sodium hydroxide solution 4 N	Carl Roth GmbH + Co. KG
Sodium hypochlorite solution	Carl Roth GmbH + Co. KG
TEMED 99%	Carl Roth GmbH + Co. KG
TRIS PUFFERAN®	Carl Roth GmbH + Co. KG
Triton® X-100	Sigma Aldrich
Tween20	Sigma Aldrich

Table 4.9.2 Solutions used in this study

Name	Company
Bleaching solution (1mL)	100µL 14 % NaClO, 200µL 4M NaOH, 700µL dd H_2O
Freezing solution (1L)	5.8g NaCl, 50mL 1M KH_2PO_4 (pH 6), 240mL glycerol, ddH_2O; before use: add 0.3mL 1M $MgSO_4$
2x Gibson Assembly Master Mix	405µL isothermal start mix, 25µL 1M DTT, 50µL 10mM dNTPs, 50µL NAD^+(NEB #M0363S), 31.25µL Phusion High Fidelity DNA Polymerase (NEB #M0530S), 437.75µL ddH_2O
50% Glycerol	50mL glycerol (100%), 50mL ddH_2O
Hybridisation solution	125µL 20% dextran sulfate, 25µL 99.5% formamide, 37.5µL Ethylene Carbonate, 50uL DEPC-treated nuclease-free H_2O
Lysis Buffer	50mM KCl, 10mM Tris (pH 8.3), 2.5mM $MgCl_2$, 0.45% Tween-20, 0.01% Gelatin before use: add 0.1mg/mL of Proteinase K
LB medium (1L), pH 7	10g Tryptone, 10g NaCl, 5g Yeast Extract, ddH_2O
LB^{Carb} medium (1L)	10g Tryptone, 10g NaCl, 5g Yeast Extract, Carbenicillin (50 µg/mL final concentration), ddH_2O
LB^{Amp} plates (1 L)	15g Agar, 10g NaCl, 5g Yeast Extract, Ampicillin (100 µg/mL final concentration), ddH_2O

$LB^{Carb+Tet}$ plates (1 L)	15g Agar, 10g NaCl, 5g Yeast Extract, Carbenicillin (50µg/mL final concentration), Tetracycline (12.5µg/mL final concentration), ddH_2O
M9 buffer (1L)	6g Na_2HPO4, 3g KH_2PO_4, 5g NaCl, 50mg Gelatine, ddH_2O; before use: add 1mL 1M $MgSO_4$
NGM (1L)	3g NaCl, 20g Agar, 2.5g Peptone, ddH_2O, after autoclaving add: 1mL Cholesterol (5mg/mL in 95% EtOH stock solution), 1mL 1M $MgSO_4$, 1mL 1M $CaCl_2$, 25mL 1M K_2PO_4, 1mL fungizone (Amphotericin B 2.5 mg/mL stock)
NGM for RNAi (1L)	Prep NGM, add after autoclaving additional 1mL 1M IPTG and 500µL Carbenicillin (50 mg/mL stock)
SDS-page	12% resolving gel for 5mL: 2mL 30% Acrylamide mix, 1.3mL 1.5M Tris (PH8.8), 0.05mL 10%SDS, 0.05mL 10% APS, 0.002mL TEMED,1.7mL H_2O Stacking gel: 0.17mL30% Acrylamide mix, 0.17mL 1.5M Tris (PH6.8), 0.01mL 10%SDS, 0.01mL 10% APS, 0.001mL TEMED, 0.68mL H_2O
SDS-page running buffer	24,8 mM Tris-HCl, 192mM Glycin, 0,01% SDS (w/v)
TBST	1X: 25mM Tris, 150mM NaCl, 0,1% Tween20, ddH_2O
3%BSA	3g BSA in 100mL 1x TBST
1%BSA	1g BSA in 100mL 1x TBST
2YT (1L)	pH7.5: 16g tryptone, 10g yeast extract, 5g NaCl, ddH_2O
TAE buffer (1L)	for 50X, pH8.5: 242g Tris base, 57.1mL glacial acetic acid, 18.6g EDTA, ddH_2O
Washing buffer (20mL)	2mL 99.5% formamide, 2mL 20x SSC (RNase-free), 100µL Triton X-100, 16mL DEPC-treated nuclease-free H_2O

Table 4.9.3 Antibiotics used in this study

Name	stock solution concentration	Company
Ampicillin	100mg/mL	Carl Roth GmbH + Co. KG
Carbenicillin	50mg/mL	Carl Roth GmbH + Co. KG
Tetracycline	12.5mg/mL	Carl Roth GmbH + Co. KG

5. Methods

5.1 Nematode specific methods

5.1.1 Nematode growth and maintenance

C. elegans strains were cultured following standard procedures (Brenner, 1974). Worms were maintained on Nematode Growth Medium (NGM) agar plates containing 3g NaCl, 20g agar, 2.5g peptone per liter of double-distilled water, supplemented with 5µg/mL cholesterol, 1mM $MgSO_4$, 1mM $CaCl_2$, 25mM K_2 HPO_4 , and 2.5µg/mL amphotericin B. OP50 bacteria served as the food source at 15°C unless otherwise specified. Heat-shock and temperature-sensitive (ts) strains were kept continuously at 15°C.

For maintenance, the worms were transferred to fresh plates at two-week intervals, either by placing an old plate upside down onto a new plate or by individually transferring worms using a worm pick, particularly when genotyping was necessary for individual identification. To maintain male populations, hermaphrodites were crossed with males of the same genotype every week. Extrachromosomal lines generated through microinjection were maintained by selecting marker-positive animals every two weeks. The list of strains used and generated in this study is provided in Table 4.1.

5.1.2 Animal synchronization

Animals were synchronized using a bleaching protocol. Gravid adult worms were exposed to a bleaching solution composed of sodium hypochlorite (NaClO) and 2M sodium hydroxide (NaOH) in ddH_2 O for approximately 5 minutes until the adults lyse and release their eggs. The sensitivity of the worms to the bleaching agents facilitated the controlled lysis necessary for egg release. The eggs are protected by their shells, which allow them to survive the bleaching process. The egg pellet was collected by centrifugation, then washed three times with M9 buffer (composed of 22mM KH_2 PO_4 , 42mM Na_2 HPO_4 , 86mM NaCl, and 1mM $MgSO_4$ in ddH_2 O). The washed eggs were subsequently placed on fresh NGM plates seeded with OP50 bacteria to hatch, until the stage desired for further experiments.

5.1.3 RNA interference treatment

For the preparation of RNAi experiments, worms were grown on NGM agar plates supplemented with 1mM IPTG and 50µg/mL carbenicillin, seeded with RNAi bacteria sourced from the Ahringer library (Source Bioscience). RNAi against Renilla luciferase (*Rluc*) was used as negative control.

5.1.3.1 F1 RNAi

For F1 RNAi, synchronized L1 larvae were initially grown at 15°C on standard NGM plates until they reached the L4 developmental stage. At this point, the worms were transferred to RNAi plates and subsequently maintained at 15°C until the majority of the F1 progeny attained the L4 stage. For reprogramming experiments, the plates were then subjected to a heat shock at 37°C for 30 minutes for overexpress the transcription factor under an inducible heat shock promotor, except the strains of *hecd-1(ok1450), hecd-1(ok1437)* and *hecd-1*$^{-/-}$ were heat shocked at 32°C for 120 minutes. After heat shock, all plates were incubated overnight at 25°C, as previously described (Seelk et al., 2016; Tursun et al., 2011). The next day (~16 h later), plates were examined under a dissecting microscope to screen the presence of ectopic fluorescent expression.

5.1.3.2 P0 RNAi

In the suppressor screen conducted in the *hecd-1* mutant background, RNAi knockdown of *hsp-90*, *lmn-1*, *cox-4*, *dpf-6*, *lsm-7*, *nuo-6* and *hda-1* were performed to assess effects after embryonic development, following the P0 experiments protocol. To achieve P0 RNAi in hecd-1 mutant background, eggs were carefully transferred from normal plates to RNAi plates to prevent damage from bleaching. The worms grown at 15°C until most of the P0 animals reached L4 stage and heat-shocked at 32°C for 120 min followed by an overnight incubation at 25°C as described above. Plates were screened for presence of ectopic GFP expression the following day under a dissecting scope.

5.1.3.3 Double RNAi

For double RNAi, bacterial cultures were grown to saturation. The optical density at 600 nm (OD600) was measured to confirm that the bacteria were mixed in

an appropriate 1:1 ratio. Following this, the bacterial mixtures were seeded onto RNAi plates for further experimentation.

For the F1 double RNAi experiment, the procedure was conducted in accordance with the protocol described in the F1 RNAi section above.

For the P0 double RNAi experiment involving *lin-53* combine with lmn-1, since the reprogramming phenotype associated with *lin-53* RNAi is not observed in the P0 generation, P0 L4-stage worms were transferred onto *lin-53* RNAi plates and maintained until they reached the F1 L1 stage. Subsequently, these F1 L1 stage animals were transferred onto double RNAi plates.

5.1.4 Auxin Feeding

For auxin feeding, a 400 mM stock solution was prepared and subsequently diluted into NGM agar plates, as described previously (Zhang et al., 2015). The plates were then seeded with RNAi bacteria, and the worms were subjected to RNAi treatment for the further experiment either the P0 or F1generation.

5.1.5 Transgenic crossing

One of the advantages of *C.elegans* is its suitability for classical genetic analyses and crossing to generate animals with diverse genetic backgrounds (Corsi et al., 2015). For mating experiments, 7-10 males were combined with 3 hermaphrodites on a plate with a single drop of OP50 bacteria. Limited food availability causes the worms to stay close together, which increases the chances of successful mating. Successful mating was identified by the presence of males or the inheritance of maternally or paternally derived markers in the subsequent generation. The heterozygous F1 progeny are individually isolated, and the F2 generation is made homozygous either by checking for fluorescence (if fluorescent reporters are used) or by genotyping (Fay, 2013). To generate males of a specific strain for further crossing, hermaphrodites were crossed with N2 males.

5.1.6 Generation of CRISPR alleles

For knock in Degron and 3xHA tag to induce AID system, a mixture of sgRNA, cas9 protein Polymerase Chain Reaction (PCR) repair template with homology arms to the site of insertion and plasmid containing a florescent marker (*myo-2::mCherry*)

was injected in the animals as described by Dokshin et al, (2018). F1 generation was screen for florescent marker in the pharynx as successful injection events, and these individuals were genotyped to verify the integration of the CRISPR-mediated knock-in insertion (Arribere et al., 2014). Positive candidates were further analyzed to establish homozygosity for the knock-in allele through single out and subsequent genotyping. The accuracy of the knock-in sequence was confirmed by Sanger sequencing.

For knock gene out experiment, the dual sgRNA-directed gene editisng approach was performed. A mixture of sgRNA1, sgRNA2, cas9 protein and plasmid containing a florescent marker (*myo-2::mCherry*) was injected in the animals (Chen, X., et al., 2014). The screening process for identifying positive homozygous was conducted using the same method described for the knock-in procedure outlined above.

Due to the fluorescent marker only reflects the success of microinjection, the *dpy-10* co-CRISPR approach, as previously described by Paix et al. (2015), was also employed for knockout and knock-in experiments to verify the activity of the Cas9 protein. The injection mixture, in addition to the components required for knockout and knock-in procedures, included *dpy-10 (cn64)* sgRNA and a PAGE-purified 99-mer single-stranded oligodeoxynucleotide (ssODN) homologous recombination (HR) template targeting *dpy-10 (cn64)*.

The list of sgRNAs, sequences of the oligonucleotides to amplify the insert and details of the CRISPR strains used are provided in the materials section.

5.1.7 Worm lysis

To facilitate worm lysis for genotyping or other applications such as genomic DNA amplification, 1-10 worms were transferred into 30µL of lysis buffer (comprising 50mM KCl, 10mM Tris pH 8.3, 2.5mM $MgCl_2$, 0.45% Tween 20 [v/v], and 0.01% gelatin [v/v] in ddH_2O) supplemented with 1mg/mL proteinase K. The rigid cuticle of the worms was disrupted by freeze cracking at -80°C for 30 minutes. Subsequently, the samples were incubated in a PCR cycler for 1 hour at 65°C, followed by inactivation of proteinase K at 95°C for 30 minutes. Worm lysates were then stored at -20°C, and 1-3µL aliquots of the lysate were used for genotyping or other PCR-based applications.

5.1.8 Worm genotyping

Genotyping was performed to confirm the presence of the correct DNA sequences in the worms following crossing or transgenesis. A volume of 1.5µL of worm lysate was used as a template in PCR reactions utilizing Mango Taq Polymerase (NEB). Deletions and insertions were identified based on size differences between PCR products derived from mutant and WT samples. In cases where deletions were too large to be detected by standard PCR, two pairs of primers were employed: one pair situated within the deletion region and another pair located outside of the deletion. Heterozygous individuals generated two PCR products: one containing the deletion and one without it. N2 animals served as the WT control. To verify the accuracy of inserted DNA sequences or point mutations, PCR products were sent for sequencing. Detailed information regarding the primers used for genotyping is provided in Table 4.3.2

5.1.9 Freezing worms for long-term storage

L1 larvae exhibit resistance to freezing, allowing worms to be kept long-term at -80°C. o prepare samples for freezing, worms were grown on NGM plates until a sufficient number of L1 larvae was obtained. The worms were then washed off the plates using M9 buffer and subjected to three additional washes with M9 to remove residual bacteria. After washing, the worms were resuspended in 1mL of M9 buffer and freezing solution (100mM NaCl; 20mM KH_2PO_4 (pH 6); 4 % glycerol (v/v) and 300mM $MgSO_4$) was added in a 1:1 ratio. 500mL of the resulting suspension containing worms were then transfer into CryoTubes and gradually frozen at -80°C within Styrofoam containers to promote slow cooling. After two weeks, one tube of the frozen stock was thawed and assessed for worm viability.

5.2 Molecular biology methods

5.2.1Polymerase Chain Reaction (PCR)

PCR was employed to amplify specific DNA fragments for applications such as genotyping, vector construction for Gibson assembly, preparation of repair templates for CRISPR genome editing, or other molecular biology procedures. Different polymerases were employed in the PCR reactions, depending on the specific

downstream applications. The PCR protocols and programs were used in this project are shown below.

5.2.1.1 NEB Mango taq polymerase

Table 5.1 Reaction mixture and PCR program NEB Mango taq polymerase

component	volume
5x Mango taq buffer	2.5 µL
$MgCl_2$	1 µL
10 mM dNTPs	0.5 µL
Primer Frw	0.5 µL
Primer Rev	0.5 µL
Template	1.5 µL
Mango Taq	0.125 µL
ddH_2O up to 12.5µL	5.875 µL

Time	Process	Temperature
10min	Initial denaturation	95°C
34cycles		
30 sec	Denaturation	95°C
50 sec	Primer Hybridization	Table
2-3 min (depending on lenth of fragment	Elongation	72°C
5 min	Final elongation	72°C
∞	Storage	4°C

Mango taq polymerase was used for genotyping.

5.2.1.2 NEB Q5 polymerase

Table 5.2 Reaction mixture and PCR protocol using NEB Q5 High-Fidelity DNA Polymerase

component	volume
5x Q5 reaction buffer	10 µL
10 mM dNTPs	1µL
Primer Frw	2.5 µL
Primer Rev	2.5 µL
Template	1 µL
Mango Taq	0.25 µL
ddH_2O up to 50µL	32.75 µL

Time	Process	Temperature
30 sec	Initial denaturation	98°C
34cycles		
10 sec	Denaturation	98°C
20 sec	Primer Hybridization	Table
1-3 min (depending on lenth of fragment	Elongation	72°C
2 min	Final elongation	72°C
∞	Storage	4°C

Q5 High-Fidelity DNA Polymerase possesses 3'-5' exonuclease activity, which enables proofreading of the amplified DNA. This property reduces the chance of

errors in the DNA sequence, making it suitable for Gbison cloning and the construction of repair templates for CRISPR gene editing.

5.2.3 Purification of PCR products

PCR products that for CRISPR repair templates were purified using the GeneJet PCR Purification Kit (Thermo Scientific). PCR products that for genotyping were purified by Nucleospin® Gel and PCR Clean-up (Macherey-Nagel).

5.2.4 Gibson cloning

For Gibson cloning, digested vector with restriction enzyme Xmal (Table 5.3) and the target gene was amplified (Table 5.2: Q5 PCR) by using specific primers (Table 4.3.4) to create overhangs compatible with the vector.

Table 5.3 Restriction enzyme for digestion ptotocol

component	volume
5x Cut Smart Buffer	5 µL
Enzyme XmaI	1 µL
Vector	01 µg
ddH_2O	Up to 50µL

Time	Process	Temperature
120min	Enzyme activation	37°C
15 min	Heat inactivated	80°C
∞	Storage	4°C

For the Gibson reaction amplified fragments were combined with the vector and 2x Gibson Mastermix was added per reaction tube and incubated at 50°C for 60 mins. Optimal cloning efficiency is achieved using the vector to insert ratio was 1:3 for inserts > 100 bp and 1:5 for inserts < 100 bp., 5µL 2x Gibson Mastermix and then filled up to 10µL with ddH_2O.

5.2.5 Agarose gel electrophoresis

To separate DNA fragments by size, agarose gel electrophoresis was performed. Smaller molecules pass more quickly through the porous agarose matrix than larger ones, resulting in size-based separation of DNA fragments. To resolve fragments ranging from 100 to 10,000 base pairs (bp), a 2% (w/v) agarose gel prepared in TAE buffer was used. For visualization, MIDORIGreen was added at a dilution of 1:25,000.

Prior to loading, 6x loading dye was mixed with each DNA sample. The samples were then loaded into the gel wells and electrophoresed at 100-120 V for 30 minutes. DNA size markers, either a 1kb plus ladder or a 100bp ladder, were run alongside the samples to facilitate size determination. The separated DNA fragments were visualized and photographed under UV illumination.

5.2.6 Transformation in *E. coli*

The production from Gibson assembly transformed to chemically competent MACH1 *E.coli* cells by using a heat shock method. Briefly, 50µL competent cells were thawed on ice and 2-5µL of Gibson assembly production were added. The mixtures were incubated on ace for 30 minutes followed by heat shock of 30-40 seconds at 42 °C, then the mixture was Immediately put back on ice for 3 minutes. Afterwards, 250µL of 2YT medium was added to the transformation mixture and incubated at 37 °C for at least 1 hour. The mixture was plated on LB-Agar containing ampicillin, incubated at 37 °C overnight (~16 hours). Successful transformation for RNAi clones were confirmed via colony PCR (Section 5.2.1.1) and plasmid sequencing (Section5.2.7). Positive clones were grown overnight, purified (Section 5.2.5), and re-transformed into HT115 *E.coli* cells for RNAi experiments, following the same procedure. These HT115 cells were plated on LB-Agar plates containing ampicillin and tetracycline as selective antibiotics.

5.2.7 Plasmid purification from RNAi clone bacteria

A single colony of bacteria from Ahringer library was used to inoculate 6 mL LB-carb medium at 37°C with shaking 200 rpm overnight. The plasmid DNA was then isolated using the NucleoSpin® Plasmid Purification Kit, following the manufacturer's instructions. The concentration of the purified DNA was determined using a Nanodrop spectrophotometer.

5.3 Biochemical methods

5.3.1 Worm protein lysates

Whole-cell protein extraction was performed on the animal samples for Western blot analysis. Worms were collected by picking into M9 buffer or washing it off with M9 buffer. The worm pellet was washed three times with M9 to remove bacteria and

5x SDS sample buffer (comprising 10% w/v SDS, 10 mM DTT, 20% v/v glycerol, 0.2 M Tris-HCl pH 6.8, and 0.05% w/v bromophenol blue) was added to the worms. The SDS in the buffer denatures proteins, disables protein-protein interactions, and imparts a negative charge to the proteins. The samples were then incubated at 96°C for 10 minutes and stored at -20°C.

5.3.2 SDS polyacrylamide gel electrophoresis

The protein lysate samples were separated by SDS polyacrylamide gel electrophoresis (SDS-PAGE). The SDS-PAGE Gel is made of stacking gel (TEMED, 10%APS, 10%SDS, 1.0M(PH6.8) Tris, 30%Acrylamide mix, ddH2O) and separating gel (TEMED, 10%APS, 10%SDS, 1.5M(PH8.8) Tris, 30%Acrylamide mix, ddH2O). After the preparation of the SDS-PAGE gel, the denatured protein lysates were loaded into the gel, and electrophoresis was performed using a vertical Mini-PROTEAN Tetra Electrophoresis system (Bio-Rad) containing 1× SDS running buffer (comprising 24.8 mM Tris-HCl, 192 mM glycine, and 0.01% SDS [w/v]). A constant voltage of 100 V was applied until the entire sample volume had migrated through the gel. The PageRuler Plus Prestained Protein Ladder (Thermo Scientific) was used as a molecular weight marker.

5.3.3 Western Blot

Proteins separated by SDS-PAGE were transferred to a nitrocellulose membrane for immunological detection by antibodies. This transfer was performed using wet blotting chambers filled with Tankblot transfer buffer (containing 25 mM Tris, 192 mM glycine, pH 8.3, and 20% methanol) at a constant voltage of 100 V for 1-2 hours.

The nitrocellulose membrane was then blocked with 3% BSA in 1x TBST (containing 25 mM Tris, pH 7.5, 150 mM NaCl, and 0.1% v/v Tween-20) for 1 hour at room temperature with gentle shaking or overnight at 4°C. After blocking, the membrane was incubated with primary antibodies for 4 hours at room temperature or overnight at 4°C. The membrane was washed three times for 10 minutes in 1x TBST. Then, it was incubated with HRP-conjugated secondary antibodies for 1 hour at room temperature. For primary antibodies coupled to peroxidase, the membranes were washed three times for 10 minutes each in 1x TBST and then immediately detected. All antibodies were diluted in 1% BSA.

The antibody-antigen complexes were detected using Radiance Q (Azure Biosystems) HRP substrate for chemiluminescence following to manufacturer's instruction. Detection was performed using a ChemiDoc™ MP Imaging System.

Antibodies used in this study are listed in Table 4.5.1 and Table 4.5.2

5.3.4 Antibody staining

For detection of anti-H3K4me3 and anti-H3K9me3 staining, Worms were sheared by slide crack, then fixed and permeabilized following a previously described method (Jones et al., 1996). Briefly, glass slides were placed on a metal tray on dry ice. A drop of worm suspension in M9 was pipetted onto each slide, and a second slide was carefully positioned on top. The slides were then gently separated and fixed in methanol for 10 minutes. Following fixation, samples were washed three times with PBST (0.1% Tween-20 in PBS). The samples were then blocked with 0.2% gelatin in PBST for 1 hour, followed by incubation with primary and secondary antibodies as described previously.

Antibodies used in this study are listed in Table 4.5.1 and Table 4.5.2

5.3.5 DAPI staining

Worms were collected by washing with M9 buffer, then washed three times with 0.01% Tween PBS. After the final wash, 1 mL of -20°C methanol was added, and samples were fixed at -20°C for 5 minutes. The methanol was aspirated, and worms were rinsed twice with 0.1% Tween PBS, followed by centrifugation. Worms were then stained with 1µL of DAPI solution for 5 minutes in the dark. After staining, samples were washed twice with 0.1% Tween PBS, and a drop was mounted on a 3% agar pad for imaging.

5.3.6 Single molecule florescence in situ hybridization (smFISH)

smFISH was performed using custom Stellaris FISH probes purchased from Biosearch Technologies, following the manufacturer's protocol. Briefly, *hecd-1(ok1437)* mutant worms and washed off plates with M9 buffer, then subjected to five washes with nuclease-free water. The animals were fixed in 4% PFA for 30 minutes, washed twice with DEPC-treated 1× PBS, and permeabilized at 4°C in 70% ethanol with rotation for 2 days.

Worms were then washed twice with wash buffer (2 mL deionized formamide, 2 mL 20× SSC (RNase-free), 100 µL Triton X-100, 16 mL DEPC-treated nuclease-free water) and resuspended in hybridization buffer (125 µL 20% dextran sulfate, 25 µL deionized formamide, 37.5 µL ethylene carbonate, with DEPC water up to 50 µL) containing the probe (12.5µM/ µL). The hybridization was performed in the dark at 37°C overnight. After incubation, worms were washed in wash buffer at 37°C for 30 minutes in the dark, followed by a 30-minute incubation with DAPI for nuclear counterstaining. Finally, worms were mounted on glass slides in a drop of ProLong™ Diamond Antifade Mountant. Or without DAPI incubation, directly mounted with ProLong™ Diamond Antifade Mountant with DAPI.

The sequences of all smFISH probes used are listed in Table 4.6.

5.3.7 Fluorescent microscopy

Imaging was performed using a Zeiss Axio Imager 2 fluorescence microscope equipped with a Sensicam camera (PCO) , Nikon fluorescence microscope and Nikon ECLISPSE Ti2 confocal microscope. Worms were mounted on 3% agar pads prepared on slides and anesthetized with 3µL of 20mM tetramisole, an acetylcholine receptor agonist that induces paralysis by depolarizing neurons. After placing a coverslip, images were acquired immediately. The obtained images were processed using Fiji software.

6. REFERENCES

Abernathy, D.G., Kim, W.K., McCoy, M.J., Lake, A.M., Ouwenga, R., Lee, S.W., Xing, X., Li, D., Lee, H.J., Heuckeroth, R.O., 2017. MicroRNAs induce a permissive chromatin environment that enables neuronal subtype-specific reprogramming of adult human fibroblasts. Cell Stem Cell 21, 332-348. e9.

Adachi, K., Kopp, W., Wu, G., Heising, S., Greber, B., Stehling, M., Araúzo-Bravo, M.J., Boerno, S.T., Timmermann, B., Vingron, M., 2018. Esrrb unlocks silenced enhancers for reprogramming to naive pluripotency. Cell Stem Cell 23, 266-275. e6.

Agrelo, R., Setien, F., Espada, J., Artiga, M.J., Rodriguez, M., Pérez-Rosado, A., Sanchez-Aguilera, A., Fraga, M.F., Piris, M.A., Esteller, M., 2005. Inactivation of the lamin A/C gene by CpG island promoter hypermethylation in hematologic malignancies, and its association with poor survival in nodal diffuse large B-cell lymphoma. J. Clin. Oncol. 23, 3940–3947.

Aguilo, F., Zhang, F., Sancho, A., Fidalgo, M., Di Cecilia, S., Vashisht, A., Lee, D.-F., Chen, C.-H., Rengasamy, M., Andino, B., 2015. Coordination of m6A mRNA methylation and gene transcription by ZFP217 regulates pluripotency and reprogramming. Cell Stem Cell 17, 689–704.

Ahrens, T.D., Caglayan, S., Staerk, J., Cieślar-Pobuda, A., 2019. Chapter 4 - Transdifferentiation—Changing Cell Identity, in: Łos, M.J., Hudecki, A., Wiecheć, E. (Eds.), Stem Cells and Biomaterials for Regenerative Medicine. Academic Press, pp. 37–56.

Aleidi, S.M., Yang, A., Sharpe, L.J., Rao, G., Cochran, B.J., Rye, K.-A., Kockx, M., Brown, A.J., Gelissen, I.C., 2018. The E3 ubiquitin ligase, HECTD1, is involved in ABCA1-mediated cholesterol export from macrophages. Biochim. Biophys. Acta BBA-Mol. Cell Biol. Lipids 1863, 359–368.

Alemán, L.M., Doench, J., Sharp, P.A., 2007. Comparison of siRNA-induced off-target RNA and protein effects. Rna 13, 385–395.

Alvarado, A.S., Yamanaka, S., 2014. Rethinking Differentiation: Stem Cells, Regeneration, and Plasticity. Cell 157, 110–119.

Andreux, P.A., Houtkooper, R.H., Auwerx, J., 2013. Pharmacological approaches to restore mitochondrial function. Nat. Rev. Drug Discov. 12, 465–483.

Ang, C.E., Ma, Q., Wapinski, O.L., Fan, S., Flynn, R.A., Lee, Q.Y., Coe, B., Onoguchi, M., Olmos, V.H., Do, B.T., 2019. The novel lncRNA lnc-NR2F1 is pro-neurogenic and mutated in human neurodevelopmental disorders. Elife 8, e41770.

Armstrong, L., 2012. Epigenetic control of embryonic stem cell differentiation. Stem Cell Rev. Rep. 8, 67–77.

Bach, S.V., Hegde, A.N., 2016. The proteasome and epigenetics: zooming in on histone modifications. Biomol. Concepts 7, 215–227.

Baharvand, H., Fathi, A., Gourabi, H., Mollamohammadi, S., Salekdeh, G.H., 2008. Identification of mouse embryonic stem cell-associated proteins. J. Proteome Res. 7, 412–423.

Bahnassawy, L., Perumal, T.M., Gonzalez-Cano, L., Hillje, A.-L., Taher, L., Makalowski, W., Suzuki, Y., Fuellen, G., Sol, A. del, Schwamborn, J.C., 2015. TRIM32 modulates pluripotency entry and exit by directly regulating Oct4 stability. Sci. Rep. 5, 13456.

Balch, W.E., Morimoto, R.I., Dillin, A., Kelly, J.W., 2008. Adapting proteostasis for disease intervention. science 319, 916–919.
Balchin, D., Hayer-Hartl, M., Hartl, F.U., 2016. In vivo aspects of protein folding and quality control. Science 353, aac4354.
Banito, A., Rashid, S.T., Acosta, J.C., Li, S., Pereira, C.F., Geti, I., Pinho, S., Silva, J.C., Azuara, V., Walsh, M., 2009. Senescence impairs successful reprogramming to pluripotent stem cells. Genes Dev. 23, 2134–2139.
Barrière, A., Félix, M.-A., 2006. Isolation of C. elegans and related nematodes. WormBook 17, 1–9.
Battersby, A., Jones, R.D., Lilley, K.S., McFarlane, R.J., Braig, H.R., Allen, N.D., Wakeman, J.A., 2007. Comparative proteomic analysis reveals differential expression of Hsp25 following the directed differentiation of mouse embryonic stem cells. Biochim. Biophys. Acta BBA-Mol. Cell Res. 1773, 147–156.
Battistelli, C., Garbo, S., Maione, R., 2022. MyoD-induced trans-differentiation: a paradigm for dissecting the molecular mechanisms of cell commitment, differentiation and reprogramming. Cells 11, 3435.
Baugh, L.R., 2013. To grow or not to grow: nutritional control of development during Caenorhabditis elegans L1 arrest. Genetics 194, 539–555.
Baumeister, R., Ge, L., 2002. The worm in us–Caenorhabditis elegans as a model of human disease. Trends Biotechnol. 20, 147–148.
Becker, S.F., Jarriault, S., 2016. Natural and induced direct reprogramming: mechanisms, concepts and general principles—from the worm to vertebrates. Curr. Opin. Genet. Dev. 40, 154–163.
Bernassola, F., Chillemi, G., Melino, G., 2019. HECT-type E3 ubiquitin ligases in cancer. Trends Biochem. Sci. 44, 1057–1075.
Bieschke, J.A.N., Zhang, Q., Bosco, D.A., Lerner, R.A., Powers, E.T., Wentworth, P., Kelly, J.W., 2006. Small molecule oxidation products trigger disease-associated protein misfolding. Acc. Chem. Res. 39, 611–619.
Blanco, S., Bandiera, R., Popis, M., Hussain, S., Lombard, P., Aleksic, J., Sajini, A., Tanna, H., Cortés-Garrido, R., Gkatza, N., 2016. Stem cell function and stress response are controlled by protein synthesis. Nature 534, 335–340.
Borkent, M., Bennett, B.D., Lackford, B., Bar-Nur, O., Brumbaugh, J., Wang, L., Du, Y., Fargo, D.C., Apostolou, E., Cheloufi, S., 2016. A serial shRNA screen for roadblocks to reprogramming identifies the protein modifier SUMO2. Stem Cell Rep. 6, 704–716.
Boulin, T., Etchberger, J.F., Hobert, O., 2006. Reporter gene fusions. WormBook Online Rev. C Elegans Biol. Internet.
Brenner, S., 1974. The genetics of Caenorhabditis elegans. Genetics 77, 71–94.
Briggs, S.D., Xiao, T., Sun, Z.-W., Caldwell, J.A., Shabanowitz, J., Hunt, D.F., Allis, C.D., Strahl, B.D., 2002. Trans-histone regulatory pathway in chromatin. Nature 418, 498–498.
Broers, J.L., Raymond, Y., Rot, M.K., Kuijpers, H., Wagenaar, S.S., Ramaekers, F.C., 1993. Nuclear A-type lamins are differentially expressed in human lung cancer subtypes. Am. J. Pathol. 143, 211.
Brosh, R., Assia-Alroy, Y., Molchadsky, A., Bornstein, C., Dekel, E., Madar, S., Shetzer, Y., Rivlin, N., Goldfinger, N., Sarig, R., 2013. p53 counteracts reprogramming by inhibiting mesenchymal-to-epithelial transition. Cell Death Differ. 20, 312–320.
Brumbaugh, J., Di Stefano, B., Hochedlinger, K., 2019. Reprogramming: identifying the mechanisms that safeguard cell identity. Development 146, dev182170.

Buchner, J., 1999. Hsp90 & Co.–a holding for folding. Trends Biochem. Sci. 24, 136–141.
Buckley, S.M., Aranda-Orgilles, B., Strikoudis, A., Apostolou, E., Loizou, E., Moran-Crusio, K., Farnsworth, C.L., Koller, A.A., Dasgupta, R., Silva, J.C., Stadtfeld, M., Hochedlinger, K., Chen, E.I., Aifantis, I., 2012. Regulation of Pluripotency and Cellular Reprogramming by the Ubiquitin-Proteasome System. Cell Stem Cell 11, 783–798.
Buganim, Y., Faddah, D.A., Jaenisch, R., 2013. Mechanisms and models of somatic cell reprogramming. Nat. Rev. Genet. 14, 427–439.
Bukowiecki, R., Adjaye, J., Prigione, A., 2014. Mitochondrial function in pluripotent stem cells and cellular reprogramming. Gerontology 60, 174–182.
Butin-Israeli, V., Adam, S.A., Goldman, A.E., Goldman, R.D., 2012. Nuclear lamin functions and disease. Trends Genet. 28, 464–471.
Capo-chichi, C.D., Cai, K.Q., Smedberg, J., Ganjei-Azar, P., Godwin, A.K., Xu, X.-X., 2011. Loss of A-type lamin expression compromises nuclear envelope integrity in breast cancer. Chin. J. Cancer 30, 415.
Chalfie, M., Tu, Y., Euskirchen, G., Ward, W.W., Prasher, D.C., 1994. Green fluorescent protein as a marker for gene expression. Science 263, 802–805.
Cheloufi, S., Elling, U., Hopfgartner, B., Jung, Y.L., Murn, J., Ninova, M., Hubmann, M., Badeaux, A.I., Euong Ang, C., Tenen, D., 2015. The histone chaperone CAF-1 safeguards somatic cell identity. Nature 528, 218–224.
Chen, J., Halappanavar, S., Th'ng, J., Li, Q., 2007. Ubiquitin-dependent distribution of the transcriptional coactivator p300 in cytoplasmic inclusion bodies. Epigenetics 2, 92–99.
Chen, J., Li, Q., 2011. Life and death of transcriptional co-activator p300. Epigenetics 6, 957–961.
Chen, Jiekai, Liu, H., Liu, J., Qi, J., Wei, B., Yang, J., Liang, H., Chen, Y., Chen, Jing, Wu, Y., 2013. H3K9 methylation is a barrier during somatic cell reprogramming into iPSCs. Nat. Genet. 45, 34–42.
Chen, Y., Greenwald, I., 2015. hecd-1 Modulates Notch Activity in Caenorhabditis elegans. G3 GenesGenomesGenetics 5, 353–359.
Chen, Y.-C., Ma, N.-X., Pei, Z.-F., Wu, Z., Do-Monte, F.H., Keefe, S., Yellin, E., Chen, M.S., Yin, J.-C., Lee, G., 2020. A NeuroD1 AAV-based gene therapy for functional brain repair after ischemic injury through in vivo astrocyte-to-neuron conversion. Mol. Ther. 28, 217–234.
Chen, Y.-S., Qiu, X.-B., 2012. Transcription-coupled replacement of histones: degradation or recycling? J. Genet. Genomics 39, 575–580.
Chiche, A., Le Roux, I., von Joest, M., Sakai, H., Aguín, S.B., Cazin, C., Salam, R., Fiette, L., Alegria, O., Flamant, P., 2017. Injury-induced senescence enables in vivo reprogramming in skeletal muscle. Cell Stem Cell 20, 407-414. e4.
Ciechanover, A., 2015. The unravelling of the ubiquitin system. Nat. Rev. Mol. Cell Biol. 16, 322–324.
Ciechanover, A., Iwai, K., 2004. The ubiquitin system: from basic mechanisms to the patient bed. IUBMB Life 56, 193–201.
Ciechanover, A., Orian, A., Schwartz, A.L., 2000. Ubiquitin-mediated proteolysis: biological regulation via destruction. Bioessays 22, 442–451.
Cohen, E., Dillin, A., 2008. The insulin paradox: aging, proteotoxicity and neurodegeneration. Nat. Rev. Neurosci. 9, 759–767.

Columbaro, M., Capanni, C., Mattioli, E., Novelli, G., Parnaik, V.K., Squarzoni, S., Maraldi, N.M., Lattanzi, G., 2005. Rescue of heterochromatin organization in Hutchinson-Gilford progeria by drug treatment. Cell. Mol. Life Sci. 62, 2669.
Condelli, V., Crispo, F., Pietrafesa, M., Lettini, G., Matassa, D.S., Esposito, F., Landriscina, M., Maddalena, F., 2019. HSP90 Molecular Chaperones, Metabolic Rewiring, and Epigenetics: Impact on Tumor Progression and Perspective for Anticancer Therapy. Cells 8, 532.
Cooper, S., Grijzenhout, A., Underwood, E., Ancelin, K., Zhang, T., Nesterova, T.B., Anil-Kirmizitas, B., Bassett, A., Kooistra, S.M., Agger, K., 2016. Jarid2 binds mono-ubiquitylated H2A lysine 119 to mediate crosstalk between Polycomb complexes PRC1 and PRC2. Nat. Commun. 7, 13661.
Coradeghini, R., Barboro, P., Rubagotti, A., Boccardo, F., Parodi, S., Carmignani, G., D'Arrigo, C., Patrone, E., Balbi, C., 2006. Differential expression of nuclear lamins in normal and cancerous prostate tissues. Oncol. Rep. 15, 609–613.
Corsi, A.K., 2006. A biochemist's guide to C. elegans. Anal. Biochem. 359, 1.
Corsi, A.K., Wightman, B., Chalfie, M., 2015. A transparent window into biology: a primer on Caenorhabditis elegans. Genetics 200, 387–407.
Damgaard, R.B., 2021. The ubiquitin system: from cell signalling to disease biology and new therapeutic opportunities. Cell Death Differ. 28, 423–426.
Das, I., Krzyzosiak, A., Schneider, K., Wrabetz, L., D'Antonio, M., Barry, N., Sigurdardottir, A., Bertolotti, A., 2015. Preventing proteostasis diseases by selective inhibition of a phosphatase regulatory subunit. Science 348, 239–242.
Davie, J.R., Lin, R., Allis, C.D., 1991. Timing of the appearance of ubiquitinated histones in developing new macronuclei of Tetrahymena thermophila. Biochem. Cell Biol. 69, 66–71.
Davis, R.L., Weintraub, H., Lassar, A.B., 1987. Expression of a single transfected cDNA converts fibroblasts to myoblasts. Cell 51, 987–1000.
Dörnen, J., Sieler, M., Weiler, J., Keil, S., Dittmar, T., 2020. Cell fusion-mediated tissue regeneration as an inducer of polyploidy and aneuploidy. Int. J. Mol. Sci. 21, 1811.
Doss, M.X., Sachinidis, A., 2019. Current challenges of iPSC-based disease modeling and therapeutic implications. Cells 8, 403.
Ebrahimi, B., 2015. Reprogramming barriers and enhancers: strategies to enhance the efficiency and kinetics of induced pluripotency. Cell Regen. 4, 4:10.
Eckschlager, T., Plch, J., Stiborova, M., Hrabeta, J., 2017. Histone deacetylase inhibitors as anticancer drugs. Int. J. Mol. Sci. 18, 1414.
Elsherbiny, A., Dobreva, G., 2021. Epigenetic memory of cell fate commitment. Curr. Opin. Cell Biol. 69, 80–87.
Endoh, M., Endo, T.A., Endoh, T., Isono, K., Sharif, J., Ohara, O., Toyoda, T., Ito, T., Eskeland, R., Bickmore, W.A., 2012. Histone H2A mono-ubiquitination is a crucial step to mediate PRC1-dependent repression of developmental genes to maintain ES cell identity. PLoS Genet. 8, e1002774.
Etchberger, J.F., Lorch, A., Sleumer, M.C., Zapf, R., Jones, S.J., Marra, M.A., Holt, R.A., Moerman, D.G., Hobert, O., 2007. The molecular signature and cis-regulatory architecture of a C. elegans gustatory neuron. Genes Dev. 21, 1653–1674.
Evangelisti, C., Cenni, V., Lattanzi, G., 2016. Potential therapeutic effects of the MTOR inhibitors for preventing ageing and progeria-related disorders. Br. J. Clin. Pharmacol. 82, 1229–1244.

Ezhkova, E., Tansey, W.P., 2004. Proteasomal ATPases link ubiquitylation of histone H2B to methylation of histone H3. Mol. Cell 13, 435–442.
Fang, L., El Wazan, L., Tan, C., Nguyen, T., Hung, S.S., Hewitt, A.W., Wong, R.C., 2018. Potentials of cellular reprogramming as a novel strategy for neuroregeneration. Front. Cell. Neurosci. 12, 460.
Fang, L., Zhang, L., Wei, W., Jin, X., Wang, P., Tong, Y., Li, J., Du, J.X., Wong, J., 2014. A methylation-phosphorylation switch determines Sox2 stability and function in ESC maintenance or differentiation. Mol. Cell 55, 537–551.
Fidalgo, M., Faiola, F., Pereira, C.-F., Ding, J., Saunders, A., Gingold, J., Schaniel, C., Lemischka, I.R., Silva, J.C., Wang, J., 2012. Zfp281 mediates Nanog autorepression through recruitment of the NuRD complex and inhibits somatic cell reprogramming. Proc. Natl. Acad. Sci. 109, 16202–16207.
Finley, D., 2009. Recognition and processing of ubiquitin-protein conjugates by the proteasome. Annu. Rev. Biochem. 78, 477–513.
Fuchs, G., Shema, E., Vesterman, R., Kotler, E., Wolchinsky, Z., Wilder, S., Golomb, L., Pribluda, A., Zhang, F., Haj-Yahya, M., 2012. RNF20 and USP44 regulate stem cell differentiation by modulating H2B monoubiquitylation. Mol. Cell 46, 662–673.
Fukushige, T., Hawkins, M.G., McGhee, J.D., 1998. The GATA-factor elt-2 is essential for formation of the Caenorhabditis elegans intestine. Dev. Biol. 198, 286–302.
Fukushige, T., Krause, M., 2005. The myogenic potency of HLH-1 reveals wide-spread developmental plasticity in early C. elegans embryos.
García-Prat, L., Sousa-Victor, P., Muñoz-Cánoves, P., 2017. Proteostatic and Metabolic Control of Stemness. Cell Stem Cell 20, 593–608.
Gilleard, J.S., McGhee, J.D., 2001. Activation of hypodermal differentiation in the Caenorhabditis elegans embryo by GATA transcription factors ELT-1 and ELT-3. Mol. Cell. Biol. 21, 2533–2544.
Giovannini, S., Fiorilli, C., Moriconi, V., Shi, Y., Candi, E., Melino, G., Bernassola, F., 2025. The role of HECT-type E3 ubiquitin ligases in DNA damage response and repair. Cell Death Discov.
Glowczewski, L., Yang, P., Kalashnikova, T., Santisteban, M.S., Smith, M.M., 2000. Histone-histone interactions and centromere function. Mol. Cell. Biol. 20, 5700–5711.
Golden, J.W., Riddle, D.L., 1984. A Caenorhabditis elegans dauer-inducing pheromone and an antagonistic component of the food supply. J. Chem. Ecol. 10, 1265–1280.
Goldknopf, I.L., Busch, H., 1977. Isopeptide linkage between nonhistone and histone 2A polypeptides of chromosomal conjugate-protein A24. Proc. Natl. Acad. Sci. 74, 864–868.
Goldknopf, I.L., Taylor, C.W., Baum, R.M., Yeoman, L.C., Olson, M.O., Prestayko, A.W., Busch, H., 1975. Isolation and characterization of protein A24, a" histone-like" non-histone chromosomal protein. J. Biol. Chem. 250, 7182–7187.
Gouveia, C., Huyser, C., Egli, D., Pepper, M.S., 2020. Lessons learned from somatic cell nuclear transfer. Int. J. Mol. Sci. 21, 2314.
Graf, T., 2011. Historical origins of transdifferentiation and reprogramming. Cell Stem Cell 9, 504–516.
Groothuis, T.A., Dantuma, N.P., Neefjes, J., Salomons, F.A., 2006. Ubiquitin crosstalk connecting cellular processes. Cell Div. 1, 21.

Gu, Y., Jones, A.E., Yang, W., Liu, S., Dai, Q., Liu, Y., Swindle, C.S., Zhou, D., Zhang, Z., Ryan, T.M., 2016. The histone H2A deubiquitinase Usp16 regulates hematopoiesis and hematopoietic stem cell function. Proc. Natl. Acad. Sci. 113, E51–E60.
Guo, Z., Zhang, L., Wu, Z., Chen, Y., Wang, F., Chen, G., 2014. In vivo direct reprogramming of reactive glial cells into functional neurons after brain injury and in an Alzheimer's disease model. Cell Stem Cell 14, 188–202.
Gurdon, J.B., Elsdale, T.R., Fischberg, M., 1958. Sexually mature individuals of Xenopus laevis from the transplantation of single somatic nuclei. Nature 182, 64–65.
Hadorn, E., 1963. Differenzierungsleistungen wiederholt fragmentierter Teilstücke männlicher Genitalscheiben von Drosophila melanogaster nach Kultur in vivo. Dev. Biol. 7, 617–629.
Hajduskova, M., Baytek, G., Kolundzic, E., Gosdschan, A., Kazmierczak, M., Ofenbauer, A., Beato del Rosal, M.L., Herzog, S., ul Fatima, N., Mertins, P., 2019. MRG-1/MRG15 is a barrier for germ cell to neuron reprogramming in Caenorhabditis elegans. Genetics 211, 121–139.
Håkelien, A.-M., Delbarre, E., Gaustad, K.G., Buendia, B., Collas, P., 2008. Expression of the myodystrophic R453W mutation of lamin A in C2C12 myoblasts causes promoter-specific and global epigenetic defects. Exp. Cell Res. 314, 1869–1880.
Hamanaka, R.B., Chandel, N.S., 2010. Mitochondrial reactive oxygen species regulate cellular signaling and dictate biological outcomes. Trends Biochem. Sci. 35, 505–513.
Hanna, J.H., Saha, K., Jaenisch, R., 2010. Pluripotency and cellular reprogramming: facts, hypotheses, unresolved issues. Cell 143, 508–525.
Hansson, J., Rafiee, M.R., Reiland, S., Polo, J.M., Gehring, J., Okawa, S., Huber, W., Hochedlinger, K., Krijgsveld, J., 2012. Highly coordinated proteome dynamics during reprogramming of somatic cells to pluripotency. Cell Rep. 2, 1579–1592.
Harfe, B.D., Branda, C.S., Krause, M., Stern, M.J., Fire, A., 1998. MyoD and the specification of muscle and non-muscle fates during postembryonic development of the C. elegans mesoderm. Development 125, 2479–2488.
Haridhasapavalan, K.K., Raina, K., Dey, C., Adhikari, P., Thummer, R.P., 2020. An Insight into Reprogramming Barriers to iPSC Generation. Stem Cell Rev. Rep. 16, 56–81.
Harr, J.C., Schmid, C.D., Muñoz-Jiménez, C., Romero-Bueno, R., Kalck, V., Gonzalez-Sandoval, A., Hauer, M.H., Padeken, J., Askjaer, P., Mattout, A., Gasser, S.M., 2020. Loss of an H3K9me anchor rescues laminopathy-linked changes in nuclear organization and muscle function in an Emery-Dreifuss muscular dystrophy model. Genes Dev. 34, 560–579.
Hartl, F.U., 2017. Protein misfolding diseases. Annu. Rev. Biochem. 86, 21–26.
Hayakawa, T., Nakayama, J., 2011. Physiological roles of class I HDAC complex and histone demethylase. BioMed Res. Int. 2011, 129383.
Heimbucher, T., Liu, Z., Bossard, C., McCloskey, R., Carrano, A.C., Riedel, C.G., Tanasa, B., Klammt, C., Fonslow, B.R., Riera, C.E., 2015. The deubiquitylase MATH-33 controls DAF-16 stability and function in metabolism and longevity. Cell Metab. 22, 151–163.
Helfand, B.T., Wang, Y., Pfleghaar, K., Shimi, T., Taimen, P., Shumaker, D.K., 2012. Chromosomal regions associated with prostate cancer risk localize to lamin

B-deficient microdomains and exhibit reduced gene transcription. J. Pathol. 226, 735–745.
Hernebring, M., Fredriksson, Å., Liljevald, M., Cvijovic, M., Norrman, K., Wiseman, J., Semb, H., Nyström, T., 2013. Removal of damaged proteins during ES cell fate specification requires the proteasome activator PA28. Sci. Rep. 3, 1381.
Hershko, A., Ciechanover, A., 1998. The ubiquitin system. Annu. Rev. Biochem. 67, 425–479.
Hertel, P., Daniel, J., Stegehake, D., Vaupel, H., Kailayangiri, S., Gruel, C., Woltersdorf, C., Liebau, E., 2013. The ubiquitin-fold modifier 1 (Ufm1) cascade of Caenorhabditis elegans. J. Biol. Chem. 288, 10661–10671.
Hipp, M.S., Park, S.-H., Hartl, F.U., 2014. Proteostasis impairment in protein-misfolding and-aggregation diseases. Trends Cell Biol. 24, 506–514.
Ho, R., Papp, B., Hoffman, J.A., Merrill, B.J., Plath, K., 2013. Stage-specific regulation of reprogramming to induced pluripotent stem cells by Wnt signaling and T cell factor proteins. Cell Rep. 3, 2113–2126.
Hobert, O., 2016. A map of terminal regulators of neuronal identity in Caenorhabditis elegans. Wiley Interdiscip. Rev. Dev. Biol. 5, 474–498.
Hochedlinger, K., Jaenisch, R., 2015. Induced pluripotency and epigenetic reprogramming. Cold Spring Harb. Perspect. Biol. 7, a019448.
Højfeldt, J.W., Laugesen, A., Willumsen, B.M., Damhofer, H., Hedehus, L., Tvardovskiy, A., Mohammad, F., Jensen, O.N., Helin, K., 2018. Accurate H3K27 methylation can be established de novo by SUZ12-directed PRC2. Nat. Struct. Mol. Biol. 25, 225–232.
Hong, H., Takahashi, K., Ichisaka, T., Aoi, T., Kanagawa, O., Nakagawa, M., Okita, K., Yamanaka, S., 2009. Suppression of induced pluripotent stem cell generation by the p53–p21 pathway. Nature 460, 1132–1135.
Huang, S.-Y., Barnard, M.B., Xu, M., Matsui, S. -l, Rose, S.M., Garrard, W.T., 1986. The active immunoglobulin kappa chain gene is packaged by non-ubiquitin-conjugated nucleosomes. Proc. Natl. Acad. Sci. 83, 3738–3742.
Hunt, L.T., Dayhoff, M.O., 1977. Amino-terminal sequence identity of ubiquitin and the nonhistone component of nuclear protein A24. Biochem. Biophys. Res. Commun. 74, 650–655.
Hutchison, C.J., 2002. Lamins: building blocks or regulators of gene expression? Nat. Rev. Mol. Cell Biol. 3, 848–858.
Hwang, C.-S., Shemorry, A., Auerbach, D., Varshavsky, A., 2010. The N-end rule pathway is mediated by a complex of the RING-type Ubr1 and HECT-type Ufd4 ubiquitin ligases. Nat. Cell Biol. 12, 1177–1185.
Ieda, M., Fu, J.-D., Delgado-Olguin, P., Vedantham, V., Hayashi, Y., Bruneau, B.G., Srivastava, D., 2010. Direct reprogramming of fibroblasts into functional cardiomyocytes by defined factors. Cell 142, 375–386.
Inoue, D., Aihara, H., Sato, T., Mizusaki, H., Doiguchi, M., Higashi, M., Imamura, Y., Yoneda, M., Miyanishi, T., Fujii, S., 2015. Dzip3 regulates developmental genes in mouse embryonic stem cells by reorganizing 3D chromatin conformation. Sci. Rep. 5, 16567.
Ishiuchi, T., Enriquez-Gasca, R., Mizutani, E., Bošković, A., Ziegler-Birling, C., Rodriguez-Terrones, D., Wakayama, T., Vaquerizas, J.M., Torres-Padilla, M.-E., 2015. Early embryonic-like cells are induced by downregulating replication-dependent chromatin assembly. Nat. Struct. Mol. Biol. 22, 662–671.

Jackson, A.L., Bartz, S.R., Schelter, J., Kobayashi, S.V., Burchard, J., Mao, M., Li, B., Cavet, G., Linsley, P.S., 2003. Expression profiling reveals off-target gene regulation by RNAi. Nat. Biotechnol. 21, 635–637.
Jacobson, T., Navarrete, C., Sharma, S.K., Sideri, T.C., Ibstedt, S., Priya, S., Grant, C.M., Christen, P., Goloubinoff, P., Tamás, M.J., 2012. Arsenite interferes with protein folding and triggers formation of protein aggregates in yeast. J. Cell Sci. 125, 5073–5083.
Jarosz, D., 2016. Hsp90: a global regulator of the genotype-to-phenotype map in cancers. Adv. Cancer Res. 129, 225–247.
Jarriault, S., Schwab, Y., Greenwald, I., 2008. A Caenorhabditis elegans model for epithelial–neuronal transdifferentiation. Proc. Natl. Acad. Sci. 105, 3790–3795.
Jayaraj, G.G., Hipp, M.S., Hartl, F.U., 2020. Functional Modules of the Proteostasis Network. Cold Spring Harb. Perspect. Biol. 12, a033951.
Jin, L., Williamson, A., Banerjee, S., Philipp, I., Rape, M., 2008. Mechanism of ubiquitin-chain formation by the human anaphase-promoting complex. Cell 133, 653–665.
Jin, Y., Hoskins, R., Horvitz, H.R., 1994. Control of type-D GABAergic neuron differentiation by C. elegans UNC-30 homeodomain protein. Nature 372, 780–783.
Jin, Y., Zeng, S.X., Lee, H., Lu, H., 2004. MDM2 mediates p300/CREB-binding protein-associated factor ubiquitination and degradation. J. Biol. Chem. 279, 20035–20043.
Jopling, C., Boue, S., Belmonte, J.C.I., 2011. Dedifferentiation, transdifferentiation and reprogramming: three routes to regeneration. Nat. Rev. Mol. Cell Biol. 12, 79–89.
Ju, D., Xie, Y., 2006. A synthetic defect in protein degradation caused by loss of Ufd4 and Rad23. Biochem. Biophys. Res. Commun. 341, 648–652.
Kagias, K., Ahier, A., Fischer, N., Jarriault, S., 2012. Members of the NODE (Nanog and Oct4-associated deacetylase) complex and SOX-2 promote the initiation of a natural cellular reprogramming event in vivo. Proc. Natl. Acad. Sci. 109, 6596–6601.
Kaletta, T., Hengartner, M.O., 2006. Finding function in novel targets: C. elegans as a model organism. Nat. Rev. Drug Discov. 5, 387–399.
Kao, S.-H., Wu, H.-T., Wu, K.-J., 2018. Ubiquitination by HUWE1 in tumorigenesis and beyond. J. Biomed. Sci. 25, 67.
Kaushik, S., Cuervo, A.M., 2015. Proteostasis and aging. Nat. Med. 21, 1406–1415.
Kerem, B., Zielenski, J., Markiewicz, D., Bozon, D., Gazit, E., Yahav, J., Kennedy, D., Riordan, J.R., Collins, F.S., Rommens, J.M., 1990. Identification of mutations in regions corresponding to the two putative nucleotide (ATP)-binding folds of the cystic fibrosis gene. Proc. Natl. Acad. Sci. 87, 8447–8451.
Keshri, R., Detraux, D., Phal, A., McCurdy, C., Jhajharia, S., Chan, T.C., Mathieu, J., Ruohola-Baker, H., 2024. Next-generation direct reprogramming. Front. Cell Dev. Biol. 12.
Kiefer, J.C., Smith, P.A., Mango, S.E., 2007. PHA-4/FoxA cooperates with TAM-1/TRIM to regulate cell fate restriction in the C. elegans foregut. Dev. Biol. 303, 611–624.
Kimble, J., Hirsh, D., 1979. The postembryonic cell lineages of the hermaphrodite and male gonads in Caenorhabditis elegans. Dev. Biol. 70, 396–417.
Kingston, R.E., Tamkun, J.W., 2014. Transcriptional regulation by trithorax-group proteins. Cold Spring Harb. Perspect. Biol. 6, a019349.

Knoblich, J.A., 2008. Mechanisms of asymmetric stem cell division. Cell 132, 583–597.
Koganti, P., Levy-Cohen, G., Blank, M., 2018. Smurfs in protein homeostasis, signaling, and cancer. Front. Oncol. 8, 295.
Kolundzic, E., Ofenbauer, A., Bulut, S.I., Uyar, B., Baytek, G., Sommermeier, A., Seelk, S., He, M., Hirsekorn, A., Vucicevic, D., Akalin, A., Diecke, S., Lacadie, S.A., Tursun, B., 2018. FACT Sets a Barrier for Cell Fate Reprogramming in *Caenorhabditis elegans* and Human Cells. Dev. Cell 46, 611-626.e12.
Kulessa, H., Frampton, J., Graf, T., 1995. GATA-1 reprograms avian myelomonocytic cell lines into eosinophils, thromboblasts, and erythroblasts. Genes Dev. 9, 1250–1262.
Kutscher, L.M., Shaham, S., 2014. Forward and reverse mutagenesis in C. elegans. WormBook Online Rev. C Elegans Biol. 1.
Labbadia, J., Morimoto, R.I., 2015. The biology of proteostasis in aging and disease. Annu. Rev. Biochem. 84, 435–464.
Ladewig, J., Koch, P., Brüstle, O., 2013. Leveling Waddington: the emergence of direct programming and the loss of cell fate hierarchies. Nat. Rev. Mol. Cell Biol. 14, 225–236.
Lampersberger, L., Conte, F., Ghosh, S., Xiao, Y., Price, J., Jordan, D., Matus, D.Q., Sarkies, P., Beli, P., Miska, E.A., 2023. Loss of the E3 ubiquitin ligases UBR-5 or HECD-1 restores Caenorhabditis elegans development in the absence of SWI/SNF function. Proc. Natl. Acad. Sci. 120, e2217992120.
Laugesen, A., Højfeldt, J.W., Helin, K., 2019. Molecular mechanisms directing PRC2 recruitment and H3K27 methylation. Mol. Cell 74, 8–18.
Lee, H.J., Gutierrez-Garcia, R., Vilchez, D., 2017. Embryonic stem cells: a novel paradigm to study proteostasis? FEBS J. 284, 391–398.
Lee, J.W., Beebe, K., Nangle, L.A., Jang, J., Longo-Guess, C.M., Cook, S.A., Davisson, M.T., Sundberg, J.P., Schimmel, P., Ackerman, S.L., 2006. Editing-defective tRNA synthetase causes protein misfolding and neurodegeneration. Nature 443, 50–55.
Lee, S.W., Oh, Y.M., Lu, Y.-L., Kim, W.K., Yoo, A.S., 2018. MicroRNAs overcome cell fate barrier by reducing EZH2-controlled REST stability during neuronal conversion of human adult fibroblasts. Dev. Cell 46, 73-84. e7.
Levinger, L., Varshavsky, A., 1982. Selective arrangement of ubiquitinated and D1 protein-containing nucleosomes within the Drosophila genome. Cell 28, 375–385.
Li, L., Martinez, S.S., Hu, W., Liu, Z., Tjian, R., 2015. A specific E3 ligase/deubiquitinase pair modulates TBP protein levels during muscle differentiation. Elife 4, e08536.
Liang, G., Zhang, Y., 2013. Embryonic stem cell and induced pluripotent stem cell: an epigenetic perspective. Cell Res. 23, 49–69.
Liao, B., Jin, Y., 2010. Wwp2 mediates Oct4 ubiquitination and its own auto-ubiquitination in a dosage-dependent manner. Cell Res. 20, 332–344.
Lin, X., Ruan, X., Anderson, M.G., McDowell, J.A., Kroeger, P.E., Fesik, S.W., Shen, Y., 2005. siRNA-mediated off-target gene silencing triggered by a 7 nt complementation. Nucleic Acids Res. 33, 4527–4535.
Lis, E.T., Romesberg, F.E., 2006. Role of Doa1 in the Saccharomyces cerevisiae DNA damage response. Mol. Cell. Biol. 26, 4122–4133.
Liu, J., Ben-Shahar, T.R., Riemer, D., Treinin, M., Spann, P., Weber, K., Fire, A., Gruenbaum, Y., 2000. Essential Roles for Caenorhabditis elegans Lamin Gene

in Nuclear Organization, Cell Cycle Progression, and Spatial Organization of Nuclear Pore Complexes. Mol. Biol. Cell 11, 3937–3947.
Liu, L., Komatsu, H., Murray, I.V., Axelsen, P.H., 2008. Promotion of amyloid β protein misfolding and fibrillogenesis by a lipid oxidation product. J. Mol. Biol. 377, 1236–1250.
Liu, Z., Miao, D., Xia, Q., Hermo, L., Wing, S.S., 2007. Regulated expression of the ubiquitin protein ligase, E3Histone/LASU1/Mule/ARF-BP1/HUWE1, during spermatogenesis. Dev. Dyn. Off. Publ. Am. Assoc. Anat. 236, 2889–2898.
Llamas, E., Alirzayeva, H., Loureiro, R., Vilchez, D., 2020. The intrinsic proteostasis network of stem cells. Curr. Opin. Cell Biol., Differentiation and disease 67, 46–55.
Llorens-Bobadilla, E., Zhao, S., Baser, A., Saiz-Castro, G., Zwadlo, K., Martin-Villalba, A., 2015. Single-cell transcriptomics reveals a population of dormant neural stem cells that become activated upon brain injury. Cell Stem Cell 17, 329–340.
Lluis, F., Pedone, E., Pepe, S., Cosma, M.P., 2008. Periodic activation of Wnt/β-catenin signaling enhances somatic cell reprogramming mediated by cell fusion. Cell Stem Cell 3, 493–507.
Machiels, B.M., Broers, J.L., Raymond, Y., de Ley, L., Kuijpers, H.J., Caberg, N.E., Ramaekers, F.C., 1995. Abnormal A-type lamin organization in a human lung carcinoma cell line. Eur. J. Cell Biol. 67, 328–335.
Malin, K., Witkowska-Piłaszewicz, O., Papis, K., 2022. The many problems of somatic cell nuclear transfer in reproductive cloning of mammals. Theriogenology 189, 246–254.
Marión, R.M., Strati, K., Li, H., Murga, M., Blanco, R., Ortega, S., Fernandez-Capetillo, O., Serrano, M., Blasco, M.A., 2009. A p53-mediated DNA damage response limits reprogramming to ensure iPS cell genomic integrity. Nature 460, 1149–1153.
Mark, K.G., Rape, M., 2021. Ubiquitin-dependent regulation of transcription in development and disease. EMBO Rep. 22, EMBR202051078.
Matoba, S., Liu, Y., Lu, F., Iwabuchi, K.A., Shen, L., Inoue, A., Zhang, Y., 2014. Embryonic development following somatic cell nuclear transfer impeded by persisting histone methylation. Cell 159, 884–895.
Mattioli, E., Andrenacci, D., Garofalo, C., Prencipe, S., Scotlandi, K., Remondini, D., Gentilini, D., Di Blasio, A.M., Valente, S., Scarano, E., 2018. Altered modulation of lamin A/C-HDAC2 interaction and p21 expression during oxidative stress response in HGPS. Aging Cell 17, e12824.
McCloskey, R.J., Kemphues, K.J., 2012. Deubiquitylation machinery is required for embryonic polarity in Caenorhabditis elegans. PLoS Genet. 8, e1003092.
Meneely, P.M., Dahlberg, C.L., Rose, J.K., 2019. Working with worms: Caenorhabditis elegans as a model organism. Curr. Protoc. Essent. Lab. Tech. 19, e35.
Merkwirth, C., Jovaisaite, V., Durieux, J., Matilainen, O., Jordan, S.D., Quiros, P.M., Steffen, K.K., Williams, E.G., Mouchiroud, L., Tronnes, S.U., 2016. Two conserved histone demethylases regulate mitochondrial stress-induced longevity. Cell 165, 1209–1223.
Mersman, D.P., Du, H.-N., Fingerman, I.M., South, P.F., Briggs, S.D., 2009. Polyubiquitination of the demethylase Jhd2 controls histone methylation and gene expression. Genes Dev. 23, 951–962.

Moehle, E.A., Shen, K., Dillin, A., 2019. Mitochondrial proteostasis in the context of cellular and organismal health and aging. J. Biol. Chem. 294, 5396–5407.
Morimoto, R.I., Cuervo, A.M., 2014. Proteostasis and the aging proteome in health and disease. J. Gerontol. Ser. Biomed. Sci. Med. Sci. 69, S33–S38.
Moss, S.F., Krivosheyev, V., De Souza, A., Chin, K., Gaetz, H.P., Chaudhary, N., Worman, H.J., Holt, P.R., 1999. Decreased and aberrant nuclear lamin expression in gastrointestinal tract neoplasms. Gut 45, 723–729.
Mosteiro, L., Pantoja, C., Alcazar, N., Marión, R.M., Chondronasiou, D., Rovira, M., Fernandez-Marcos, P.J., Muñoz-Martin, M., Blanco-Aparicio, C., Pastor, J., 2016. Tissue damage and senescence provide critical signals for cellular reprogramming in vivo. Science 354, aaf4445.
Muraoka, N., Yamakawa, H., Miyamoto, K., Sadahiro, T., Umei, T., Isomi, M., Nakashima, H., Akiyama, M., Wada, R., Inagawa, K., 2014. MiR-133 promotes cardiac reprogramming by directly repressing Snai1 and silencing fibroblast signatures. EMBO J. 33, 1565–1581.
Murray-Nerger, L.A., Cristea, I.M., 2021. Lamin post-translational modifications: emerging toggles of nuclear organization and function. Trends Biochem. Sci. 46, 832–847.
Nakagawa, T., Nakayama, K., 2015. Protein monoubiquitylation: targets and diverse functions. Genes Cells 20, 543–562.
Nandi, D., Tahiliani, P., Kumar, A., Chandu, D., 2006. The ubiquitin-proteasome system. J. Biosci. 31, 137–155.
Nickel, B.E., Allis, C.D., Davie, J.R., 1989. Ubiquitinated histone H2B is preferentially located in transcriptionally active chromatin. Biochemistry 28, 958–963.
Noormohammadi, A., Calculli, G., Gutierrez-Garcia, R., Khodakarami, A., Koyuncu, S., Vilchez, D., 2018. Mechanisms of protein homeostasis (proteostasis) maintain stem cell identity in mammalian pluripotent stem cells. Cell. Mol. Life Sci. 75, 275–290.
Noormohammadi, A., Khodakarami, A., Gutierrez-Garcia, R., Lee, H.J., Koyuncu, S., König, T., Schindler, C., Saez, I., Fatima, A., Dieterich, C., 2016. Somatic increase of CCT8 mimics proteostasis of human pluripotent stem cells and extends C. elegans lifespan. Nat. Commun. 7, 13649.
Okita, Y., Nakayama, K.I., 2012. UPS delivers pluripotency. Cell Stem Cell 11, 728–730.
Olguín, H.C., 2022. The Gentle Side of the UPS: Ubiquitin-Proteasome System and the Regulation of the Myogenic Program. Front. Cell Dev. Biol. 9.
Onder, T.T., Kara, N., Cherry, A., Sinha, A.U., Zhu, N., Bernt, K.M., Cahan, P., Mancarci, B.O., Unternaehrer, J., Gupta, P.B., 2012. Chromatin-modifying enzymes as modulators of reprogramming. Nature 483, 598–602.
Opperman, K.J., Mulcahy, B., Giles, A.C., Risley, M.G., Birnbaum, R.L., Tulgren, E.D., Dawson-Scully, K., Zhen, M., Grill, B., 2017. The HECT family ubiquitin ligase EEL-1 regulates neuronal function and development. Cell Rep. 19, 822–835.
Pang, Z.P., Yang, N., Vierbuchen, T., Ostermeier, A., Fuentes, D.R., Yang, T.Q., Citri, A., Sebastiano, V., Marro, S., Südhof, T.C., 2011. Induction of human neuronal cells by defined transcription factors. Nature 476, 220–223.
Patel, T., Hobert, O., 2017. Coordinated control of terminal differentiation and restriction of cellular plasticity. eLife 6, e24100.

Patel, T., Tursun, B., Rahe, D.P., Hobert, O., 2012. Removal of Polycomb repressive complex 2 makes C. elegans germ cells susceptible to direct conversion into specific somatic cell types. Cell Rep. 2, 1178–1186.
Pathare, G.R., Nagy, I., Bohn, S., Unverdorben, P., Hubert, A., Körner, R., Nickell, S., Lasker, K., Sali, A., Tamura, T., 2012. The proteasomal subunit Rpn6 is a molecular clamp holding the core and regulatory subcomplexes together. Proc. Natl. Acad. Sci. 109, 149–154.
Pavri, R., Zhu, B., Li, G., Trojer, P., Mandal, S., Shilatifard, A., Reinberg, D., 2006. Histone H2B monoubiquitination functions cooperatively with FACT to regulate elongation by RNA polymerase II. Cell 125, 703–717.
Pellegrini, C., Columbaro, M., Capanni, C., D'Apice, M.R., Cavallo, C., Murdocca, M., Lattanzi, G., Squarzoni, S., 2015. All-trans retinoic acid and rapamycin normalize Hutchinson Gilford progeria fibroblast phenotype. Oncotarget 6, 29914.
Pellegrino, M.W., Nargund, A.M., Haynes, C.M., 2013. Signaling the mitochondrial unfolded protein response. Biochim. Biophys. Acta BBA-Mol. Cell Res. 1833, 410–416.
Pengelly, A.R., Kalb, R., Finkl, K., Müller, J., 2015. Transcriptional repression by PRC1 in the absence of H2A monoubiquitylation. Genes Dev. 29, 1487–1492.
Pereira, C.F., Terranova, R., Ryan, N.K., Santos, J., Morris, K.J., Cui, W., Merkenschlager, M., Fisher, A.G., 2008. Heterokaryon-based reprogramming of human B lymphocytes for pluripotency requires Oct4 but not Sox2. PLoS Genet. 4, e1000170.
Pereira, M., Birtele, M., Shrigley, S., Benitez, J.A., Hedlund, E., Parmar, M., Ottosson, D.R., 2017. Direct reprogramming of resident NG2 glia into neurons with properties of fast-spiking parvalbumin-containing interneurons. Stem Cell Rep. 9, 742–751.
Pickart, C.M., 2001. Mechanisms underlying ubiquitination. Annu. Rev. Biochem. 70, 503–533.
Pickart, C.M., Fushman, D., 2004. Polyubiquitin chains: polymeric protein signals. Curr. Opin. Chem. Biol. 8, 610–616.
Pozhidaeva, A., Bezsonova, I., 2019. USP7: Structure, substrate specificity, and inhibition. DNA Repair 76, 30–39.
Qian, M.-X., Pang, Y., Liu, C.H., Haratake, K., Du, B.-Y., Ji, D.-Y., Wang, G.-F., Zhu, Q.-Q., Song, W., Yu, Y., 2013. Acetylation-mediated proteasomal degradation of core histones during DNA repair and spermatogenesis. Cell 153, 1012–1024.
Qin, H., Diaz, A., Blouin, L., Lebbink, R.J., Patena, W., Tanbun, P., LeProust, E.M., McManus, M.T., Song, J.S., Ramalho-Santos, M., 2014. Systematic identification of barriers to human iPSC generation. Cell 158, 449–461.
Quintin, S., Michaux, G., McMahon, L., Gansmuller, A., Labouesse, M., 2001. The Caenorhabditis elegans gene lin-26 can trigger epithelial differentiation without conferring tissue specificity. Dev. Biol. 235, 410–421.
Raizen, D.M., Zimmerman, J.E., Maycock, M.H., Ta, U.D., You, Y., Sundaram, M.V., Pack, A.I., 2008. Lethargus is a Caenorhabditis elegans sleep-like state. Nature 451, 569–572.
Rasmussen, K.D., Helin, K., 2016. Role of TET enzymes in DNA methylation, development, and cancer. Genes Dev. 30, 733–750.
Rasmussen, M.A., Holst, B., Tümer, Z., Johnsen, M.G., Zhou, S., Stummann, T.C., Hyttel, P., Clausen, C., 2014. Transient p53 suppression increases

reprogramming of human fibroblasts without affecting apoptosis and DNA damage. Stem Cell Rep. 3, 404–413.
Rastogi, A., Joshi, P., Contreras, E., Gama, V., 2019. Remodeling of mitochondrial morphology and function: an emerging hallmark of cellular reprogramming. Cell Stress 3, 181.
Ricci, A.R., Genereaux, J., Brandl, C.J., 2002. Components of the SAGA histone acetyltransferase complex are required for repressed transcription of ARG1 in rich medium. Mol. Cell. Biol. 22, 4033–4042.
Richard, L., Gauvin, L., Raine, K., 2011. Ecological models revisited: their uses and evolution in health promotion over two decades. Annu. Rev. Public Health 32, 307–326.
Riddle, D.L., Blumenthal, T., Meyer, B.J., Priess, J.R., 1997. C. elegans ii.
Riddle, M.R., Weintraub, A., Nguyen, K.C., Hall, D.H., Rothman, J.H., 2013. Transdifferentiation and remodeling of post-embryonic C. elegans cells by a single transcription factor. Development 140, 4844–4849.
Romani, B., Baygloo, N.S., Hamidi-Fard, M., Aghasadeghi, M.R., Allahbakhshi, E., 2016. HIV-1 Vpr protein induces proteasomal degradation of chromatin-associated class I HDACs to overcome latent infection of macrophages. J. Biol. Chem. 291, 2696–2711.
Ross, A.J., Li, M., Yu, B., Gao, M.X., Derry, W.B., 2011. The EEL-1 ubiquitin ligase promotes DNA damage-induced germ cell apoptosis in C. elegans. Cell Death Differ. 18, 1140–1149.
Rothman, J., Jarriault, S., 2019. Developmental plasticity and cellular reprogramming in Caenorhabditis elegans. Genetics 213, 723–757.
Roy, S., Ghosh, M.K., 2025. Ubiquitin proteasome system (UPS): a crucial determinant of the epigenetic landscape in cancer. Epigenomics 17, 625–644.
Sala, A.J., Bott, L.C., Morimoto, R.I., 2017. Shaping proteostasis at the cellular, tissue, and organismal level. J. Cell Biol. 216, 1231–1241.
Samavarchi-Tehrani, P., Golipour, A., David, L., Sung, H., Beyer, T.A., Datti, A., Woltjen, K., Nagy, A., Wrana, J.L., 2010. Functional genomics reveals a BMP-driven mesenchymal-to-epithelial transition in the initiation of somatic cell reprogramming. Cell Stem Cell 7, 64–77.
Sampson, C., Wang, Q., Otkur, W., Zhao, H., Lu, Y., Liu, X., Piao, H., 2023. The roles of E3 ubiquitin ligases in cancer progression and targeted therapy. Clin. Transl. Med. 13, e1204.
Santi, S., Cenni, V., Capanni, C., Lattanzi, G., Mattioli, E., 2020. PCAF involvement in lamin A/C-HDAC2 interplay during the early phase of muscle differentiation. Cells 9, 1735.
Saretzki, G., Armstrong, L., Leake, A., Lako, M., von Zglinicki, T., 2004. Stress defense in murine embryonic stem cells is superior to that of various differentiated murine cells. Stem Cells 22, 962–971.
Sarkar, A.A., Zohn, I.E., 2012. Hectd1 regulates intracellular localization and secretion of Hsp90 to control cellular behavior of the cranial mesenchyme. J. Cell Biol. 196, 789–800.
Scheuermann, J.C., de Ayala Alonso, A.G., Oktaba, K., Ly-Hartig, N., McGinty, R.K., Fraterman, S., Wilm, M., Muir, T.W., Müller, J., 2010. Histone H2A deubiquitinase activity of the Polycomb repressive complex PR-DUB. Nature 465, 243–247.

Schläpfer, T., 1963. Der Einfluß des adulten Wirtsmilieus auf die Entwicklung von larvalen Augenantennen-Imaginalscheiben von Drosophila melanogaster. Wilhelm RouxArchiv Für Entwicklungsmechanik Org. 154, 378–404.
Schuettengruber, B., Bourbon, H.-M., Di Croce, L., Cavalli, G., 2017. Genome regulation by polycomb and trithorax: 70 years and counting. Cell 171, 34–57.
Schuettengruber, B., Chourrout, D., Vervoort, M., Leblanc, B., Cavalli, G., 2007. Genome regulation by polycomb and trithorax proteins. Cell 128, 735–745.
Seelk, S., Adrian-Kalchhauser, I., Hargitai, B., Hajduskova, M., Gutnik, S., Tursun, B., Ciosk, R., 2016. Increasing Notch signaling antagonizes PRC2-mediated silencing to promote reprograming of germ cells into neurons. Elife 5, e15477.
Segref, A., Kevei, É., Pokrzywa, W., Schmeisser, K., Mansfeld, J., Livnat-Levanon, N., Ensenauer, R., Glickman, M.H., Ristow, M., Hoppe, T., 2014. Pathogenesis of human mitochondrial diseases is modulated by reduced activity of the ubiquitin/proteasome system. Cell Metab. 19, 642–652.
Selenina, A.V., Tsimokha, A.S., Tomilin, A.N., 2017. Proteasomes in protein homeostasis of pluripotent stem cells. Acta Naturae 9, 39.
Sewduth, R.N., Baietti, M.F., Sablina, A.A., 2020. Cracking the monoubiquitin code of genetic diseases. Int. J. Mol. Sci. 21, 3036.
Shahbazian, M.D., Grunstein, M., 2007. Functions of site-specific histone acetylation and deacetylation. Annu Rev Biochem 76, 75–100.
Shao, L.-W., Peng, Q., Dong, M., Gao, K., Li, Yumei, Li, Yi, Li, C.-Y., Liu, Y., 2020. Histone deacetylase HDA-1 modulates mitochondrial stress response and longevity. Nat. Commun. 11, 4639.
Shemorry, A., Hwang, C.-S., Varshavsky, A., 2013. Control of protein quality and stoichiometries by N-terminal acetylation and the N-end rule pathway. Mol. Cell 50, 540–551.
Shmueli, M.D., Sheban, D., Eisenberg‐Lerner, A., Merbl, Y., 2022. Histone degradation by the proteasome regulates chromatin and cellular plasticity. FEBS J. 289, 3304–3316.
Signer, R.A., Magee, J.A., Salic, A., Morrison, S.J., 2014. Haematopoietic stem cells require a highly regulated protein synthesis rate. Nature 509, 49–54.
Silva, J., Chambers, I., Pollard, S., Smith, A., 2006. Nanog promotes transfer of pluripotency after cell fusion. Nature 441, 997–1001.
Simic, M.S., Moehle, E.A., Schinzel, R.T., Lorbeer, F.K., Halloran, J.J., Heydari, K., Sanchez, M., Jullié, D., Hockemeyer, D., Dillin, A., 2019. Transient activation of the UPRER is an essential step in the acquisition of pluripotency during reprogramming. Sci. Adv. 5, eaaw0025.
Singh, R.K., Gonzalez, M., Kabbaj, M.-H.M., Gunjan, A., 2012. Novel E3 ubiquitin ligases that regulate histone protein levels in the budding yeast Saccharomyces cerevisiae. PLoS One 7, e36295.
Singh, R.K., Kabbaj, M.-H.M., Paik, J., Gunjan, A., 2009. Histone levels are regulated by phosphorylation and ubiquitylation-dependent proteolysis. Nat. Cell Biol. 11, 925–933.
Smith, Z.D., Sindhu, C., Meissner, A., 2016. Molecular features of cellular reprogramming and development. Nat. Rev. Mol. Cell Biol. 17, 139–154.
Sonnhammer, E.L., Durbin, R., 1997. Analysis of protein domain families inCaenorhabditis elegans. Genomics 46, 200–216.
Sprecher, S.G., Desplan, C., 2008. Switch of rhodopsin expression in terminally differentiated Drosophila sensory neurons. Nature 454, 533–537.

Srivastava, D., DeWitt, N., 2016. In Vivo Cellular Reprogramming: The Next Generation. Cell 166, 1386–1396.
Stefanakis, N., Carrera, I., Hobert, O., 2015. Regulatory logic of pan-neuronal gene expression in C. elegans. Neuron 87, 733–750.
St-Germain, J.R., Chen, J., Li, Q., 2008. Involvement of PML nuclear bodies in CBP degradation through the ubiquitin-proteasome pathway. Epigenetics 3, 342–349.
Sugrue, K.F., Sarkar, A.A., Leatherbury, L., Zohn, I.E., 2019. The ubiquitin ligase HECTD1 promotes retinoic acid signaling required for development of the aortic arch. Dis. Model. Mech. 12, dmm036491.
Sulston, J.E., Horvitz, H.R., 1977. Post-embryonic cell lineages of the nematode, Caenorhabditis elegans. Dev. Biol. 56, 110–156.
Sulston, J.E., Schierenberg, E., White, J.G., Thomson, J.N., 1983. The embryonic cell lineage of the nematode Caenorhabditis elegans. Dev. Biol. 100, 64–119.
Sun, Z.-W., Allis, C.D., 2002. Ubiquitination of histone H2B regulates H3 methylation and gene silencing in yeast. Nature 418, 104–108.
Tada, M., Takahama, Y., Abe, K., Nakatsuji, N., Tada, T., 2001. Nuclear reprogramming of somatic cells by in vitro hybridization with ES cells. Curr. Biol. 11, 1553–1558.
Taipale, M., Tucker, G., Peng, J., Krykbaeva, I., Lin, Z.-Y., Larsen, B., Choi, H., Berger, B., Gingras, A.-C., Lindquist, S., 2014. A quantitative chaperone interaction network reveals the architecture of cellular protein homeostasis pathways. Cell 158, 434–448.
Takahashi, A., Imai, Y., Yamakoshi, K., Kuninaka, S., Ohtani, N., Yoshimoto, S., Hori, S., Tachibana, M., Anderton, E., Takeuchi, T., 2012. DNA damage signaling triggers degradation of histone methyltransferases through APC/CCdh1 in senescent cells. Mol. Cell 45, 123–131.
Takahashi, K., Tanabe, K., Ohnuki, M., Narita, M., Ichisaka, T., Tomoda, K., Yamanaka, S., 2007. Induction of pluripotent stem cells from adult human fibroblasts by defined factors. cell 131, 861–872.
Takahashi, K., Yamanaka, S., 2016. A decade of transcription factor-mediated reprogramming to pluripotency. Nat. Rev. Mol. Cell Biol. 17, 183–193.
Takahashi, K., Yamanaka, S., 2015. A developmental framework for induced pluripotency. Development 142, 3274–3285.
Takahashi, K., Yamanaka, S., 2006. Induction of pluripotent stem cells from mouse embryonic and adult fibroblast cultures by defined factors. cell 126, 663–676.
Taylor, R.C., Dillin, A., 2011. Aging as an event of proteostasis collapse. Cold Spring Harb. Perspect. Biol. 3, a004440.
Theodoraki, M.A., Nillegoda, N.B., Saini, J., Caplan, A.J., 2012. A network of ubiquitin ligases is important for the dynamics of misfolded protein aggregates in yeast. J. Biol. Chem. 287, 23911–23922.
Tormos, K.V., Anso, E., Hamanaka, R.B., Eisenbart, J., Joseph, J., Kalyanaraman, B., Chandel, N.S., 2011. Mitochondrial complex III ROS regulate adipocyte differentiation. Cell Metab. 14, 537–544.
Tra, T., Gong, L., Kao, L.-P., Li, X.-L., Grandela, C., Devenish, R.J., Wolvetang, E., Prescott, M., 2011. Autophagy in human embryonic stem cells. PloS One 6, e27485.
Tran, H., Bustos, D., Yeh, R., Rubinfeld, B., Lam, C., Shriver, S., Zilberleyb, I., Lee, M.W., Phu, L., Sarkar, A.A., 2013. HectD1 E3 ligase modifies adenomatous polyposis coli (APC) with polyubiquitin to promote the APC-axin interaction. J. Biol. Chem. 288, 3753–3767.

Trempe, J.-F., 2011. Reading the ubiquitin postal code. Curr. Opin. Struct. Biol. 21, 792–801.
Turner, S.D., Ricci, A.R., Petropoulos, H., Genereaux, J., Skerjanc, I.S., Brandl, C.J., 2002. The E2 ubiquitin conjugase Rad6 is required for the ArgR/Mcm1 repression of ARG1 transcription. Mol. Cell. Biol. 22, 4011–4019.
Tursun, B., 2012. Cellular reprogramming processes in Drosophila and C. elegans. Curr. Opin. Genet. Dev. 22, 475–484.
Tursun, B., Patel, T., Kratsios, P., Hobert, O., 2011. Direct conversion of C. elegans germ cells into specific neuron types. Science 331, 304–308.
Uchida, O., Nakano, H., Koga, M., Ohshima, Y., 2003. The C. elegans che-1 gene encodes a zinc finger transcription factor required for specification of the ASE chemosensory neurons.
Vabulas, R.M., Raychaudhuri, S., Hayer-Hartl, M., Hartl, F.U., 2010. Protein folding in the cytoplasm and the heat shock response. Cold Spring Harb. Perspect. Biol. 2, a004390.
Van Steensel, B., Belmont, A.S., 2017. Lamina-associated domains: links with chromosome architecture, heterochromatin, and gene repression. Cell 169, 780–791.
Vidal, S.E., Amlani, B., Chen, T., Tsirigos, A., Stadtfeld, M., 2014. Combinatorial modulation of signaling pathways reveals cell-type-specific requirements for highly efficient and synchronous iPSC reprogramming. Stem Cell Rep. 3, 574–584.
Vierbuchen, T., Ostermeier, A., Pang, Z.P., Kokubu, Y., Südhof, T.C., Wernig, M., 2010. Direct conversion of fibroblasts to functional neurons by defined factors. Nature 463, 1035–1041.
Vierbuchen, T., Wernig, M., 2011. Direct lineage conversions: unnatural but useful? Nat. Biotechnol. 29, 892–907.
Vilchez, D., Boyer, L., Morantte, I., Lutz, M., Merkwirth, C., Joyce, D., Spencer, B., Page, L., Masliah, E., Berggren, W.T., 2012. Increased proteasome activity in human embryonic stem cells is regulated by PSMD11. Nature 489, 304–308.
Vilchez, D., Saez, I., Dillin, A., 2014. The role of protein clearance mechanisms in organismal ageing and age-related diseases. Nat. Commun. 5, 5659.
Vousden, K.H., 2000. p53: death star. Cell 103, 691–694.
Wang, H., Yang, Y., Liu, J., Qian, L., 2021. Direct cell reprogramming: approaches, mechanisms and progress. Nat. Rev. Mol. Cell Biol. 22, 410–424.
Wang, T., Chen, K., Zeng, X., Yang, J., Wu, Y., Shi, X., Qin, B., Zeng, L., Esteban, M.A., Pan, G., 2011. The histone demethylases Jhdm1a/1b enhance somatic cell reprogramming in a vitamin-C-dependent manner. Cell Stem Cell 9, 575–587.
Weber, J., Polo, S., Maspero, E., 2019. HECT E3 Ligases: A Tale With Multiple Facets. Front. Physiol. 10.
Weintraub, H., Tapscott, S.J., Davis, R.L., Thayer, M.J., Adam, M.A., Lassar, A.B., Miller, A.D., 1989. Activation of muscle-specific genes in pigment, nerve, fat, liver, and fibroblast cell lines by forced expression of MyoD. Proc. Natl. Acad. Sci. 86, 5434–5438.
Weissman, A.M., 2001. Themes and variations on ubiquitylation. Nat. Rev. Mol. Cell Biol. 2, 169–178.
Werner, A., Manford, A.G., Rape, M., 2017. Ubiquitin-Dependent Regulation of Stem Cell Biology. Trends Cell Biol. 27, 568–579.

Wernig, M., Meissner, A., Foreman, R., Brambrink, T., Ku, M., Hochedlinger, K., Bernstein, B.E., Jaenisch, R., 2007. In vitro reprogramming of fibroblasts into a pluripotent ES-cell-like state. nature 448, 318–324.
White, J.G., Southgate, E., Thomson, J.N., Brenner, S., 1986. The structure of the nervous system of the nematode Caenorhabditis elegans. Philos. Trans. R. Soc. Lond. B Biol. Sci. 314, 1–340.
Whitesell, L., Lindquist, S.L., 2005. HSP90 and the chaperoning of cancer. Nat. Rev. Cancer 5, 761–772.
Willis, N.D., Cox, T.R., Rahman-Casañs, S.F., Smits, K., Przyborski, S.A., van den Brandt, P., van Engeland, M., Weijenberg, M., Wilson, R.G., de Bruïne, A., 2008. Lamin A/C is a risk biomarker in colorectal cancer. PloS One 3, e2988.
Wilmut, I., Schnieke, A.E., McWhir, J., Kind, A.J., Campbell, K.H., 1997. Viable offspring derived from fetal and adult mammalian cells. Nature 385, 810–813.
Wolff, S., Weissman, J.S., Dillin, A., 2014. Differential scales of protein quality control. Cell 157, 52–64.
Wong, K.S., Houry, W.A., 2006. Hsp90 at the crossroads of genetics and epigenetics. Cell Res. 16, 742–749.
Worman, H.J., Östlund, C., Wang, Y., 2010. Diseases of the nuclear envelope. Cold Spring Harb. Perspect. Biol. 2, a000760.
Wu, R.-C., Feng, Q., Lonard, D.M., O'Malley, B.W., 2007. SRC-3 coactivator functional lifetime is regulated by a phospho-dependent ubiquitin time clock. Cell 129, 1125–1140.
Wu, Z., Wu, L., Weng, D., Xu, D., Geng, J., Zhao, F., 2009. Reduced expression of lamin A/C correlates with poor histological differentiation and prognosis in primary gastric carcinoma. J. Exp. Clin. Cancer Res. 28, 8.
Xie, H., Ye, M., Feng, R., Graf, T., 2004. Stepwise reprogramming of B cells into macrophages. Cell 117, 663–676.
Xu, X., Duan, S., Yi, F., Ocampo, A., Liu, G.-H., Belmonte, J.C.I., 2013. Mitochondrial regulation in pluripotent stem cells. Cell Metab. 18, 325–332.
Xue, Y., Ouyang, K., Huang, J., Zhou, Y., Ouyang, H., Li, H., Wang, G., Wu, Q., Wei, C., Bi, Y., Jiang, L., Cai, Z., Sun, H., Zhang, K., Zhang, Y., Chen, J., Fu, X.-D., 2013. Direct conversion of fibroblasts to neurons by reprogramming PTB-regulated microRNA circuits. Cell 152, 82–96.
Yamanaka, S., Blau, H.M., 2010. Nuclear reprogramming to a pluripotent state by three approaches. Nature 465, 704–712.
Yamano, K., Matsuda, N., Tanaka, K., 2016. The ubiquitin signal and autophagy: an orchestrated dance leading to mitochondrial degradation. EMBO Rep. 17, 300–316.
Yang, W., Lee, Y.-H., Jones, A.E., Woolnough, J.L., Zhou, D., Dai, Q., Wu, Q., Giles, K.E., Townes, T.M., Wang, H., 2014. The histone H2A deubiquitinase Usp16 regulates embryonic stem cell gene expression and lineage commitment. Nat. Commun. 5, 3818.
Yanger, K., Zong, Y., Maggs, L.R., Shapira, S.N., Maddipati, R., Aiello, N.M., Thung, S.N., Wells, R.G., Greenbaum, L.E., Stanger, B.Z., 2013. Robust cellular reprogramming occurs spontaneously during liver regeneration. Genes Dev. 27, 719–724.
Ye, J., Blelloch, R., 2014. Regulation of pluripotency by RNA binding proteins. Cell Stem Cell 15, 271–280.

Yoneda, T., Benedetti, C., Urano, F., Clark, S.G., Harding, H.P., Ron, D., 2004. Compartment-specific perturbation of protein handling activates genes encoding mitochondrial chaperones. J. Cell Sci. 117, 4055–4066.
You, K.T., Park, J., Kim, V.N., 2015. Role of the small subunit processome in the maintenance of pluripotent stem cells. Genes Dev. 29, 2004–2009.
Yu, J., Vodyanik, M.A., Smuga-Otto, K., Antosiewicz-Bourget, J., Frane, J.L., Tian, S., Nie, J., Jonsdottir, G.A., Ruotti, V., Stewart, R., 2007. Induced pluripotent stem cell lines derived from human somatic cells. science 318, 1917–1920.
Yu, S., Avery, L., Baude, E., Garbers, D.L., 1997. Guanylyl cyclase expression in specific sensory neurons: a new family of chemosensory receptors. Proc. Natl. Acad. Sci. 94, 3384–3387.
Yuzyuk, T., Fakhouri, T.H.I., Kiefer, J., Mango, S.E., 2009. The polycomb complex protein mes-2/E (z) promotes the transition from developmental plasticity to differentiation in C. elegans embryos. Dev. Cell 16, 699–710.
Zahreddine, H., Zhang, H., Diogon, M., Nagamatsu, Y., Labouesse, M., 2010. CRT-1/calreticulin and the E3 ligase EEL-1/HUWE1 control hemidesmosome maturation in C. elegans development. Curr. Biol. 20, 322–327.
Zerafati-Jahromi, G., Oxman, E., Hoang, H.D., Charng, W.-L., Kotla, T., Yuan, W., Ishibashi, K., Sebaoui, S., Luedtke, K., Winrow, B., 2025. Sequence variants in HECTD1 result in a variable neurodevelopmental disorder. Am. J. Hum. Genet. 112, 537–553.
Zhang, L., Ward, J.D., Cheng, Z., Dernburg, A.F., 2015. The auxin-inducible degradation (AID) system enables versatile conditional protein depletion in C. elegans. Development 142, 4374–4384.
Zhang, P., Chang, W.-H., Fong, B., Gao, F., Liu, C., Al Alam, D., Bellusci, S., Lu, W., 2014. Regulation of induced pluripotent stem (iPS) cell induction by Wnt/β-catenin signaling. J. Biol. Chem. 289, 9221–9232.
Zhang, T., Joubert, P., Ansari-Pour, N., Zhao, W., Hoang, P.H., Lokanga, R., Moye, A.L., Rosenbaum, J., Gonzalez-Perez, A., Martinez-Jimenez, F., 2021. Genomic and evolutionary classification of lung cancer in never smokers. Nat. Genet. 53, 1348–1359.
Zhao, X., Heng, J.I.-T., Guardavaccaro, D., Jiang, R., Pagano, M., Guillemot, F., Iavarone, A., Lasorella, A., 2008. The HECT-domain ubiquitin ligase Huwe1 controls neural differentiation and proliferation by destabilizing the N-Myc oncoprotein. Nat. Cell Biol. 10, 643–653.
Zhou, G., Meng, S., Li, Y., Ghebre, Y.T., Cooke, J.P., 2016. Optimal ROS signaling is critical for nuclear reprogramming. Cell Rep. 15, 919–925.
Zhou, Q., Brown, J., Kanarek, A., Rajagopal, J., Melton, D.A., 2008. In vivo reprogramming of adult pancreatic exocrine cells to β-cells. nature 455, 627–632.
Zhu, J., Fukushige, T., McGhee, J.D., Rothman, J.H., 1998. Reprogramming of early embryonic blastomeres into endodermal progenitors by a Caenorhabditis elegans GATA factor. Genes Dev. 12, 3809–3814.
Zink, D., Fischer, A.H., Nickerson, J.A., 2004. Nuclear structure in cancer cells. Nat. Rev. Cancer 4, 677–687.
Zubarev, I.V., Podenkova, U.I., Tomilin, A.N., Tsimokha, A.S., 2022. Ubiquitin–Proteasome System in the Induction and Maintenance of Cellular Pluripotency. Russ. J. Dev. Biol. 53, 373–388.
Zuryn, S., Ahier, A., Portoso, M., White, E.R., Morin, M.-C., Margueron, R., Jarriault, S., 2014. Sequential histone-modifying activities determine the robustness of transdifferentiation. Science 345, 826–829

Supplementary

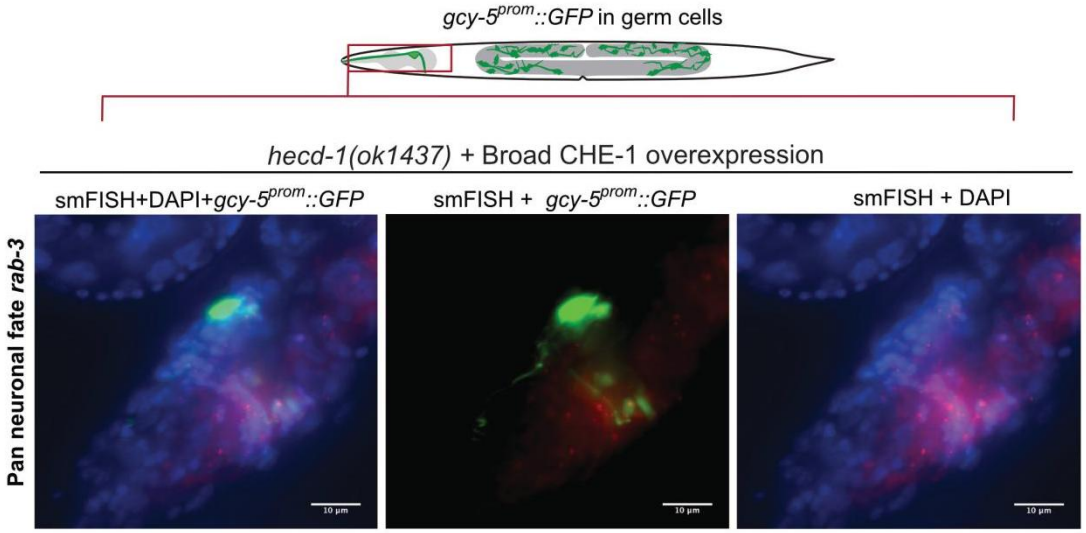

S.1 Endogenous Expression of Neuronal Genes in neuron cells. smFISH-based visualization of transcripts originating from endogenous neuronal *rab-3* in the neuson cells of *hecd-1(ok1437)* mutant background upon CHE-1^{oe} animals. The mRNAs are displayed as red dots. Scale bar: 10 µm.

List of Figures

List of Tables

List of Abbreviations

°C	Degree Celsius
AID	Auxin Inducible Degron
Amp	Auxin Inducible Degron
ASE	Amphid neurons (single ciliated endings)
bp	base pairs
DIC	Differential Interference Contrast
DNA	Deoxyribonucleic acid
dNTPs	deoxyribonucleotide triphosphate
E. coli	Escherichia Coli
g	gram
kDA	kilodalton
LB	Luria-Bertani
min	minute
mL	mililiters
mM	mili Molar
PCR	Polymerase Chain Reaction
PFA	Paraformaldehyde
Rluc	Renilla luciferase

RNA	ribonucleic acid
RNAi	RNA interference
rpm	revolutions per minute
s	second
SCNT	Somatic cell nuclear transfer
SDS-PAGE	SDS-polyacrylamide gel electrophoresis
SEM	Standard error of the mean
smFISH	single molecule fluorescent in situ hybridization
TAE	Tris Acetat EDTA
TBST	Tris-Buffered Saline-Tween 20
TF	Transcription Factor
WB	Western Blot
WT	wild type
µg	microgram
µM	micro Molar
µm	micrometer

Acknowledgements

First, I would like to thank Baris for giving me the opportunity to work in his lab, and for his patience and support throughout the years. As a girl who grew up in a small town, he gave me the chance to see the world beyond China. I am truly grateful and deeply appreciate having him as my supervisor.

I am profoundly thankful to Iris for being my friend, for appearing in my life and supporting me from the very beginning of this journey to the very end. And this friendship will continue for the rest of my life. I feel so lucky to know you. I would also like to thank Ismail, Selman, Amin, Sophia, Gizem, Marcel E., Marcel S., Levi, and Tina for their support.

I want to thank my mom and dad — you are the greatest parents in the world. You have always supported everything I wanted to do. Whenever I felt sad or lost, your love healed me and carried me through.

A special thanks to my fiancé, Zhaoyong. You have always been my best friend all these years. Even though we are thousands of miles apart, we still share everything in our lives and remain as close as if we were one person.

Finally, a few words to myself: stay hungry, stay foolish — always remain curious and humble.